Structural Behavior of Full Scale Totally Precast Concrete Counterfort Retaining Wall System

BY

Maen Farhat
B.S., Lebanese University, Beirut, Lebanon, 2012

THESIS

Submitted as partial fulfillment of the requirements
for the degree of Doctor of Philosophy in Civil Engineering
in the Graduate College of the
University of Illinois at Chicago, 2016

Chicago, Illinois

Defense Committee:

Professor Mohsen Issa, Chair and Advisor
Professor Ahmed Shabana, Mechanical and Industrial Engineering
Professor Craig Foster
Professor Krishna Reddy
Professor Alexander Chudnovsky

DEDICATION

To Leila and Ali…

ACKNOWLEDGEMENTS

I would like to express my sincere gratitude to my advisor Professor Mohsen Issa for his continuous support and guidance. Professor Issa has always motivated me to advance my understanding of fundamentals of materials and structural engineering.

I would also like to express my appreciation to my PhD committee members; Professor Ahmed Shabana, Professor Craig Foster, Professor Krishna Reddy, and Professor Alexander Chudnovsky. Their recommendation and advice in my research, is deeply appreciated.

Thanks to my colleagues who greatly assisted me in performing the experimental texting program; Mustapha Ibrahim and Momenur Rahman. Their help was important in completing the experimental testing required in this research.

I would like to extend my thanks to the National University Rail Center (NURail) for supporting me for several semesters. Also thanks to Utility Concrete Products (UCP), LLC. Morris, Illinois for performing the fabrication, erection procedures and providing the facility to perform the full scale experimental testing part of the study. Thanks to UIC for providing all the means to perform both the full scale and the elementary experimental testing programs such as instrumentation, testing equipment, machines, data analysis, and finite element modeling.

Finally I am grateful to the University of Illinois at Chicago, Department of Civil and Materials Engineering, to the faculty, and staff. In particular, thanks to the technicians at the UIC machine shop; David Mecha and Eric Schmidt for all their help with the testing fixtures and setups, the technical support personnel; Kassem Saad and Douglas Perzan for their help and support throughout my time at UIC, and UIC staff; Mary Ann Borjal, Sara Arevalo, Pam Woodard and Dansel Abando for their help with the administration and financial affairs.

CONTRIBUTION OF THE AUTHORS

The content of this thesis was based on articles in which I was the first author. Chapter 1 presents introduction about the topic. The introduction was taken from the introductions of each paper. Chapter 2 presents a literature review. The literature review was gathered from the literature reviews presented in these papers. Chapter 3 presents the design guidelines of the proposed Totally Precast Concrete Counterfort Retaining Wall system and it was primarily taken from Paper 1. Chapter 4 presents the fabrication procedures of the proposed system and it was primarily taken from Paper 2. Chapter 5 presents the experimental testing program and finite element analysis and it was mainly taken from Paper 3. Chapter 6 presents the pullout behavior and it was taken from Paper 4. Chapter 7 presents summary and conclusions of this work and it was collected from the conclusions of all the papers.

1. Farhat, M., and Issa, M.A., "Design Principles of Totally Precast Concrete Counterfort Retaining Wall System Compared to Existing Cast-In-Place Structures," *PCI Journal*, Accepted for publication in PCI Journal on October 31, 2016

2. Farhat, M., and Issa, M.A., "Fabrication and Construction of Totally Precast Concrete Counterfort Retaining Wall System for Highways," Practice Periodical of Structural Engineering, *ASCE*, Accepted for publication on October 8, 2016.

3. Farhat, M., Ibrahim, M., Issa, M.A., and Rahman, M., "Full Scale Experimental Testing and Finite Element Analysis of Totally Precast Concrete Counterfort Retaining Wall System," *PCI Journal*, Accepted for publication in PCI Journal on October 31, 2016

4. Farhat, M., Issa, M.A., and Jose Prado, B. F. “Pullout Behavior of Headed Anchors Used in Totally Precast Concrete Counterfort Retaining Wall System,” Paper Submitted to *PCI Journal*, Under review.
5. Farhat, M., Rahman, M., Ibrahim, M., and Issa, M. A., “Design Optimization and Modeling of a Totally Precast Concrete Counterfort Retaining Wall System” In the proceedings of the European Bridge Conference, Edinburgh., UK, 22-25 June 2015.
6. Farhat, M., Rahman, M., Ibrahim, M., and Issa, M. A., “Design, Fabrication, Modeling and Experimental Study of a Totally Precast Concrete Counterfort Retaining Wall System for Highways” In the proceedings of the 2014 PCI/NBC conference, Washington D.C., CA, 06-09 September 2014.

In Papers 1 and 2, my advisor (Professor Mohsen Issa) provided the necessary guidance to perform the experimental and analytical work. He assisted in reviewing the content of the paper and enriching it with valuable ideas and information. In Papers 3, 5, and 6, Mustapha Ibrahim and Professor Issa greatly assisted in conducting the experimental testing program. Momenur Rahman helped in performing part of the finite element analysis. Professor Issa guided us through his experience in experimental testing. In Paper 4, Professor Mohsen Issa assisted in providing the necessary guidance in order to conduct the experimental testing program. Bruno Fusari Jose Prado helped me with the experimental testing program. Bruno was an exchange undergraduate student in summer 2016.

TABLE OF CONTENTS

LIST OF TABLES

LIST OF FIGURES

ABSTRACT

Totally Prefabricated Concrete Counterfort Retaining Wall (TPCCRW) provides an alternative for conventional construction techniques to reduce the drawbacks associated with cast-in-place construction. TPCCRW is composed of a precast concrete wall component (face panel and counterforts) and a base slab connected, on-site, through headed anchors. The anchors extend downward from the counterforts into shear pockets located in the precast base slab. While the structural design of TPCCRW shares some features with cast-in place systems, it also has specific requirements for anchor connections, strength of shear pockets, and counterfort design. The design of TPCCRW was developed according to AASHTO LRFD (2012) specifications and compared to an existing cast-in-place counterfort system in Chicago, IL, for both structural and economic performances. The design strength of TPCCRW (moment and shear) surpassed that of the existing system with an overall reduction in concrete volume of 57%. A parametric study identified a counterfort spacing-to-base length ratio of 0.35 and a counterfort extension-to-heel length ratio of 0.6 as optimal values.

In addition, the overall structural behavior of TPCCRW was examined experimentally and analytically using Nonlinear Finite Element Analysis (NLFEA). A full scale prototype (20 ft 2 in. high and 13 ft 10 in. wide) was designed meeting the requirements of AASHTO LRFD specifications, assembled, constructed, instrumented and tested at the precast concrete plant. The design was optimized and validated using NLFEA. The precast components were connected through five headed anchors at each counterfort. The results showed that the wall experienced a deflection of 0.2 in. at its middle. The anchors succeeded to maintain serviceability and ultimate strength requirements. The

proposed system required a unique method of construction. Therefore, the fabrication and construction procedures and guidelines required to accelerate the erection process on site were detailed. The system components can be fully assembled and set in place in less than 2 hours.

Finally, the pullout behavior of headed anchors used in TPCCRW was examined experimentally and analytically using NLFEA. Eighteen precast concrete blocks (21 in. x 20 in.) having a truncated shear pocket identical to those used in TPCCRW were prepared, grouted with headed anchors, instrumented, and experimentally tested. The study took into consideration two different block thicknesses (14 in. and 6 in.), two IDOT certified types of headed anchors and types of concrete grout, different bar sizes (#6, #7, #8, #9), and different embedment depths (12.5 in., 10 in., 8 in, and 6 in.). The structural behavior of the pullout specimens was characterized by yielding and fracture of steel anchors regardless of their size. Concrete breakout was witnessed in 14 in. thick concrete specimens made with #9 headed anchors and 6 in. embedment depth when the specimen was tested to ultimate. The experimental test results were verified using finite element analysis and compared to design codes and other studies in the literature. The result showed close correlation with the AISC design guide for base plates and headed rods.

EXECUTIVE SUMMARY

The structural and concrete research laboratory at the University of Illinois at Chicago designed and tested a Totally Precast Concrete Counterfort Retaining Wall System (TPCCRW) as an innovative retaining wall solution for highway and bridge construction. It was optimized and developed as a response to the growing needs of multiple requirements such as the speed of construction, strength and durability, minimizing the interruption of traffic flow, safety and cost competency. TPCCRW consists of two prefabricated units: 1) the wall unit consisting of a precast concrete face-panel and three precast counterforts and 2) a precast concrete base-slab. Headed anchors are used to connect each counterfort to the base-slab and thus enforcing the integrity of the system as one unit. The headed anchors extend from the bottom of the precast counterforts into shear pockets located in the base slab. The shear pockets are grouted after erection to achieve full composite action between the counterforts and the base slab.

This research work presented herein was conducted to evaluate the structural integrity and performance of TPCCRW. The design principles of the proposed system were presented with special focus on the new design concepts of this system, which are different from conventional concepts. The system was compared to an existing counterfort cast-in-place retaining wall system from design, structural efficiency, and economic perspectives. A parametric study also was performed to assess the performance of the proposed system with increasing heights to facilitate its design procedures.

In addition, description and illustrations of the construction procedures and practices involved in TPCCRW were presented. The guidelines for off-site fabrication and the construction processes were detailed taking into account the challenges that might face the contactors in order to accelerate construction procedures and reduce errors.

After detailing the design, and fabrication processes, the proposed wall system was optimized using conventional beam theory and finite element analysis to achieve the most efficient geometric configuration. Then, a full scale experimental testing and nonlinear finite element analysis was performed to examine the overall structural behavior of the proposed system. The tested prototype was 20 ft - 2 in. (6.09 m) high and 13 ft – 10 in. (4.21 m) wide. The prototype was subjected to soil backfilling, live load surcharge, and additional load using hydraulic cylinders reaching up to 192.4 kips (855.83 kN) to carry the system to ultimate load. The deflection in the face panel at H/3 and H/2 was monitored. In addition, strain readings in the headed anchors, counterforts main reinforcement, face panel, and base slab were monitored and presented. The results of the finite element analysis were compared and validated with the experimental testing results.

Finally, the headed anchors are subjected to tensile loads under the effect of the applied soil pressure. Therefore, an experimental study and nonlinear finite element analysis were also performed to examine the overall breakout behavior of headed anchors used in this system. Eighteen precast concrete blocks (21 in. x 20 in.) having a shear pocket identical to those used in TPCCRW were prepared, grouted with headed anchors, instrumented and experimentally tested. The study took into consideration two different block thicknesses (14 in. and 6 in.), two IDOT certified types of headed anchors and grouts, different bar sizes (#7, #8, #9), and different embedment depths (12.5 in., 10 in., 8 in, and 6 in.). The blocks were tested under axial tensile loading conditions to simulate actual loading conditions. Based on the results of these tests, conclusions were drawn regarding the design, fabrication and structural behavior of the proposed system.

1. INTRODUCTION

1.1. Background

Substructure systems, specifically retaining walls and abutments, constitute a major facet of the bridge construction process. Currently, a majority of the substructure construction work is carried out using cast-in-place concrete. However, cast-in-place construction can be associated with several difficulties and drawbacks, such as prolonged site preparation procedures, mitigated work zone safety due to exposure of workers to active traffic, traffic congestion, the requirement for skilled workmanship, and environmental costs. As a result, the need for shorter construction periods is shifting the interest towards Accelerated Bridge Construction (ABC) methods, such as incorporating precast concrete products in construction. The implementation of precast concrete products in construction provides several economic, safety and environmental advantages. Precast concrete products are cast using high performance concrete under high level of quality control, which enhances the consistency and uniformity of the materials during mass production and therefore improves the durability of the final product.

Precast concrete products are made in a controlled environment, which eliminates problems that can be found on job sites and affect the quality of concrete like temperature; curing conditions, and human errors on site. Moreover, the modularity of precast concrete products gives the precast retaining walls the ability to be installed faster which saves time and money. These advantages allow the precast concrete retaining walls to be produced with aesthetically appealing wall panel.

Although precast systems provide several economic, social, and environmental advantages, plenty of research is still required to develop precast systems for substructures such as retaining walls and abutments. As a response, the structural and concrete laboratory at the University of Illinois at Chicago proposed the totally Precast Concrete Counterfort Retaining Wall System (TPCCRW) as an innovative retaining wall solution for highway application (Farhat et al. 2014 and 2015). The proposed system was optimized and developed as a response to the growing needs of multiple requirements such as the speed of construction, strength and durability, minimization of traffic flow interruption, safety and cost.

TPCCRW consists of two precast concrete components: the wall component consisting of a face-panel with three counterforts and the base-slab component. Counterforts act as stiffeners to the face panel and connection between the wall and the base slab. Headed anchors are used to connect each counterfort to the base-slab and thus enforcing the integrity of the system to achieve full composite action.

Counterforts are added along the length of the wall at discrete locations to enhance the serviceability of the face-panel and to increase the stiffness of the system without affording to increase the thickness of the face-panel along the entire length of the wall. In fact, counterfort retaining wall systems also exhibit lower stress states then their cantilever counterparts.

1.2. <u>Problem Statement</u>

The increasing traffic demand imposes further expansion on highways and bridges components such as substructure systems. The conventional construction processes performed to accommodate this expansion is generally accompanied with drawbacks such as traffic interruptions, lane closures, and long construction periods that increase the economic cost. As a result, several departments of transportation are seeking accelerated construction techniques to reduce the impact of the aforementioned drawbacks associated with conventional construction methods. These accelerated construction techniques involve using proposed precast concrete systems. These systems require detailed experimental and theoretical investigations to confirm their applicability before introducing them to the DOTs.

When TPCCRW was introduced, the structural design of the connections between the precast components required attention. In addition, the construction procedures of this system required detailing to facilitate the process for designers and contractors. Moreover, the structural performance of TPCCRW on the full-scale measure must be verified to meet the requirements of serviceability and strength as per AASHTO LRFD. In addition to presenting the proposed system, a comparison between this system and other existing systems was needed to understand its suitability to widespread adoption.

1.3. Research Objectives

The aim of this work is to study the structural behavior of TPCCRW. This involves performing detailed structural design assessment according to design codes and using finite element analysis, detailing the fabrication procedures, optimization, and conducting full-scale experimental testing. Therefore, this study develops the design principles of the proposed system. It also presents a comparison between this system and an existing typical cast-in-place counterfort retaining wall system in Chicago, IL. The study highlights the main details, parameters, and assumptions taken in both systems. The advantages of using the proposed precast concrete system and its suitability for widespread adoption in the specified site are examined from the economical point of view. In addition, the general guidelines for the fabrication and construction of the Totally Precast Concrete Counterfort Retaining Wall system must be standardized.

Moreover, the structural performance of the proposed totally precast concrete counterfort retaining wall system (TPCCRW) was examined through full scale experimental testing and nonlinear finite element analysis. After studying the global behavior through full scale testing, the elementary behavior at the level of headed anchors was performed to examine its mode of failure.

1.4. Thesis Organization

Chapter 1: This chapter gives a general background on the retaining walls and substructure systems. It also presents the problem statement and the research objective of this report.

Chapter 2: This chapter presents a detailed description of the past literature research documenting the current advances and state-the-art regarding fully precast concrete systems used in highways and bridges.

Chapter 3: This chapter presents the design principles of totally precast concrete counterfort retaining wall system compared to existing cast-in-place structures

Chapter 4: This chapter presents the fabrication and construction procedures of the totally precast concrete counterfort retaining wall system for highways.

Chapter 5: This chapter entails the full scale experimental testing and finite element analysis of totally precast counterfort retaining wall system. The experimental testing program and results in addition to the finite element analysis results are presented in this section

Chapter 6: This chapter presents the experimental testing program and finite element analysis results of the pullout behavior of headed anchors used in totally precast concrete counterfort retaining wall system.

Chapter 7: This chapter presents the summary and conclusions of the presented work. In addition, it presents recommendations for future work.

2. LITERATURE REVIEW

2.1. Background

The use of precast concrete elements for bridge construction and rehabilitation is considered economically efficient, as it requires less time of operation (Biswas, 1986). Although cast-in-place abutments, piers, and deck slabs are widely used in bridge applications, their construction sequences and procedures are considered time intensive (Hieber et al., 2005). Several activities related to cast-in-place procedures had raised problems related to time schedules, safety priorities, and environment. These activities include:

- Site preparation procedures like installation of formwork, casting, curing of concrete,
- Traffic detouring and lane closures causing traffic congestion,
- Construction works causing labor exposure to active traffic,
- Finishing works which require skilled workmanship.

These challenges have led to increasing focus on precast concrete products as it provides a potential solution due to the efficiency of the production and assembly processes. Moreover, precast concrete products are made in a controlled environment taking advantage of the uniformity and consistency of the high performance concrete properties and therefore, reducing the risk of error on-site.

Precast concrete bridge components are divided into superstructure elements (decks, beams, etc...) and substructure elements (Piers, abutment, retaining walls, etc…). Generally, majority of the research found in literature was focused on developing precast concrete superstructure systems. The research resulted in details and guidelines for using partial or precast concrete superstructure systems.

2.2. Precast systems for superstructures

Precast concrete bridge components are divided into superstructure elements (decks, beams, etc..) and Substructure elements (Piers, abutment, retaining walls, etc…). Goldberg D. (1987) proposed guidelines to design, manufacture, and erect stay-in-place (SIP) concrete bridge deck panels with cast in place topping. In addition, Guidelines has been detailed for the use of partial and full-depth precast superstructure deck systems in new bridge construction and rehabilitation (PCI-NER, 2001 and 2002).

Special focus was made on rapid replacement of deteriorated cast in place bridge decks. Efficient bridge deck replacement and demolition techniques were presented and an efficient continuous precast prestressed stay in place system that is 20% faster than conventional cast in place systems was developed (Tadros et al., 1998).

Issa et al. (1995a) proposed a phased bridge deck replacement procedure using full depth precast concrete panels that allow maintaining full daytime traffic flow during rehabilitation process. The advantages of proposed procedure are that it all precast units can precast and prepared prior to demolition work of existing bridge deck to be replaced. The procedure is divided into two phases such that the contractor can perform replacement works on each half of the bridge deck without interrupting the traffic flow.

Throughout visual inspection of over 40 bridges in 12 states, the importance of shear keys among fully precast elements and shear connections and between the slabs and the supporting system was highlighted. Female to female shear keys proved to be the most effective type of connection (Issa et al. 1995b).

Issa et al. (1995c) conducted as survey to the departments of transportation (DOT). Transverse and longitudinal prestressing in full depth precast panels would protect the panels from cracking during handling and installation and would keep the joints in compression to prevent the failure of the grout. This was verified by conducting experimental static and fatigue test to conclude that prestressing is important in crack arrest and extending the service life of the panel system (Issa et al., 2000). The minimum prestressing required within a grouted joint is 200psi for simply supported spans determined using finite element analysis (Issa et al,. 1998).

2.3. <u>Substructure systems</u>

The use of precast concrete technologies in bridge substructure construction such as bent caps, column and footings has been implemented and frequently reported (Medlock et al., 2002 and Hewes, 2013). However, few studies have been found that cover any development or optimisation for the end supports of bridges like retaining walls and abutments.

One such study was conducted by Michigan Department of Transportation to implement the use of totally precast cantilever retaining wall system as shown in Figure 2-1 (Darwish et al., 2013). The system consisted of a two components: a precast base slab, and a precast stem. The components were cast off-site and transported to the construction site where were assembled. The length of the segments was limited to 3.65 m (12 ft). The recorded wall height ranged from 1.21 m (4 ft) to 7.92 m (26 ft) in order to facilitate shipping and handling.

However, the main disadvantage of using the conventional cantilever retaining wall is that a relatively thick stem cross section might be required, depending on the wall height, to control cracking and deflections. This imposes difficulties related to shipping and handling as the weight of the component will increase with the increase in the thickness.

Figure 2-1. Precast cantilever retaining wall in Michigan (Darwish et al., 2013)

As a second example, the New Hampshire Department of Transportation (NHDOT) conducted a project in which a fully precast concrete bridge was constructed (Stamnas et al., 2005). The bridge is 35.05 m (115 ft) long and 0.91 m (3 ft) deep with a precast box beam superstructure. A fully precast abutment system was proposed in which a precast abutment stem was connected to a precast base-slab. Steel rebars were extended from the base-slab and embedded in the precast stem through grouted sleeves to maintain full moment connection (Figure 2-2). The system is said to cut down the time required to construct a typical abutment from approximately one month for the CIP (cast-in-place) version to only two days for the precast version. In order to maintain full composite action between the stem and the base, a large number of grouted sleeves may be required. This may impose time-consuming alignment difficulties and require specially trained workmanship.

Figure 2-2. Precast bridge in “only eight days” was made in New Hampshire, 2005 (Stamnas et al., 2005)

Donkada and Menon (2012) presented an optimization approach of variable heights cast in place counterfort retaining walls taking into account geometric, reinforcement and cost parameters. The study was conducted over three different types of walls: the cantilever walls, counterfort walls, and relieving platforms walls. The study utilized heuristic rules to proportion the wall dimensions taking into account the cost perspective. The study concluded that cantilever retaining wall systems can be more cost effective compared to counterfort walls for heights exceeding 8m (26.25 ft).

State of the practice report showed details for connections in precast bridge components including retaining walls and abutments used in different states (Culmo, 2009). The study focused on presenting the state-of-the-art practice with respect to connection details between precast components used in bridge applications for Accelerated Bridge Construction.

A segmental substructure pier system was proposed for the Texas Department of Transportation (TxDOT) in 1999 (Billington 1998, 2001). The system is mainly composed of match cast column segments (Figure 2-3): template segments and inverted-T cap components. The erection procedure starts by placing a starter template column segment followed by stacking the column segments that are post-tensioned after erecting each segment. The template segment is then erected and placed followed by the prestressed precast cap. Joints between every segment are filled with epoxy before post-tensioning.

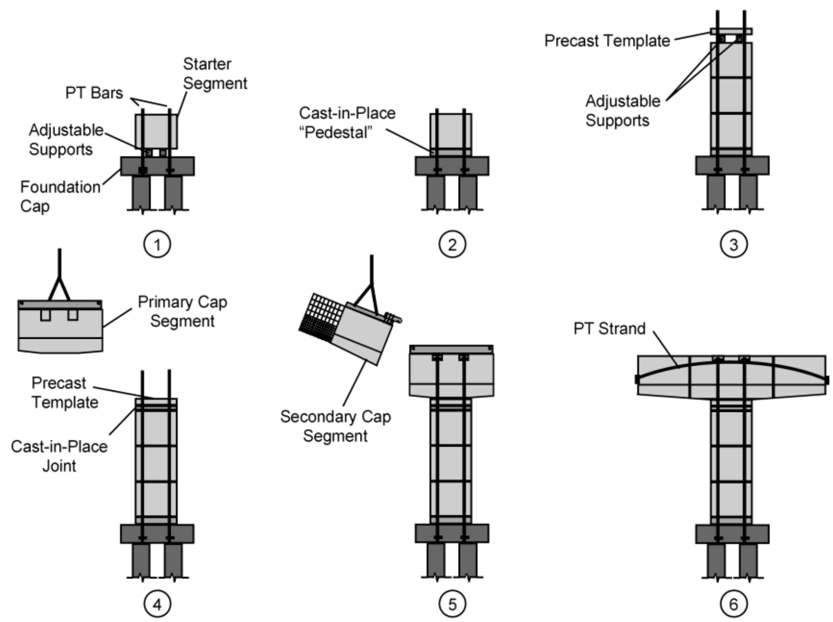

Figure 2-3. guidelines for Precast Pier erection sequence (Billington et al., 2001)

2.4. Finite element analysis for retaining wall systems

Abundant research which covers development of precast superstructure elements for bridges was found. However, the work that covers development of fully precast substructure systems was limited. Senthil et al (2014) performed a three-dimensional finite element analysis to study the effect of lateral earth pressure on cantilever and counterfort-type retaining walls. The study concluded that the amount of stress in the counterfort the height of the counterfort plays an important role in the normal stress distribution. Retaining walls with high counterforts reaching 1.2 m (3.93 ft) below the top face of the face-panel show lower stress distribution when compared to retaining walls with counterforts reaching 4.0 m (13.12 ft) from the top face of the face-panel.

Chugh et al. (2011) performed numerical simulation of an instrumented cantilever retaining wall. The result concluded that displacement-based analysis method should be used to calculate lateral earth pressure for walls founded on soils. Clough et al. (1971) used one-dimensional elements to simulate the interface between the two-dimensional elements of the soil and the retaining wall in a finite element analysis. The study showed the general behavior of the system is in agreement with the classical theory at ultimate loading conditions. Liu et al. (2006) performed finite element analysis on a 5 m (16.4 ft) high retaining wall to investigate the deformed profile of the backfill. In this study, the author discussed the relationship between displacement and distribution of the backfill from one side and between displacement and maximum plastic strain of the backfill with variant friction angle from the other side. It was found the wall friction angle has insignificant effect on the deformed soil profile.

2.5. <u>Pullout Behavior of headed anchors</u>

There are few studies in the literature that was performed on large-size headed bars subjected to pullout load. Most of the studies focused on the pullout behavior of small shear studs at a shallow depth (Rodriguez et al., 1997 and 2001, Eligehausen et al., 1995, Sattler, 1962, McMakin et al., 1973, and Cannon et al., 1975).

Lee et al. (2007) performed experimental testing on large headed anchors (more than 2 in. diameter) and large embedment depths in concrete (greater than 25 in.). The objective of the test was to investigate the anchors' suitability to be used in nuclear power plants. The authors showed that the breakout cone with the concrete surface varied from 20^o to 30^o.

According to ACI 318 -14 provisions (Chapter 17), the tensile capacity of headed anchor is controlled either by the nominal strength of an anchor in tension, N_{sa}, (17.4.1.2) or by the concrete breakout strength of anchor in tension (17.4.2). The nominal strength of the anchor in tension, N_{sa}, shall not exceed $A_{se,N}$ * f_{uta} (17.4.1.2), where $A_{se,N}$ is the effective cross sectional area of the anchor bar and f_{uta} shall not be taken greater than the smaller of $1.9f_{ya}$ and 125,000 psi. The concrete capacity design (CCD) method is used in the formulas adopted by ACI 318 for concrete breakout formulas. According to ACI 318-14, the average concrete breakout capacity of headed anchors in uncracked concrete is given by Eq. (4). The basic concrete breakout strength of a single anchor in tension in cracked concrete is given by Eq. (5), where $\boldsymbol{k_c}$ is taken as 24 for cast in place anchors and 17 for post-installed anchors. The value of k_c is permitted to be between 17 and 24 for post-installed anchors. The values of ***kc*** were determined from test results on uncracked concrete (Fuchs et al., 1995) at the 5% fractile (ACI 318-14) . Eq. (6) can be used for cast-in headed studs and headed bolts with 11 in. $\leq$ hef $\leq$ 25 in. The CCD design method presented in AISC steel design guide for base plate and anchor rods is based on the ACI-318 code (Guid, S. D., 2006). Table 2-1 summarizes the concrete breakout/pullout equations developed in the design codes and past literature.

Table 2-1. Breakout/pullout equations developed in the design codes and past literature

No.	Code reference	Equation	Remark
(1)	AISC Guide 2	$P = 0.85 f_c' A_1 \sqrt{\frac{A_2}{A_1}}$	Concentric Compressive Axial Load
(2)	AISC Guide 2	$\varphi N_p = 8\, \varphi\, \psi_4\, A_{brg}\ f_c'$	Concrete Pullout Strength
(3)	AISC Guide 2	$\varphi N_{cgb} = \varphi\, \psi_3\, k_c \sqrt{f_c'}\, h_{ef}^{1.5}\ \frac{A_N}{A_{N0}}$	CCD method
(4)	ACI 318-14 (17.4.2.1a)	$N_{cb} = \frac{A_{Nc}}{A_{Nco}} \Psi_{ed,N} \Psi_{c,N} \Psi_{cp,N} \mathrm{N}_b$	Nominal concrete (uncracked) breakout strength for single anchor
(5)	ACI 318-14 (17.4.2.2a)	$N_b = k_c\, \lambda_a \sqrt{f_c'}\, h_{ef}^{1.5}$	The basic concrete (cracked) breakout strength of a single anchor in tension.
(6)	ACI 318-14 (17.4.2.2b)	$N_b = 16\, \lambda_a \sqrt{f_c'}\, h_{ef}^{5/3}$	Cast-in headed studs and headed bolts with 11 in. ≤ *hef* ≤ 25 in.,
(7)	ACI 318-14 (17.4.3.1 and 17.4.3.4)	$N_{pn} = \Psi_{c,P}\, N_p$, and $N_p = 8\, A_{brg}\, f_c'$	Pullout strength of headed anchors
(8)	UT, FHWA/ TX-04/1855-3	$f_{s,head} = 2\, n_{5\%} \sqrt{\frac{A_{nh}}{A_b}} \left(\frac{c_1}{\sqrt{d_b}}\right) \Psi f_c'$ $\Psi = 0.6 + 0.4 \frac{c_2}{c_1}$	Bearing strength of headed anchors.
(9)	DeVries, Ph.D. thesis, TX, 1996	$P_u = \Psi \frac{A_{b0}}{A_{bon}} \left(\frac{c_1 \sqrt{A_n f_c'}}{80}\right)$ $\Psi = 0.7 + 0.3 \frac{c_2}{c_1}$	Pullout strength of headed anchors

DeVries (1996) tested over 140 concrete blocks with headed reinforcement bars as part of an extensive study conducted by the University of Texas at Austin. The study was based on assuming a value for the embedment depth to clear cover ratio of five for the shallow embedded tests and more for the deep tests. The bearing strength and pullout capacity of a single headed anchor were developed as shown in Eqs. (8) and (9). In the second phase of this project, Bashandy (1996) performed 14 pullout tests. The purpose was to study the applicability of using plate-anchored bars as shear reinforcement under cyclic loading. It was found that the anchorage was not significantly affected in the first 15 cycles with a stress level of 5% to 80%.

Delhomme et al. (2015) performed pullout tension tests on cast in place concrete blocks with (1) a plate (10 x 10 x 1 in) welded to four ribbed bars or (2) headed studs. The study considered different bar sizes and embedment depths. It was found that headed anchors provide better ductility than bonded bars. It was also found that Eurocode 2 tends to underestimate the mean ultimate strength of the concrete breakout cone.

The damage process in engineered cementitious composites reinforced with fibers around headed anchors subjected to tensile load was examined using experimental testing and finite element analysis (Qian and Li (2011)). The study considered small headed-anchors with 8 mm diameter, 5 mm thick head, 15 mm diameter head, and 30 mm embedment depth. It was found using experimental testing that the ductility preset in the concrete mix due to fibers caused a chance in the mode of failure of the pullout headed anchors from brittle to ductile.

3. DESIGN PRINCIPLES OF TOTALLY PRECAST CONCRETE COUNTERFORT RETAINING WALL SYSTEM COMPARED TO EXISTING CAST-IN-PLACE STRUCTURES

3.1. Introduction

Substructure systems, specifically retaining walls and abutments, constitute a major facet of the bridge construction process. Currently, a majority of the substructure construction work is carried out using cast-in-place concrete. However, cast-in-place construction can be associated with several difficulties and drawbacks, such as prolonged site preparation procedures, mitigated work zone safety due to exposure of workers to active traffic, traffic congestion, the requirement for skilled workmanship, and environmental costs (Heiber et al., 2005). As a result, the need for shorter construction periods is shifting the interest towards Accelerated Bridge Construction (ABC) methods, such as incorporating precast concrete products in construction. The implementation of precast concrete products in construction provides several economic, safety and environmental advantages (Kim 2013, Billington et al., 2001). Precast concrete products are cast using high performance concrete under high level of quality control, which enhances the consistency and uniformity of the materials during mass production and therefore improves the durability of the final product (Olvia et al., 2011).

This chapter develops the design principles of the proposed system. It also presents a comparison between this system and an existing typical cast-in-place counterfort retaining wall system in Chicago, IL. The chapter highlights the main details, parameters, and assumptions taken in both systems. The advantages of using the proposed precast concrete system and its suitability for widespread adoption in the specified site are examined from the economical point of view. Finally, a parametric study was performed considering different design parameters such as various wall heights (H), counterfort extension-to-heel length ratio (R_{ch}), and anchor bar size in order to facilitate the design process for precast producers.

3.2. Existing Cast-in-place counterfort retaining wall

The existing structure chosen for this study is a cast-in-place counterfort retaining wall located Chicago, IL. The wall is 6.55 m (21 ft – 6 in.) high measured from the bottom of the base to the top of the wall. The total width of the base slab is 4.87 m (16 ft). The typical details for geometry and reinforcement are represented in Figure 3-1. The existing counterforts are 45.7 cm (1ft – 6in.) thick and regularly spaced every 3.35 m (11 ft).

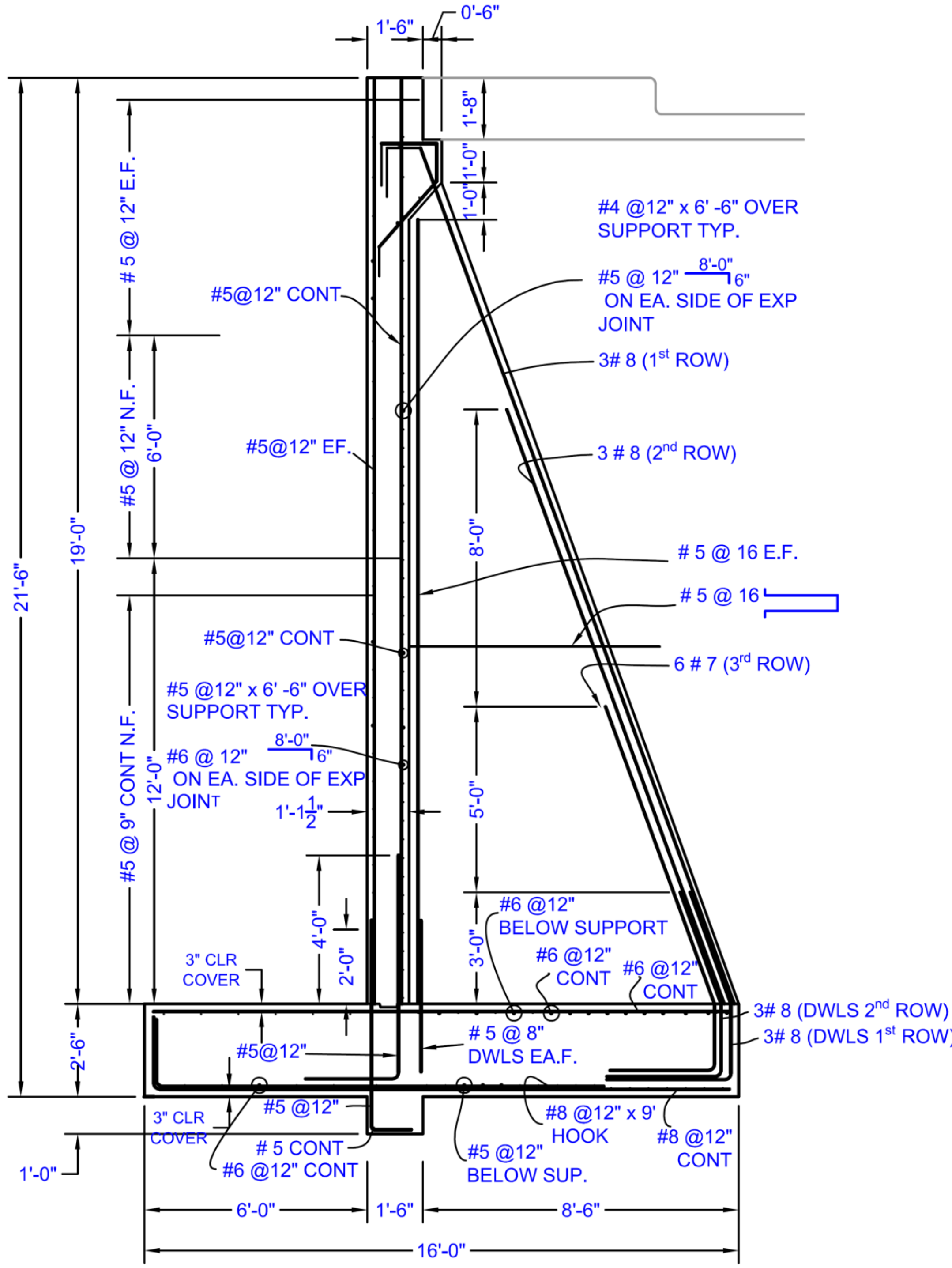

Figure 3-1. The typical details for geometry and reinforcement (1 in. = 25.4 mm)

The counterfort spacing-to-base length ratio can be calculated by dividing the spacing between the counterforts by the total length of the base slab. The typical counterfort spacing-to-base length ratio for the existing structure is 0.84. For a typical base length of 3.96 m (13 ft), the counterfort-spacing-to-base length ratio will increase if the spacing between the counterforts increases and vice-versa. The ratio can be optimized to yield a more efficient design as will be shown in later sections. A high counterfort spacing-to-base length ratio indicates that each counterfort is designed to resist a significant amount of load from soil pressure and surcharge loads distributed over 3.35 m (11 ft) tributary area per counterfort. This affects the existing typical design in 3 major aspects:

The counterforts require a large cross section and additional steel reinforcement. The counterforts, which act as T-beam, will also be extended to a longer distance to increase web depth and therefore increase the moment arm to resist applied load. In most cases, the counterfort will be extended to the end of the base slab as shown in Figure 3-1.

The face-panel is designed as one-way slab spanning between the counterforts which act as supports. The increased spacing between the counterforts requires additional thickness and steel reinforcement to resist the applied positive and negative moments at midspan between the counterforts and over the counterforts, respectively. Furthermore, some additional thickness may be required to control the shear demand in the section at the supports (counterforts).

The base slab requires similar attention to that of the face-panel. The base slab is assumed to act as one-way slab spanning between the counterforts which act as supports.

3.3. Proposed Totally Precast Counterfort Retaining Wall System

The proposed substructure system is composed of two structural components: 1) the wall component which encompasses the face panel and the counterforts, and 2) the base slab as shown in Figure 3-2. The system is cast off-site, transported to the construction site, and erected in the least possible time.

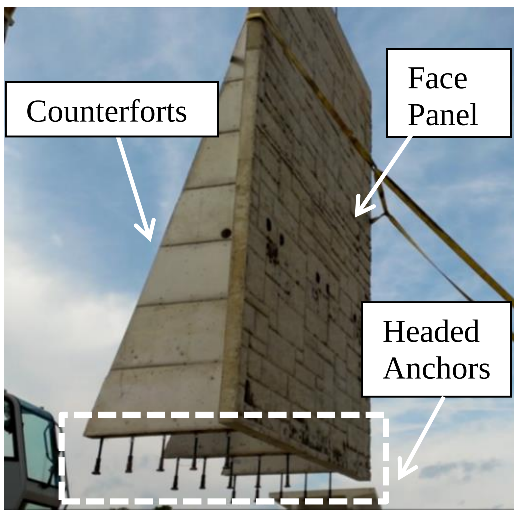

(a) Wall component of the proposed system

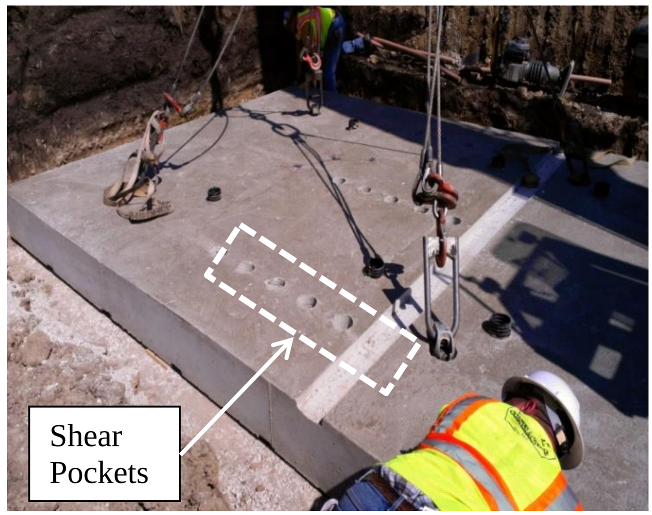

(b) Base component of the proposed system

Figure 3-2. Wall Component Structural component of the proposed system

The wall component is connected to the base slab using headed anchors. The headed anchors play the most important role in maintaining full composite action between the structural components. Moreover, the anchors are designed to resist the overturning moments and shear forces applied on the system. The counterforts are connected to the face panel through extended L-shape bars, which enforces the full composite action between them. As a result, counterforts were designed and analyzed as T-beams with the face panel as flange and the counterfort as web. Figure 3-3 represents typical details for the new features introduced in the totally precast counterfort retaining wall, which distinguish it from the conventional cast in place counterfort retaining wall.

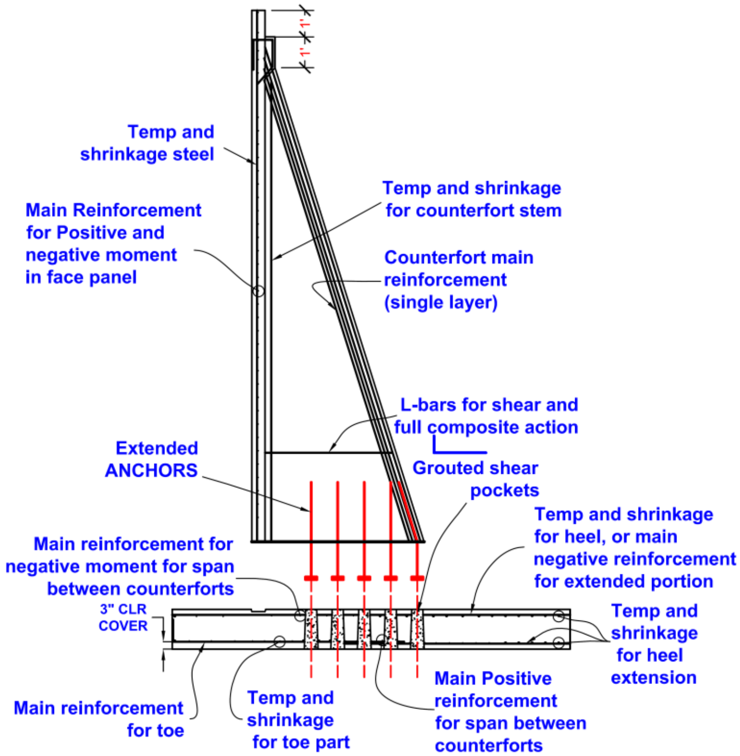

(a) Components of proposed wall

(b) Tapered cylinder with de-bonding layer

(c) Two types of available headed anchors

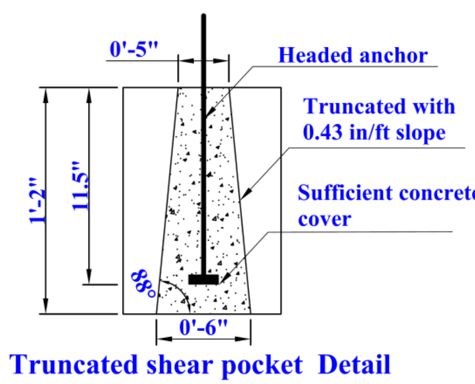

(d) details for truncated shear pocket

Figure 3-3. Anchor details for typical construction of the proposed wall (1 in. =25.4 mm)

The tapered concrete cylinder shown in Figure 3-3 is used to create the truncated shear pockets in the base slab in which the extended headed anchors are embedded. The cylinders are wrapped with greased layer to facilitate de-bonding and placed in the corresponding location before concrete is poured. They are then removed after the concrete sets to create the truncated shear pockets. The final assembly of the proposed system is shown in Figure 3-4.

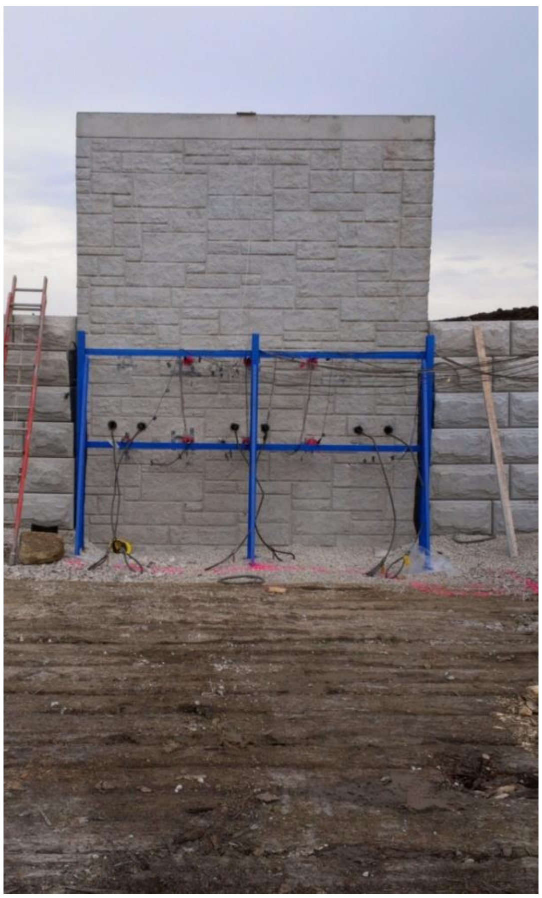

(a) Front Elevation of assembled wall

(b) Rear elevation of assembled wall

Figure 3-4. Final assembly of the proposed system

3.4. Main concepts used for designing TPCCRW

Strengthening a retaining wall with counterforts changes the structural behavior of the retaining wall. In conventional cantilever retaining wall systems, the face panel is the load resisting component. However, when counterforts are added to the cantilever wall, the counterforts become the main load resisting component with the face panel simply acting as a continuous one way slab spanning over the counterforts. This allows the cross section of the wall to be reduced significantly while satisfying the strength and serviceability requirements of AASHTO LRFD code. The critical locations in the counterfort retaining wall system to which the special attention must be given are highlighted as follows:

1. Counterfort and anchors: Bottom section of the counterfort at which the bending moment and shear forces are maximum for cantilever type retaining walls.
2. Face-panel design: For a transverse strip taken at the bottom of the face panel, the midspan between the counterforts for positive moment, and over the counterforts for negative moment.
3. Base slab design: For a transverse strip taken at the base slab, the midspan between the counterforts for positive moment and over the counterforts for negative moment.

   The critical locations and load application for the design is presented in Figure 3-5.

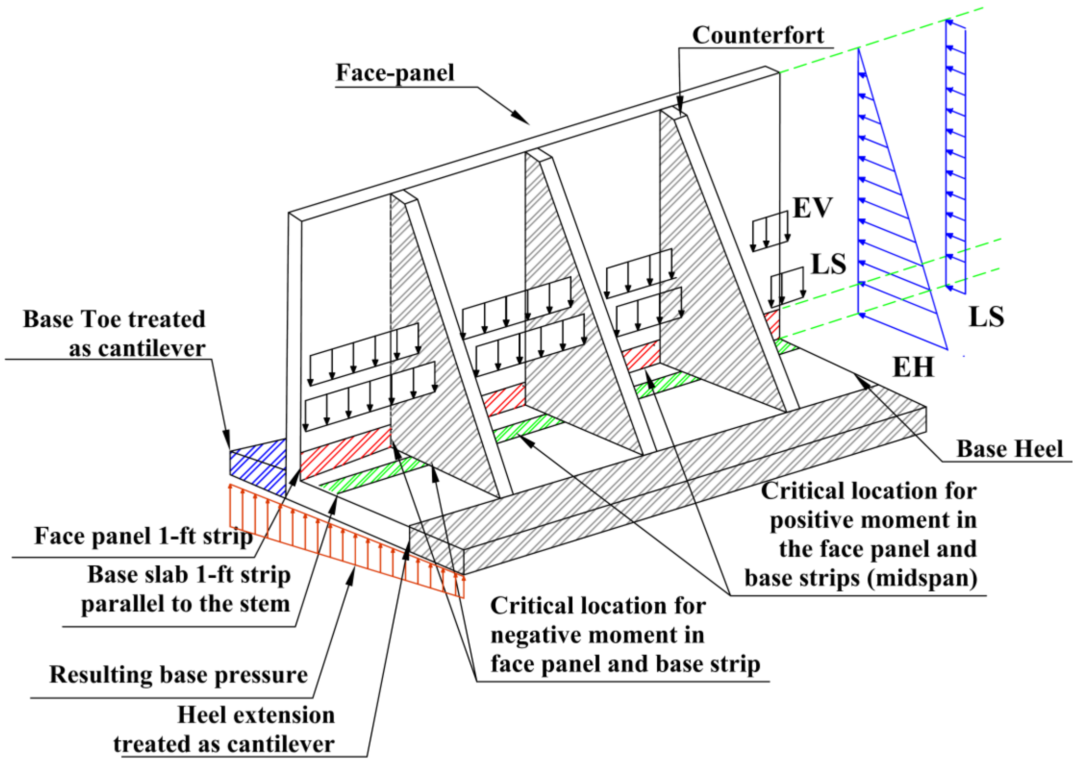

Figure 3-5. Critical locations and load application for designing counterfort retaining wall

The load calculations are divided into vertical and lateral loads applied on the retaining wall as per AASHTO LRFD specifications section 3.3.2.

1. DC: Self-weight of each component
2. EV: Vertical earth pressure
3. EH: Horizontal earth pressure
4. LS: Horizontal and vertical surcharge load

Per IDOT BM 3.8.8, a live load surcharge (LS) of 61 cm (2 ft.) soil should be added to the earth pressure to account for live load. Two cases are considered for placing live load surcharge as per AASHTO LRFD (Fig. C11.5.6.3). In case 1, live load surcharge is placed behind the base slab heel. This configuration helps maximize the lateral overturning forces applied on the retaining wall without simultaneously increasing the stabilizing vertical forces. It is used for checking the stability of the system against overturning and sliding. In case 2, the live load surcharge is extended over the base slab heel. The configuration in case 2 maximizes both lateral and vertical forces. It is used to study the bearing capacity and eccentricity limits of the system.

3.5. Design Assumptions to be considered for TPCCRW

1) **Geometry:** Two main geometric parameters highly contribute to the structural behavior of TPCCRW: (1) the counterfort spacing-to-base length ratio and (2) the length of the counterfort extension along the heel.

   Counterfort spacing-to-base length ratio controls the tributary load area assigned to each counterfort. When the ratio is reduced, the load applied to each counterfort is reduced and therefore the required thickness of the counterforts is reduced. Moreover, when the counterfort spacing-to-base length ratio is reduced, the tributary load area applied to the continuous spans face-panel and base slab is reduced. Therefore, this ratio has a major influence on the structural design of the face-panel and base slab in the longitudinal direction.

   In addition, the bottom depth of the counterfort measured along the interface with the base slab is an important factor that controls the design of the counterfort. The increase in the counterfort-base slab interface distance (counterfort extension) enhances the flexural moment capacity of the counterfort by enlarging the effective depth of the cross section. In the present study, a spacing-to-base length ratio of 0.35 and a counterfort extension-to-heel length ratio of 0.6 were considered.

2) **Headed anchors and main steel reinforcements in the counterforts**: The design of headed anchors and counterfort main reinforcement is based on two main assumptions:

   a) The anchors are assumed to maintain full composite action between the counterforts and the base slab. As a result, the main steel is designed to resist the entire flexural load applied on the counterfort.

   b) The headed anchors connecting counterforts to base-slab are designed to fully resist the bending moments and shear forces at the bottom of the counterforts.

3) **Face-panel**: the face-panel is assumed to act as continuous slab spanning over the counterforts which act as support to the face-panel. The optimized geometry of the face-panel allows the positive and negative bending moments within the face-panel to be equalized and significantly reduced. Therefore, the thickness of the face-panel is reduced to 152 mm (6 in.) and one layer of steel is provided that is capable of resisting both the negative and positive moments. The optimization of the cross section of the face-panel is described in the following sections.

4) **L-bars connecting the counterforts to the face panel:** L-bars are used to maintain composite action between face-panel and counterforts. They are designed to have sufficient development length inside the counterfort and the face-panel.

5) **Base slab (heel and toe):** The design of the heel in the base-slab is divided into two parts: the cantilever portion extending to the back of the counterforts and the continuous slab portion spanning between the counterforts. The heel is subjected to the soil pressure acting below the footing slab and the vertical weight of the soils and surcharge acting above the footing slab. The toe part is treated as a cantilever beam subjected to upward soil pressure.

3.6. Design procedure

The design procedure of the proposed system is similar to the design of a typical cast-in-place counterfort retaining wall for the typical components. However, it is different for the components where the headed anchors are introduced. It is reasonable to highlight the main aspects of the design procedure for TPCCRW. The design procedure can be summarized as follows:

1) Calculate all the applicable loads in compliance with AASHTO LRFD specifications.
2) Determine the loads acting per each counterfort.
3) Perform the necessary stability checks to ensure that the system meets all the required safety factors for stability. The system is checked against overturning, sliding, failure due to loss of contact (eccentricity), and bearing pressure.
4) Assume the counterforts to be acting as T-section with the face panel as flange and the counterfort as web. In this case, the counterforts are assumed to be in full composite action with the base slab. Design for the required moment capacity and provide steel reinforcement which meets the minimum reinforcement requirements. Check for crack control requirements and provide temperature and shrinkage steel.
5) For the same loads taken at the bottom of the counterfort, the headed anchors are designed to resist all the applied flexural and shear loads. The design of the anchors should also meet the specifications for minimum reinforcement. Moreover, the resistance of the shear pockets against pullout failure should be examined as per the requirements of ACI 318-11 code[16] to prevent premature failure in the shear pockets before yielding of the anchors.

Finally, the development length of the headed anchor should be studied and provided based on the selected bar size.

6) Consider 30.5 cm (1 ft) strip for the face panel assuming that the face-panel acts as one-way slab spanning over the counterforts (which act as support). Design the necessary reinforcement for the positive moment at midspan and similarly for the negative over the counterforts. The main reinforcement is the longitudinal reinforcement. Provide temperature and shrinkage reinforcement as vertical steel bars.
7) For the base slab, consider 30.5 cm (1 ft) strip between the counterforts, assuming the slab to act as one way slab between the counterforts. The bearing pressure should be calculated along with the moment due to the vertical loads (vertical soil pressure and vertical surcharge load) acting behind the face-panel. The strip is designed for the negative moment at the counterforts and the positive moment between counterforts. Longitudinal top and bottom steel bars are the main reinforcement for negative and positive moments, respectively. For base slabs with extended heel (i.e. counterforts do not reach the end of the base slab), the extended portion should be treated as cantilever and provided with main reinforcement as transverse top bars. The toe is designed as cantilever with trapezoidal bearing pressure acting below. The toe is provided with main steel as transverse bottom reinforcement.
8) Check for shear capacity at all the locations designed in steps 3 through 7.
9) Check for development length, pullout load, and bearing load for the headed anchors at the level of the base slab to ensure that it meets the code requirements for pull-out resistance and development length.

3.7. <u>Optimization</u>

The number and spacing of counterforts has a great influence on the structural design of the face-panel and the base slab. When the counterfort spacing-to-base length ratio is reduced, the bending moments in the face-panel are minimized and a relatively thinner concrete face-panel may be used. The choice of the counterfort spacing-to-base length ratio is simply based on the conventional beam theory. Using the conventional beam theory, the bending moment in the face-panel at midspan between counterforts is equivalent to the negative moment over each counterfort if the length of overhang is $0.41L$, where L is the spacing center to center between two adjacent counterforts. The resulting distribution of bending and shear stresses allows reducing the face-panel thickness and using only one layer of steel reinforcements. One layer of steel is capable of resisting equivalent positive and negative moments simultaneously (Farhat 2014). The spacing of the counterforts resulted from the optimization process is clarified in Figure 3-6.

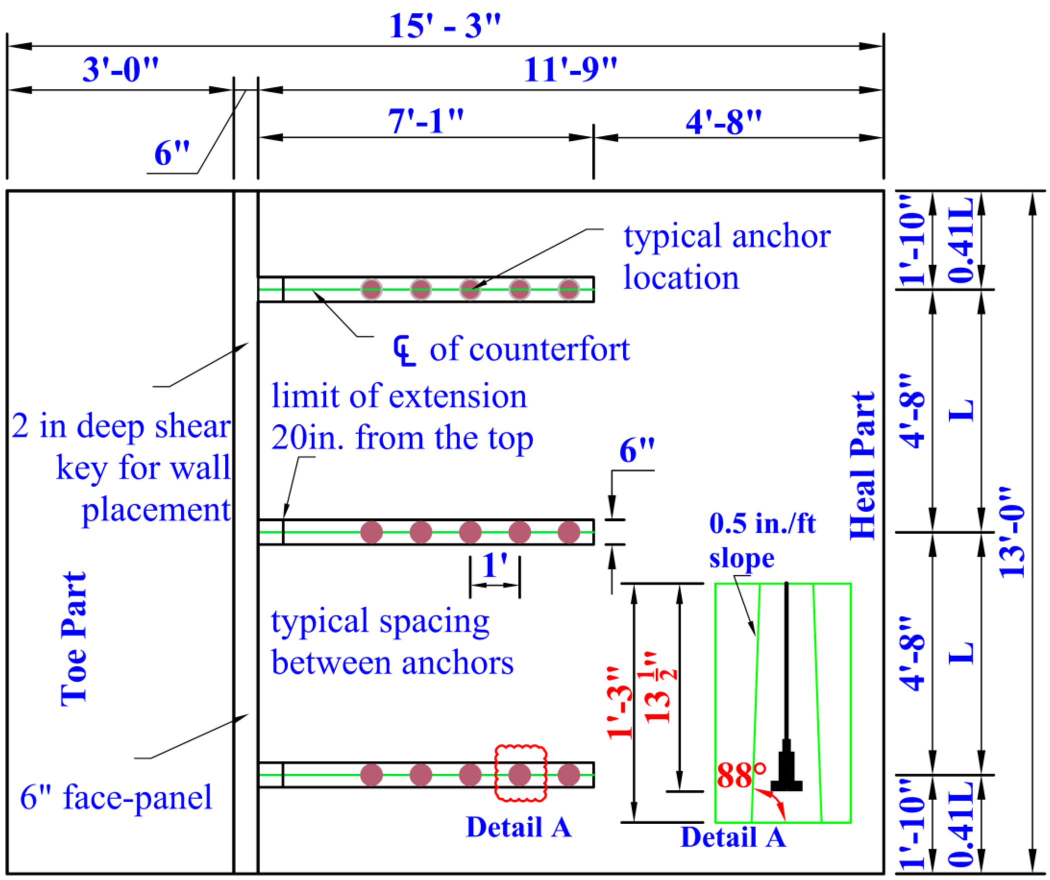

Figure 3-6 Details of the base-slab geometry after optimization (1 in. =25.4 mm)

3.8. Material properties

The material properties used in the design and analysis of the proposed system are presented in Table 3-1. The soil properties were obtained from the geotechnical report. Concrete compressive strength is determined from sample cylinders obtained from the precast concrete producer.

Table 3-1. Material properties used in the design of the proposed system

Property	Value	Description
c_l	3.81 cm (1.5 in)	Clear cover for precast components
f_y	413.6 Mpa (60 ksi)	Reinforcement yield strength

E_s	200 Gpa (29000 ksi)	Steel modulus of elasticity
f'_c	51.75 Mpa (7.5ksi)	Concrete strength
γ_c	23.56 KN/m^3 (150 pcf)	Unit weight of concrete
E_c	33.7 Gpa (4888 ksi)	Modulus of elasticity of concrete
n	6	Modular Ratio, Es/Ec = n, per AASHTO LRFD [5.7.1]
γ_s	19.63 KN/m^3 (125 pcf)	Dry earth weight
φ_s	30	Angle of internal friction
k_a	0.51	Coefficient of active earth pressure, AASHTO LRFD 3.11.5.7.1
q_{all_prov*}	478 Kpa (10 ksf)	Allowable soil bearing resistance provided by geotechnical report
q_{u_prov*}	718.2 (15 ksf)	Factored soil bearing resistance provided by geotechnical report

* Actual soil conditions in the field

3.9. <u>Design Limit States and stability requirements</u>

Service I and Strength I design limit states are used for load calculations as per AASHTO LRFD specifications Table 3.4.1-1. The load notations and factors are shown in Table 3-2.

Stability requirements are checked at the service limit state for overturning, bearing resistance, eccentricity, and sliding. At the strength limit state, stability is checked for bearing resistance, eccentricity and sliding taking into account the minimum and maximum load combinations in accordance to AASHTO LRFD 11.6.3.2, 11.6.3.3, and 11.6.3.6 respectively.

Table 3-2. Load Notations and Load Factors

Load Description	Notation	Load Factors		
		Service I	**Strength I**	
			Min.	**Max.**

Vertical Loads	Self-weight of face panel	DC1	1.0	0.9	1.25
	Self-weight of base	DC2	1.0	0.9	1.25
	Self-weight of counterfort stem	DC3	1.0	0.9	1.25
	Vertical earth pressure on the base heel	EV4	1.0	1.0	1.35
	Vertical earth pressure on the base toe	EV5	1.0	1.0	1.35
	Vertical surcharge load	LS_v	1.0	0.0	1.75
Lateral Load	Horizontal Earth pressure	P_{EH}	1.0	0.9	1.50
	Horizontal surcharge load	LS_h	1.0	0.0	1.75

The proposed system was chosen to have equivalent height as the existing type of retaining wall. The typical width of the retaining wall is limited to 3.96 m (13 ft). This dimension is generally limited by transportation restrictions. For a total wall height of 6.55 m (21 ft - 6 in.), a 4.64 m (15.25 ft) long base slab is chosen to sufficiently satisfy the stability requirements of AASHTO LRFD at service and strength limit states. The results for the stability checks are summarized in Table 3-3.

Table 3-3. Stability checks based on AASHTO LRFD 11.6.3.

Limit State	Stability check	F.O.S. Limit	Calculated F.O.S.	Check
Service I	Failure due to Overturning	2	2.31	O.K.
	Failure due to Sliding	1.5	5.58	O.K.
	Eccentricity limits (middle 2/3 of footing)	1/3 base = 152 cm (5 ft)	82.3 cm (2.7 ft)	O.K.
	Bearing Capacity Failure	478.8 kPa (10 ksf)	199.2 kPa (4.16 ksf)	O.K.
Strength I	Failure due to Sliding	1.5	3.63	O.K.
	Eccentricity limits (middle 2/3 of footing)	1/3 base = 152 cm (5 ft)	147.5 cm (4.84 ft)	O.K.
	Bearing Capacity Failure	718.2 kPa (15 ksf)	324.6 Kpa (6.78 ksf)	O.K.

3.10. Final Design for Flexure

1. **Counterfort reinforcement:** The main reinforcement in the counterfort is designed to resist the entire applied lateral load on the system AASHTO LRFD. Three rows of #22 (#7) bars and 2 rows of #19 (#6) bars were provided in the form of one layer as per the provisions AASHTO LRFD 8.16.1.2 and 5.7.3.3.2 for flexural design and minimum required reinforcement, respectively. In addition, #16 (#5) bars at 150 mm (6 in.) spacing were provided as vertical steel reinforcement in the web for temperature and shrinkage. Moreover, #4 L-shaped bars spaced at 230 mm (9 in.) were provided in the horizontal direction for two purposes; 1) shear resistance in the counterfort web, and 2) maintain full composite action between the counterfort and the face-panel.
2. **Headed anchors:** The anchors constitute the most important component as they provide the connection between the counterforts and the face-panel. Similar to the design of the counterforts, the anchors are designed to fully resist the total applied lateral load. The lateral loads applied are divided into flexural moment and shears. The provided anchors were 3#19 (#6) and 2#22 (#7) headed anchors starting from the end of the counterfort extension.
3. **Base slab:** The design of the base slab is divided into three sections: design of toe, heel between counterforts, and extended part of the heel. The toe is subjected to soil pressure generated below the base slab. The provided main reinforcement in the toe was #25 (#8) bars at 150 mm (6 in.) spacing. The section of the heel between the counterforts is treated as a continuous slab spanning between the counterforts which act as supports. It is subjected to the applied vertical load of the soil. In case of a rigid pavement, the vertical

component of the live load surcharge can be neglected. The main reinforcement of the heel between the counterforts was #19 (#6) bars at 300 mm (12 in.) spacing for positive moment (top) and #16 (#5) bars at 300 mm (12 in.) spacing for negative moment (bottom) provided in the transverse direction. The cantilever part of the heel is assumed fixed at the end of the counterfort extension. The provided top steel reinforcement was #19 (#6) bars at 300 mm (12 in.) spacing, which replaced the top reinforcement for temperature and shrinkage.

4. **Face-panel:** The face panel is designed as a continuous one-way slab spanning between the counterforts which act as supports. The optimization process using the beam theory led to equivalent positive bending moments at the midspan between the counterforts and negative bending moment over the counterforts. As a result, the thickness of the face-panel can be reduced to 150 mm (6 in.) and one layer of steel (#16 (#5) at 250 mm (10 in.)) can be used to resist both equivalent positive and negative bending moments. The vertical reinforcement in the face panel was provided as (#16 (#5) at 300 mm (12 in.)) for temperature and shrinkage reinforcement.

The layout of the base-slab and the reinforcement details of the proposed wall are presented in Figure 3-6 and Figure 3-7, respectively.

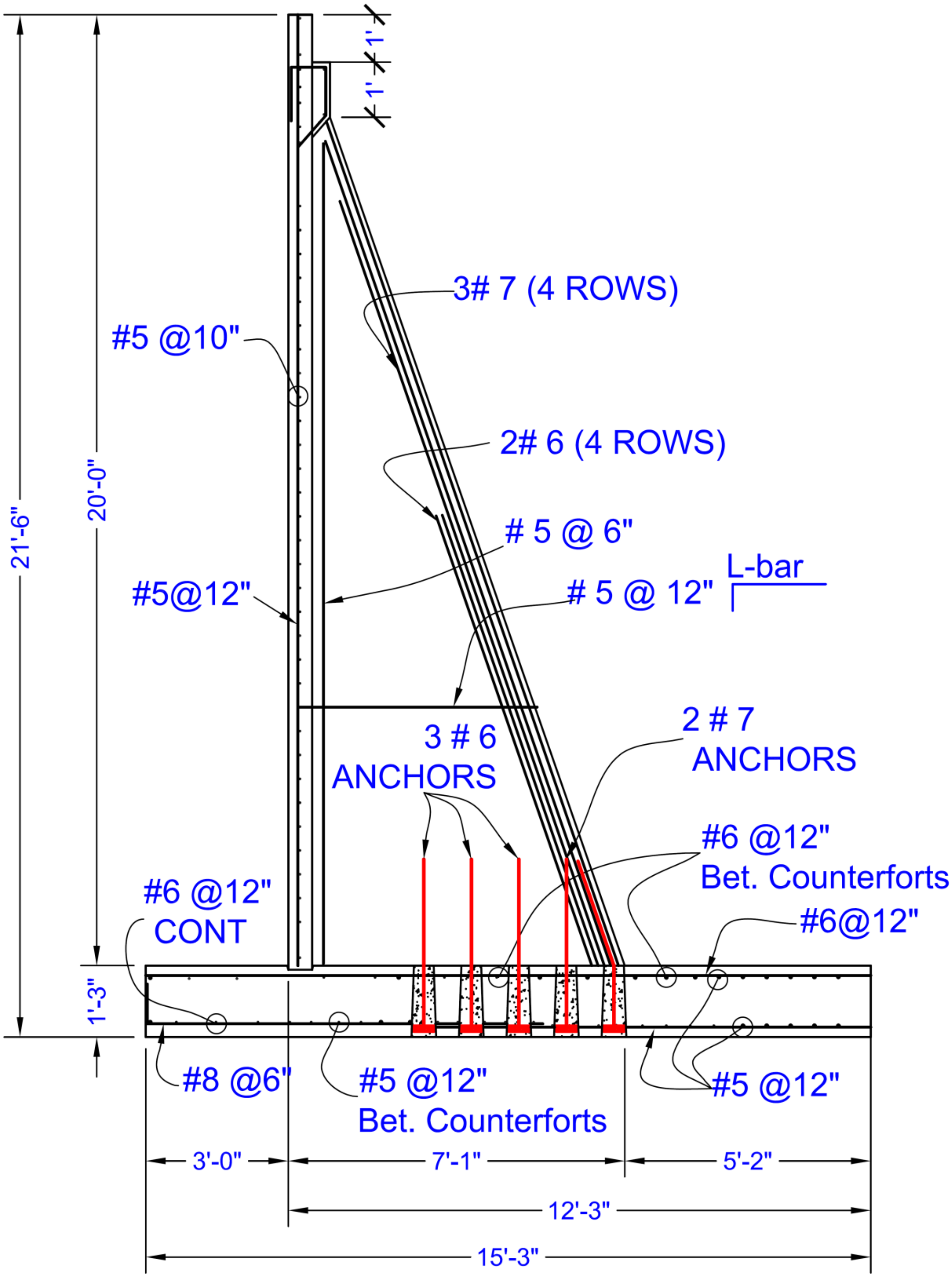

Figure 3-7. Details of the reinforcement in the proposed system (1 in. = 25.4 mm)

3.11. Check for Shear Resistance

The location of the shear critical section for “d_v” is calculated according to LRFD 5.8.2.9. The shear resistance of concrete is checked at six critical locations depending on the loading application for each component:

1. The critical section for shear at the face-panel at distance d_v from the counterfort.
2. At the level of concrete at the bottom of the counterfort.
3. At the level of anchors between the counterfort and the base-slab.
4. At the critical section for shear in the toe part of the base slab.
5. At the assumed fixity point of the cantilever section in the base heel.
6. At the critical section for shear in the base slab.

Anchors are distributed along the interface distance between the counterfort and the heel. When the loads are applied, the internal anchors will be subjected to tension. Therefore, cracks will generate in the concrete around the anchors and propagate towards the inside of the counterfort web causing shear failure as shown in Figure 3-8. In order to prevent this situation, the spacing between the temperature and shrinkage reinforcement bars (vertical steel) was reduced from 16 in. to 6 in. to create an arrest mechanism to the crack propagation.

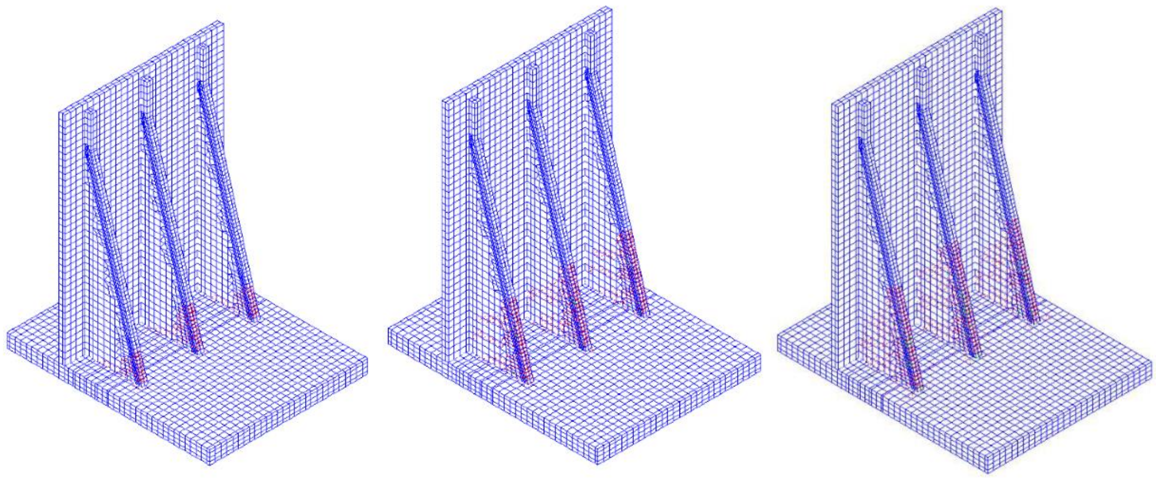

(a) 67 kip (298.03 kN) (b) 144 kip (640.54 kN) (c) 216.5 kip (963.03 kN)

Figure 3-8. Crack propagation in the counterforts and base slab with the load increase

(Taken from Farhat 2015)

3.12. <u>Development Length and Pullout Resistance of Anchors</u>

3.12.1. <u>Development length</u>

The headed anchors are responsible for maintaining full composite action between the counterforts and the base slab. The anchors are subjected to fail either by yielding of steel or by failure in the shear pocket. Therefore, it is important to check whether sufficient resistance to anchor pullout is provided along with sufficient development length to prevent failure in the shear pocket. According to the specifications of ACI 318-11 12.6.1 for development length of headed anchors, the net bearing area of the head (i.e. area of the head minus area of the bar) is required to be greater than 4 times the area of the bar. In addition, the spacing of the anchors is required to be greater than 4 times the bar diameter. The required properties needed for development length and pullout resistance calculations are summarized in Table 3-4.

Table 3-4. Required properties needed for development length and pullout resistance

Properties	Value, cm (in)	Notes
d_b	2.2 cm (0.875 in)	Bar diameter (#22 (#7))
A_b	3.87 cm^2 (0.6 in^2)	Bar Area (#22 (#7))
d_{ha}	7.1 cm (2.8 in)	Diameter of head
t_{ha}	1.6 cm (0.625 in)	Thickness of head
n_{ta}	8	Number of threads per inch
A_{ha}	39.74 cm^2 (6.16 in^2)	Area of the head
$A_{net\_bearing}$	35.9 cm^2 (5.56 in^2)	Net bearing area = A_{ha}-A_b
S_a	30.5 cm (12 in)	Spacing between anchors
$A_{net\_bearing}$ - 4A_b	20.4 cm^2 (3.16 in^2)>0 **OK**	Check if net bearing area greater than 4 times Area of the bar , ACI 318-11 12.6.1
S_a - 4 d_b = >0	21.6 cm (8.5 in) > 0 **OK**	Check if anchor spacing is greater than 4 times the bar diameter, ACI 318-11 12.6.1

$$l_{dt} = \left(\frac{0.016\, \psi_e\, f_y}{\sqrt{f'_{cdt}}}\right) d_b \qquad \text{(ACI 318-11 12.6.2)} \qquad (1)$$

Where:

l_{dt} = required development length for headed anchors inside the base slab, ACI 318-11 12.6.2

ψ_e= Modification factor for epoxy coated bars, ACI 318-11 12.6.2

f_y= Yield stress of steel equals to 413 Mpa (60,000 psi)

f'_{cdt}= Concrete compressive strength not exceeding 41.3 Mpa (6000 psi).

The required development length for the headed anchor calculated by Eq. (1) was found to be 330 mm (13 in.). The minimum required base slab thickness to ensure full development of the anchors is calculated as follows: development length + clear cover +

thickness of the head ($l_{dt} + cl + t_{ha}$) = 380 (15 in), whereas the base slab thickness used was 406 mm (16 in.).

3.12.2. Pullout resistance

The resistance to pullout is divided into two parts: 1) resistance against shear failure, and 2) resistance against bearing pressure. The properties, which are used to calculate the shear and bearing resistance of the grouted pocket, are represented in Table 3-5.

Table 3-5. Properties of the shear and bearing resistance of the grouted pocket

Properties	Value	Notes
D_{pocket_top}	12.7 cm (5 in)	Top diameter of shear pocket
D_{pocket_bot}	15.2 cm (6 in)	Bottom diameter of shear pocket
$A_{surface}$	2989.1 cm^2 (463.31 in^2)	Loaded area of contact between concrete and grout
φ_v	0.75	Reduction factor for shear ACI 318-11 9.3.2.4
$\varphi_{bearing}$	0.65	Reduction factor for bearing ACI 318-11 9.3.2.4
$Slope_{angle}$	88 deg	Angle of the truncated shear pocket sides
T_u	160.13 KN (36 kip)	Ultimate design tensile axial load in the anchor

The value for the nominal shear strength of the grouted shear pocket is calculated using Eq. (2).

$$V_n = 0.17\lambda \sqrt{f_c'}\, A_{surface} \sin\theta \qquad \text{(ACI 318-11 Eq.11-3)} \qquad (2)$$

The calculated value of nominal shear strength, V_n is 357 kN (80.25 kip) using the data presented in Table 3-5. The nominal shear resistance, f_v Vn, is 276.68 kN (60.2 kip). The ultimate pullout load which would cause yielding in the anchor is T_u = 160 kN (36 kip) as shown in Table 3-5. This indicates that the shear strength of the concrete interface with the grout is capable of resisting the shear component of the applied pullout load.

In a similar manner, the bearing strength of the grouted shear pocket can be calculated using Eq. (3). The surface are of the conical frustum was calculated from the top to the level of the provided development length of the headed anchor.

$$R_u = 0.85\, \varphi_{bearing}\, f_c'\, A_{surface} \cos\theta \qquad \text{(ACI 318-11 - 10.14.1)} \qquad (3)$$

The value of the nominal bearing load was 298 kN (67 kip) using eq. (3) which exceeded the ultimate pullout load necessary to cause yielding in the anchor. This indicates that the bearing strength of the concrete interface with the grout is capable of resisting the bearing component of the applied pullout load. The value of the bearing strength ensures yielding in the steel anchor before crushing in the concrete inside the shear pocket.

3.13. Comparison between proposed totally precast counterfort retaining wall system and cast in place system

The proposed system was optimized to have geometric efficiency that can be reflected in the form of reduction in the weight, sizes, and concrete volume of all the wall components compared to the existing wall. A comparison of the general properties of the existing wall and the proposed wall is presented in Table 3-6.

Analysis of Table 3-6 shows a significant reduction in the concrete volume in the proposed system reaching 57% compared to the volume of concrete in the existing system. Table 3-6 also shows a significant reduction in the weight of the structure in the proposed system, reaching 53% of the total weight. The large weight reduction provides an important advantage in transportation and handling purposes.

Table 3-6. Comparison of the general properties of the existing wall and the proposed wall

	Properties	Existing structure	Proposed wall	% reduction in proposed wall
Weight of component	Weight of base slab, kN (kip)	347.1 (78)	165.5 (37.2)	52
	Weight of wall component, kN (kip)	344.8 (35.46)	157.7 (35.46)	54
	Total weight, kN (kip)	691.9 (72.63)	323.2 (72.63)	53
Geometry	Thickness of base slab, cm (in)	76.2 (30)	38.1 (15)	50
	Thickness of face-panel, cm (in)	34.29 (13.5)	15.24 (5)	56
	Thickness of counterforts, cm (in)	45.72 (18)	15.24 (6)	67
	Number of counterforts	2	3	-50
Concrete volume for components	Volume of Face-panel (ft^3)	7.87 (277.9)	3.72 (131.6)	53
	Volume of base slab (ft^3)	14.72 (520)	7.01 (247.8)	52
	Volume of all counterforts (ft^3)	6.96 (245.9)	2.96 (104.8)	57

The existing retaining wall was designed in 1968 using AASHTO standard specifications. In order to provide a reasonable comparison between the existing structure and the proposed system, the design of the existing was re-evaluated using AASHTO LRFD design specification. Table 3-7 shows a comparison between the existing retaining wall using AASHTO standard specifications and AASHTO LRFD 2012, and the proposed precast wall using AASHTO LRFD 2012 for a typical base width of 3.96 m (13 ft). The comparison focuses on bending moment and shear forces at the critical location in every wall component. The ratio of the design moment to the applied factored moment (M_r/M_u) is used. This ratio provides an indication of the safety factor present in the section and therefore the effectiveness of the section. Similarly, the ratio of the design shear capacity to the applied factored shear

(V_r/V_u) is considered at the critical location for shear. For locations where the loading is on the same face undergoing tension, the critical location for shear is assumed to be at the face of the section. For locations where the loading is on the same face undergoing compression, the critical section for shear (location d_v) is calculated per AASHTO LRFD 5.8.2.9.

Table 3-7. Comparison between the existing retaining wall using both AASHTO standard specifications and AASHTO LRFD 2012, and the proposed precast wall using AASHTO LRFD 2012

Component	**Property**	**Location**	**Existing structure**		**Proposed wall**
			LFD	LRFD	LRFD
Face Panel	M_r/M_u	Midspan	1.42	1.57	7.01
	M_r/M_u	Counterfort	1.67	1.75	7.01
	V_r/V_u	Distance d_v from face	1.53	1.22	2.2
counterfort	M_r/M_u	Bottom of counterfort	2.13	1.9	1.42
	V_r/V_u	Bottom of counterfort	2.23	1.81	1.7
Toe	M_r/M_u	Face of stem	1.7	1.11	1.25
	V_r/V_u	Distance d_v from face	1.71	1.26	1.47
Heel (continuous strip)	M_r/M_u	Midspan	1.97	1.9	2.19
	M_r/M_u	Counterfort	2.77	2.3	3.07
	V_r/V_u	Distance d_v from face	2.17	1.84	3.21
Heel (Cantilever strip)	M_r/M_u	End of counterfort	N.A.	N.A.	3.07
	V_r/V_u	End of counterfort	N.A.	N.A.	3.84
Anchors	M_r/M_u	Top face of base slab	N.A.	N.A.	1.43
	V_r/V_u	Top face of base slab	N.A.	N.A.	1.053

Analysis of Table 3-7 shows that the LRFD design of the existing retaining wall exhibits lowers values for the moment and shear ratios compared to the standard specifications design. However, the comparison between the proposed wall and the existing wall using LRFD specifications shows that the proposed wall generally exhibits higher moment and shear ratios. This reflects the efficiency in the design of the proposed system. The moment and shear ratios at the bottom of the counterfort and the anchors show a lower value compared to the same location in the existing wall. This is because the fact that the design was based on choosing the optimum extension for the counterfort from the rear side of the face-panel along the length of the heel. This was done to control and minimize the weight of the wall component. The values of the moments and shear ratios at the bottom of the counterfort can be simply raised by increasing the extension distance that increases the moment arm and therefore increases the moment and shear capacities.

3.14. Parametric study

A parametric study was conducted to evaluate the structural performance of the proposed system for a variety of configurations. It was used to provide a basis to compare the effect of increasing wall height on anchor selection, counterfort reinforcement, base slab thickness, and total weight of the wall components. When the wall height increases, the flexural moment and shear force increase. Therefore, additional strength was required to meet the code requirements. This can be attained by either increasing the length of the extension of the counterfort or by increasing the amount of steel reinforcement within the allowable strain limits. From the development length calculations presented earlier, the minimum thickness of the base slab is controlled by the development length to be provided for the headed anchors. The minimum base thickness is calculated as the required development length that varies according to the anchor diameter plus the thickness of the head and the clear cover. Table 8 presents the required minimum base thickness for increasing anchor bar diameter and the corresponding weight assuming a typical 3.96 m (13 ft) wide slab. The required development length increases with bar size causing the thickness of the base slab to increase as shown in

Table 3-8. The increasing base thickness imposes difficulties and restrictions for transportation and handling. As a result, the parametric study was performed to optimize the design so that minimum base and wall weights were obtained.

Table 3-8. Required minimum base thickness for increasing anchor bar diameter

Anchor bar	**Anchor diameter**	**Head Thickness**	**Development length**	**Min. Base Thickness**	**Weight of slab per longitudinal length**
No	mm (in)	cm (in)	cm (in)	cm (in)	kN/m (kip/ft)
#16 (#5)	16 (0.625)	1.27 (0.5)	23.6 (9.3)	30.48 (12)	29.18 (2.0)
#19 (#6)	19 (0.75)	1.4 (0.56)	27.94 (11)	33.02 (13)	30.64 (2.1)
#22 (#7)	22 (0.875)	1.6 (0.625)	32.7 (12.9)	38.1 (15)	35.02 (2.4)
#25 (#8)	25 (1.0)	1.6 (0.625)	37.8 (14.9)	43.18 (17)	40.86 (2.8)
#29 (#5)	29 (1.128)	1.7 (0.68)	42.6 (16.8)	48.26 (19)	45.24 (3.1)

Generally, the length of the base slab increases when the height of the wall increases in order to maintain the stability requirements assuming constant soil properties. To account for this change, the ratio of the counterfort extension-to-heel length ratio (R_{ch}) is introduced in the parametric study. The same soil conditions introduced in the design were used in the parametric study. The results of the parametric study are presented in Table 3-9.

Table 3-9. Results of the parametric study showing all the included variables

H	**L_b**	**R_{ch}**	**ρ_c**	**Anchors reinf.**	**ρ_a**	**t_b**	**w_w**	**w_b**	**Anchors**	**Cfrt**	**Cfrt**
									M_r/M_u	M_r/M_u	V_r/V_u
m (ft)	m (ft)	--	%	No	%	cm (in)	kN (kip)	kN (kip)	--	--	--
4.87 (16)	3.65 (12)	0.5	0.4	4#19	0.82	33.02 (13)	95.63 (21.5)	112.98 (25.4)	1.3	1	1.35
		0.6	0.34	2#19 + 2#16	0.52	33.02 (13)	101.42 (22.8)	112.98 (25.4)	1.5	1.2	1.15

		0.7	0.37	1#19 + 3#16	0.4	33.02 (13)	107.64 (24.2)	104.09 (23.4)	1.7	1.7	1.05
		0.8	0.42	1#19 + 3#16	0.34	33.02 (13)	112.98 (25.4))	104.09 (23.4)	2	2	1.05
5.18 (17)	3.96 (13)	0.5	0.46	5#19	1.03	33.02 (13)	106.31 (23.9)	122.32 (27.5)	1.4	1.2	1.48
		0.6	0.39	1#19 + 4#16	0.57	33.02 (13)	112.98 (25.4)	122.32 (27.5)	1.5	1.4	1.13
		0.7	0.4	5#16	0.44	30.48 (12)	119.65 (26.9)	112.98 (25.4)	1.6	1.8	1.04
		0.8	0.44	5#16	0.37	30.48 (12)	126.77 (28.5)	112.98 (25.4)	1.9	2.4	1.04
5.48 (18)	4.11 (13.5)	0.5	0.47	1#22 +4#19	0.98	38.1 (15)	113.87 (25.6)	146.34 (32.9)	1.4	1.1	1.44
		0.6	0.4	2#19 +3#16	0.57	33.02 (13)	122.32 (27.5)	126.77 (28.5)	1.4	1.3	1.08
		0.7	0.44	2#19 + 3#16	0.46	33.02 (13)	129.44 (29.1)	126.77 (28.5)	1.7	1.8	1.08
		0.8	0.48	1#19 + 4#16	0.37	33.02 (13)	137.45 (30.9)	126.77 (28.5)	1.9	2.4	1.01
5.79 (19)	4.26 (14)	0.5	0.48	4#22	0.84	38.1 (15)	123.21 (27.7)	151.68 (34.1)	1.4	1.1	1.31
		0.6	0.44	2#22 +2#19	0.56	38.1 (15)	131.22 (29.5)	151.68 (34.1)	1.6	1.4	1.13
		0.7	0.48	1#22 +3#19	0.43	38.1 (15)	139.22 (31.3))	151.68 (34.1)	1.8	1.9	1.04
		0.8	0.52	1#22 +3#19	0.37	38.1 (15)	147.68 (33.2)	151.68 (34.1)	2.1	2.5	1.04
6.09 (20)	4.42 (14.5)	0.5	0.5	5#22	1.12	38.1 (15)	132.11 (29.7)	157.02 (35.3)	1.4	1	1.46
		0.6	0.45	5#19	0.63	33.02 (13)	142.78 (32.1)	136.11 (30.6)	1.3	1.3	1.05
		0.7	0.52	5#19	0.52	33.02 (13)	151.68 (34.1)	136.11 (30.6)	1.6	1.8	1.05
		0.8	0.55	5#19	0.44	33.02 (13)	161.47 (36.3)	136.11 (30.6)	2	2.4	1.05
6.4 (21)	4.57 (15)	0.5	0.58	1#25 +4#22	1.09	43.18 (17)	140.56 (31.6)	184.15 (41.4)	1.5	1.2	1.42
		0.6	0.53	1#22+4#19	0.62	38.1 (15)	151.68 (34.1)	162.80 (36.6)	1.4	1.4	1.03
		0.7	0.55	1#22+4#19	0.51	38.1 (15)	161.91 (36.4)	162.80 (36.6)	1.7	1.9	1.03

		0.8	0.59	1#22+4#19	0.43	38.1 (15)	172.14 (38.7)	162.80 (36.6)	2	2.5	1.03
6.7 (22)	4.72 (15.5)	0.5	0.59	2#25 +3#22	1.07	43.18 (17)	150.34 (33.8)	190.38 (42.8)	1.5	1.1	1.36
		0.6	0.57	5#22	0.77	38.1 (15)	162.8 (36.6)	168.14 (37.8)	1.6	1.4	1.19
		0.7	0.6	3#22 + 2#19	0.55	38.1 (15)	173.92 (39.1)	168.14 (37.8)	1.7	1.9	1.06
		0.8	0.66	3#22 + 2#19	0.47	38.1 (15)	185.04 (41.6)	168.14 (37.8)	2.1	2.6	1.06
7.01 (23)	4.87 (16)	0.5	0.64	3#25 +2#22	1.07	43.18 (17)	160.13 (36)	196.6 (44.2)	1.4	1.1	1.31
		0.6	0.61	5#22	0.73	38.1 (15)	173.92 (39.1)	173.48 (39)	1.4	1.4	1.08
		0.7	0.64	4#22+1#19	0.56	38.1 (15)	186.38 (41.9)	173.48 (39)	1.7	1.9	1.02
		0.8	0.7	4#22+1#19	0.47	38.1 (15)	198.39 (44.6)	173.48 (39)	2	2	1.02
Note: Bar Conversion (Metric to Imperial)						#16 is equivalent to #5 #19 is equivalent to #6 #22 is equivalent to #7 #25 is equivalent to #8 #29 is equivalent to #9					

The data provided in Table 3-9 is divided into three sections. The first section is the reinforcement ratio in the counterfort (ρ_c). It can be noticed that ρ_c increases with the increase of R_{ch} except for the 0.6 ratio. For R_{ch} of 0.5, the steel ratio is controlled by the moment strength value. When R_{ch} is increased to 0.6, the ratio of steel drops for all the studied cases. This is due to the increase in the moment arm of the counterfort which increases the moment capacity and this reduces the required area of steel. However, when R_{ch} is raised to 0.7 and 0.8, ρ_c shows an increasing trend. At this level, the moment arm is enormously increased and the steel ratio is controlled by the control of cracking requirement.

The second section is the reinforcement ratio of the anchors (ρ_a). The reinforcement ratio of the anchors is highest with extension to heel length ratio of 0.5. It decreases with the increase of the R_{ch}. However, for R_{ch} values of 0.7 and 0.8, the design is controlled by shear forces at the interface between the counterfort and the base slab. This can be deduced from the shear capacity to ultimate shear force values ($\varphi V_n/V_u$) shown in Table 3-9. As a result, the area of anchors provided cannot be further reduced. Additional analysis of Table 3-9 shows that an a R_{ch} value of 0.6 allows reduction of the bar size for wall heights above 20 ft. This reduction is pronounced in Figure 3-9 that represents the variation of the ratios of steel in the counterfort and anchors versus the counterfort extension-to-heel length ratio. For example, a 20 ft high wall requires 5#22 (#7) anchor bars for extension to heel length ratio of 0.5 and 5#19 (#6) anchor bars for a ratio of 0.6. This reduction permits to reduce the minimum required thickness of the base slab resulting in significant weight reduction as indicated by Table 3-8. It can be observed that the lowest steel ratio required in the counterforts at all heights is when R_{ch} is 0.6. In addition, the value of ρ_a exhibits a sharp drop when increasing the value of R_{ch} from 0.5 to 0.6. When the ratio is increased to 0.7 and 0.8, the value of ρ_a drops at a shallower slope. The ratio of steel in the anchors and counterforts can be interpolated for counterfort extension to heel ratios other than the specified. This relation can be very useful in determining the optimum geometry and steel reinforcement to obtain the lightest possible structure while satisfying all code requirements.

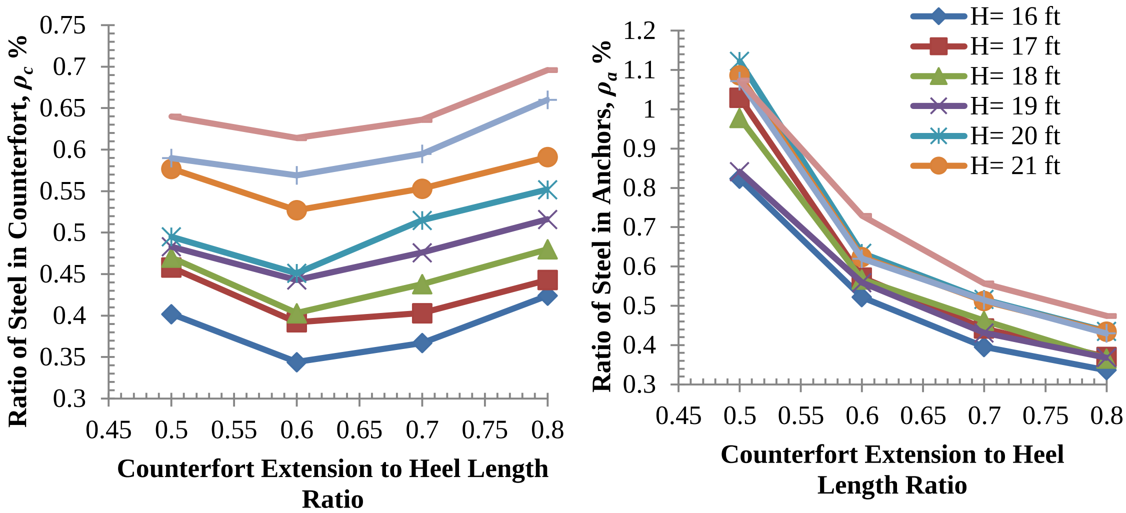

(a) ρ_c vs R_{ch} (b) ρ_a vs.R_{ch}

Figure 3-9. Variation of steel ratios in the counterfort and anchors versus the extension to heel ratio.

The third section is the weight of the components. It can be noticed that the 0.5 ratio has the lowest wall weight (w_w) and the highest base slab weight (w_b). The low extension to heel ratio helps in reducing the weight of the wall component, however it requires the use of larger anchor bars which causes the minimum base thickness to increase. With the increase in the extension to heel length ratio, the wall weight increases and the base slab weight reduces.

3.15. Conclusion

This chapter develops the design principles for TPCCRW. In addition, a comparison between the proposed system and an existing counterfort cast in place retaining wall system was established. The comparison is focused on design, structural efficiency, and performance. A parametric study was performed to assess the performance of the proposed system in increasing heights. From the study, the following conclusions can be drawn:

1. Totally precast concrete counterfort retaining wall system is an efficient solution for fast track construction. It also provides the advantage of minimal energy use, accelerated construction, the use of high strength construction materials in a consistent and accurate fabrication process, congestion reduction, and safety promotion.
2. A reduction in the counterfort spacing-to-base length ratio from 0.84 for a typical design to 0.35 causes a significant reduction in concrete volume reaching 57%. This results in cost savings in both materials and time of construction.
3. Counterfort extension to heel length ratio of 0.6 has shown to be optimum for the design of the proposed system. It results in significant reduction in the weight of the components reaching 54% compared to the existing structure. Simultaneously, it satisfies the code requirements for moment and shear strengths.
4. The tapered design of the shear pocket enhances the resistance of the anchors against pullout loads. The results show that the grout used is capable of resisting the shear and bearing forces and maintain the integrity between the wall component and the base slab.
5. The headed anchors, which extend from the counterforts to the base slab, are verified to maintain the integrity of the system by resisting the shear forces at the interface between the wall and the base components.
6. The proposed system is a cost-efficient and structurally adequate alternative that can be used in bridge and highway applications.

4. FABRICATION AND CONSTRUCTION PROCEDURES OF TOTALLY PRECAST CONCRETE COUNTERFORT RETAINING WALL SYSTEM FOR HIGHWAYS

4.1. Introduction

Advances in concrete material technology, and construction techniques accompanied with increasing traffic flow and highway demand increase the need for advanced and rapidly-constructed concrete structural components such as substructure systems for highways and bridges. Combining high performance materials with rapid fabrication methods is an advantage provided by precast concrete systems. This combination allows the precast producers to produce durable and uniform structural components in large quantities. Moreover, precast concrete construction techniques provide potential reduction in construction times, minimizes waste and labor involvement in unsafe work zones compared to conventional construction methods. Despite these advantages of the precast systems, it is essential to standardize precast construction techniques to maintain efficiency and fast track the construction process.

This work is focused on detailing the fabrication and erection processes of the Totally Precast Concrete Counterfort Retaining Wall (TPCCRW) system proposed at the University of Illinois at Chicago (Farhat et al. 2014). The proposed system consists of two precast components: the wall component which consists of a face-panel with three counterforts and the base-slab component. Both components are cast off-site and transported to the construction site for final assembly.

Counterforts are used to strengthen the face panel of the wall. It allows reducing the thickness of the face panel and increase its flexural capacity. Headed anchors are used to connect the wall components to the base slab on site. The anchors are embedded in the counterforts during the fabrication process. They extend from the bottom of the counterforts and are placed in tapered cylindrical shear pockets in the base slab which facilitates the connection on-site. The shear pockets are grouted to maintain full composite action between the counterforts and the base slab. The proposed system is shown in Figure 4-1.

This system reduces construction time, causing less traffic congestion, and requires less of specialized labor. The general guidelines for the fabrication and construction of the Totally Precast Concrete Counterfort Retaining Wall system has been standardized so as to expedite the construction.

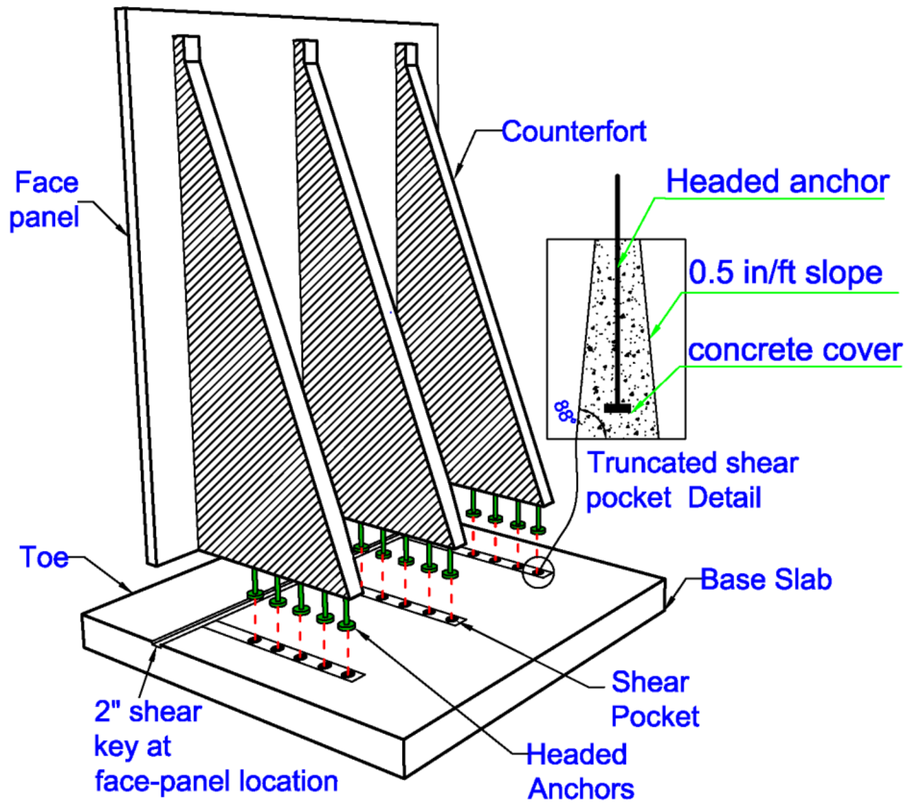

Figure 4-1 Components of the proposed Totally Precast Concrete Counterfort Retaining Wall (TPCCRW) system

4.2. <u>Fabrication process of the proposed system</u>

The fabrication process of TPCCRW is divided into two parts:

1. The fabrication of the base component which is a base slab with shear pockets.
2. The fabrication of the wall component which is comprises the face-panel and the counterforts.

4.2.1. <u>Fabrication of the base slab</u>

The base slab must be designed to satisfy the stability requirements and to resist the applied vertical loads due to soil weight and surcharge loads which generate the soil pressure below the base footing as per the requirements of AASHTO LRFD (2012) specifications. The location of each headed anchor in the counterforts and the corresponding shear pocket is identified based on the structural design. Shear pockets are created in the form of tapered cylinders with a 41.6 mm/m (0.5 in/ft) slope with a top diameter of 127 mm (5 in). The top diameter of the shear pocket is designed to ease the alignment of the headed anchor as it is lowered into the pocket, therefore facilitating the erection process. The shear pockets are generally placed at around 30.5 cm (1 ft) spacing. The fabrication processes for the base slab are shown in Figure 4-2 and Figure 4-3.

Figure 4-2 Fabrication of the base slab

Figure 4-3 Casting of the base slab

The shear pockets are created by using tapered concrete cylinders which form the desired shape and can be removed after hardening of the concrete as shown in Figure 4-4. The cylinders are wrapped with de-bonding agent to enable separation from the base slab when the concrete hardens. In addition, duct openings can be created in separate locations in the base slab to allow grouting below the slab at the construction stage to ensure uniform contact between the base slab and the supporting soil as shown in Figure 4-5. When the shear pockets are created, they must be sandblasted or water-jet blasted to remove any grease remains from the de-bonding agents. Special handles are inserted before casting to facilitate the handling and lifting processes.


(a) Base slab with cylinders used to create openings (b) Tapered cylinders

Figure 4-4. Base slab with tapered concrete cylinders used to create shear pockets


(a) Shear pockets created in the base slab (b) grouting below base slab for uniform load distribution

Figure 4-5. Grouting through duct opening to ensure uniform pressure distribution below base slab

4.2.2. Fabrication of the wall component

The fabrication of the wall component starts with the face-panel. The face panel is formed on the ground and one steel layer is placed with L-bars extending vertically upwards. The L-shaped bars serve as the transverse shear reinforcement for the counterforts. They are also used to maintain full composite action between the counterfort and the face-panel. The L-bars must be extended from the face-panel during the casting of the face-panel as shown in Figure 4-6 and Figure 4-7.

Figure 4-6. Fabrication of the face-panel with extended L-bars

Figure 4-7 Casting the face-panel

In the proposed system, the spacing between the counterforts is optimized to equalize the bending stresses in the face-panel at midspan between the counterforts and above the counterforts. This configuration provides reduction in the thickness of the face-panel to 15.25 cm (6 in.) compared to typical cast-in-place panels that can reach up to 457 mm (18 in.) and allows providing only one layer of steel in the middle of the section. The single steel layer is designed to resist both positive and negative bending stresses.

The main reinforcement of the counterforts is placed in the form of inclined steel bars along the height of the counterfort (Figure 4-8 and Figure 4-9). Temperature and shrinkage reinforcement are placed in the form of vertical steel bars inside the web of the counterfort. However, additional investigation using finite element analysis (Farhat et al. 2015) reveals that the spacing of the vertical bars based on temperature and shrinkage requirements can be insufficient. As the system is loaded, the anchors are loaded in tension and cracks tend to generate at the anchor location. With the increment of the load, the cracks tend to propagate towards the web of the counterforts. As a result, the vertical steel bars in the counterfort are used as an arrest mechanism for the crack propagation. The spacing between these bars should be reduced to 15.25 cm (6 in.). The headed anchors are placed and extended from the bottom of the counterforts before casting. An opening is made in each exterior counterfort at around two thirds of the height of the counterfort for erection and handling purposes as shown in Figure 4-8. The reinforcement in the counterforts are shown in Figure 4-9 and Figure 4-10. It can be seen that the L-bars extended from the face-panel serve as the transverse shear reinforcement for the counterforts. It can also be seen that the anchors are extended from the bottom of the counterforts.

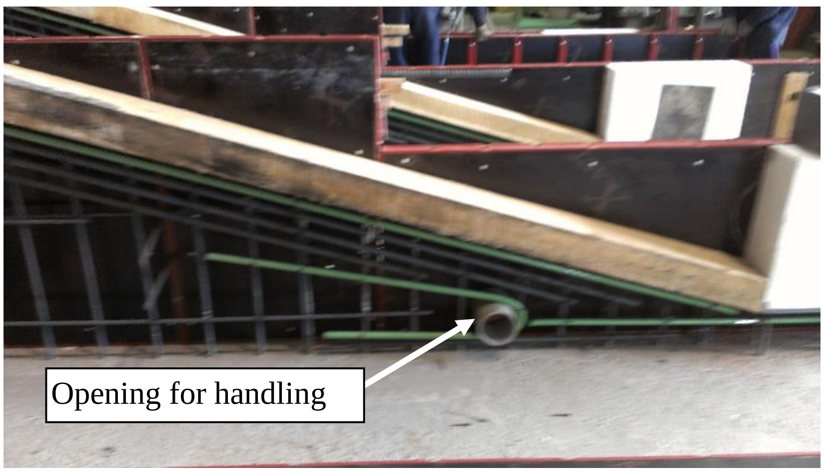

Figure 4-8. Creating an opening at two thirds the height of the wall for handling purposes

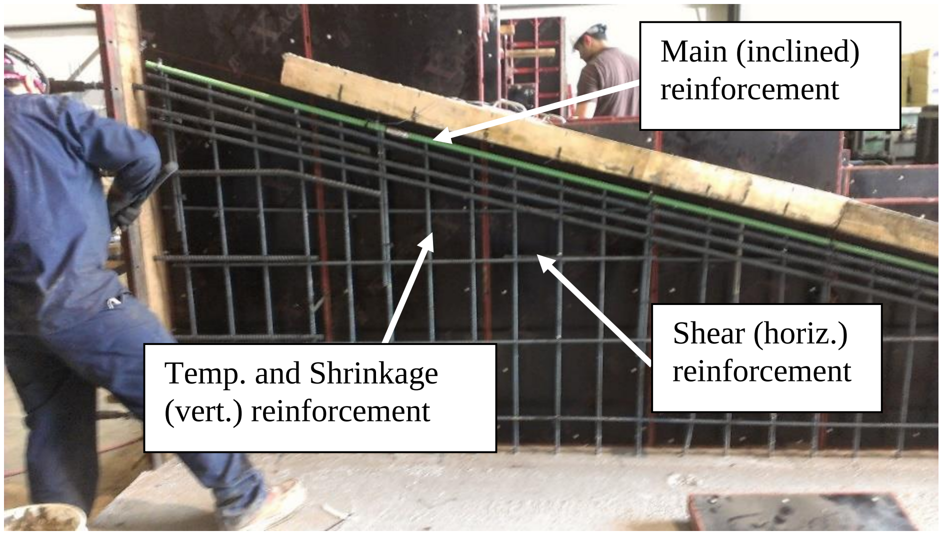

Figure 4-9. Reinforcement of the counterforts

Figure 4-10. Headed anchors extended from the bottom of the counterforts

4.3. <u>Construction Procedure</u>

The construction process is divided into four stages:

Stage 1: Site Preparation Procedures. The construction site is prepared by performing the necessary excavation and leveling procedures. The soil below the base slab is compacted and leveled so that the slab will be placed in horizontal position. Site preparation procedures are shown in Figure 4-11.

Figure 4-11. Site preparation and soil compaction below the base slab

Stage 2: Placement of the base slab. After fabrication and curing of base slab are done, the base slab is transported to the prepared construction site. The slab is lifted by a crane using steel cables at 4 points and placed at the final location. The base slab is grouted and vibrated to ensure uniform contact with the soil beneath. Foam sealants are used around the perimeter of the slab to prevent grout leakage. The grout poured beneath the base slab is used to transfer the load to the soil beneath. Any type of available grout can be used. The placement, leveling, and grouting of the base slab are shown in Figure 4-12 to Figure 4-14.

Figure 4-12. Site preparation and leveling before placing the base slab

Figure 4-13. Base slab during handling and erection

Figure 4-14. Grouting and vibrating the base slab after placement

Stage 3: Erection of the face-panel and counterforts. The wall is transported to the construction site. It is lifted with a crane using steel cables connected to steel rods inserted in openings provided on the counterforts. The steel cables are used instead of fiber straps to prevent accidental tearing of the straps when exposed to the sharp concrete edges. The wall is then positioned on the base slab such that the anchors are aligned with the shear pockets. The geometry of the wall and the presence of the counterforts allows the erection of the wall without the need for temporary bracing.

The main advantage of this erection processes of the wall and the base slab is that a smaller number of skilled labor and equipment is required compared to conventional construction methods. The erection process of the wall is illustrated in Figure 4-15.

(a) Transportation of wall face and counterforts (b) Lifting the wall component

(c) Erecting the wall component (d) Leveling the wall component over the base slab

Figure 4-15. Retaining wall transportation, erection, leveling and assembly of the proposed system

Stage 4: Grouting the shear pockets Shear pockets are grouted to maintain full composite action between the counterforts and the base-slab through the headed anchors. After the wall has been erected, 2.5 cm (1 in.) gap is kept between the base slab and the counterfort to allow the flow of the grout to the shear pockets as shown in Figure 4-16. The gap must also be grouted and sealed. Fast setting (15 minutes) high performance grout (DOT certified) should be used to fill the shear pockets. The fast setting grout provides fast initial stability and strength to the system so that the soil backfilling process can be started in a short time after erection. This process provides the advantage of fast track construction where the estimated construction time for one unit is around 2 hours. The final assembly of the retaining wall system is shown in Figure 4-17. A general sketch showing the application of the proposed system is presented in Figure 4-18.

(a) Grouting the shear pockets

(b) 2.5 cm (1 in.) gap for grout flow

(c) Grouting the gaps between the wall and the slab

(d) Soil backfilling and compaction

Figure 4-16. Grouting the shear pockets after wall erection and beginning of soil backfilling

(a) Front view of the final wall assembly (b) Rear view of the final wall assembly

Figure 4-17. Final assembly of TPCCRW

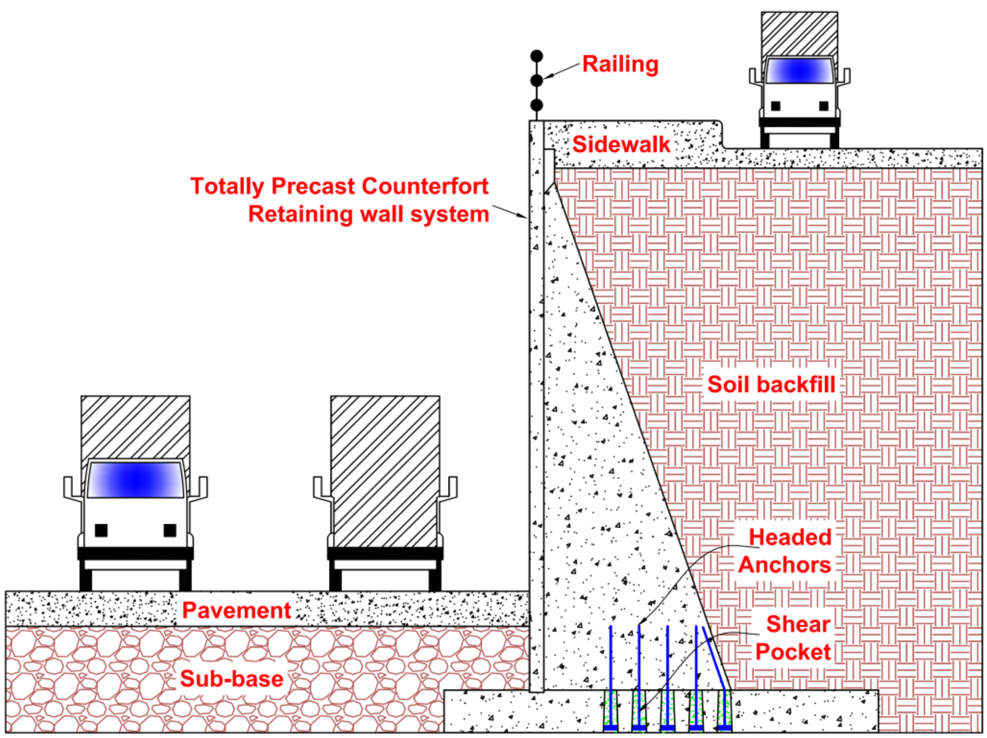

Figure 4-18. General application of TPCCRW

As the site preparation procedures are minimized, it is possible to maintain traffic flow during the construction process. The construction sequence for the proposed wall is summarized in Fig. 19.

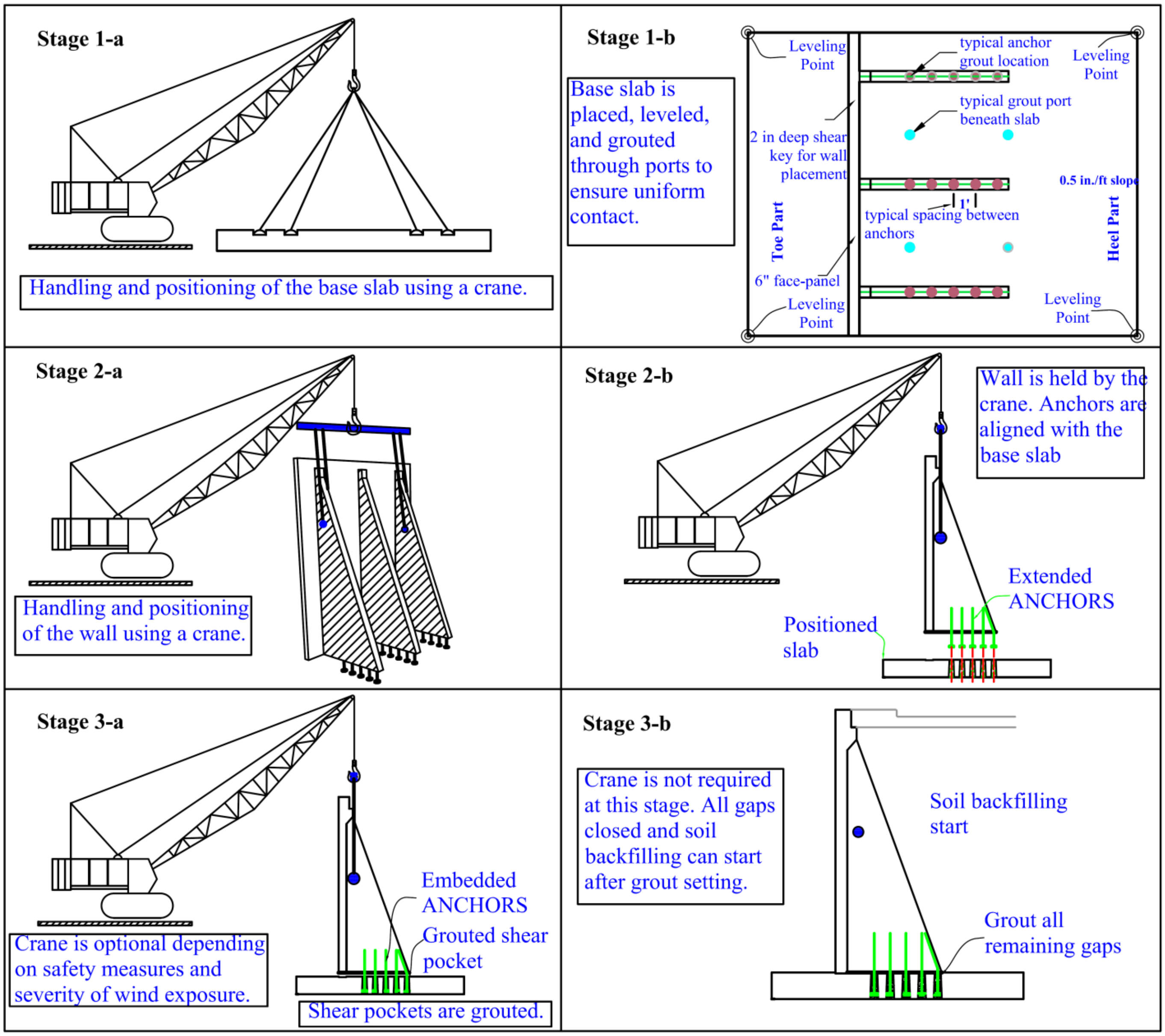

Figure 4-19. Summary of the construction sequence for TPCCRW

5. FULL SCALE EXPERIMENTAL TESTING AND FINITE ELEMENT ANALYSIS OF TOTALLY PRECAST CONCRETE COUNTERFORT RETAINING WALL SYSTEM

5.1. Introduction

The increasing traffic demand imposes further expansion on highways and bridges components such as substructure systems. The conventional construction processes performed to accommodate this expansion is generally accompanied with traffic interruptions, lane closures, and elongated construction periods which enlarges the economic expenses. As a result, several departments of transportation are seeking accelerated construction techniques to reduce the impact of the prolonged construction periods associated with conventional construction methods. The current accelerated construction techniques involve using precast concrete systems which provide several economic advantages over the conventional cast-in-place construction methods. The use of precast concrete systems for highway and bridge construction provide potential reduction in the site preparation procedures, overall construction period, and environmental impact. Moreover, it is credited to promoting work zone safety and reducing the number of injuries caused by labor exposure to active traffic.

Although precast systems provide several economic, social, and environmental advantages, plenty of research is still required to develop precast systems for substructures such as retaining walls and abutments. As a response, the structural and concrete laboratory at the University of Illinois at Chicago proposed the Totally Precast Concrete Counterfort Retaining Wall (TPCCRW) system as an innovative retaining wall solution for highway application. The proposed system was optimized and developed as a response to the growing needs of multiple requirements such as the speed of construction, strength and durability, minimization of traffic flow interruption, safety and cost.

TPCCRW consists of two precast concrete components: the wall component consisting of a face-panel with three counterforts and the base-slab component as shown in Figure 5-1 and Figure 5-2. Counterforts act as stiffeners to the face panel and connection between the wall and the base slab. Headed anchors are used to connect each counterfort to the base-slab and thus enforcing the integrity of the system to achieve full composite action.

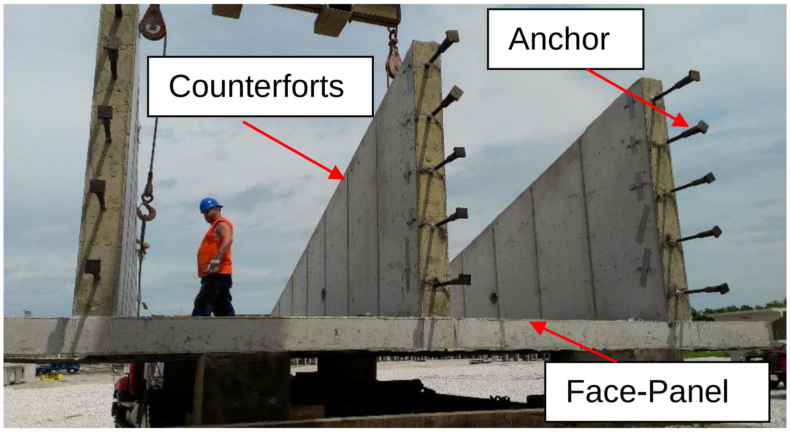

Figure 5-1. TPCCRW during erection showing anchors extended from the counterfort

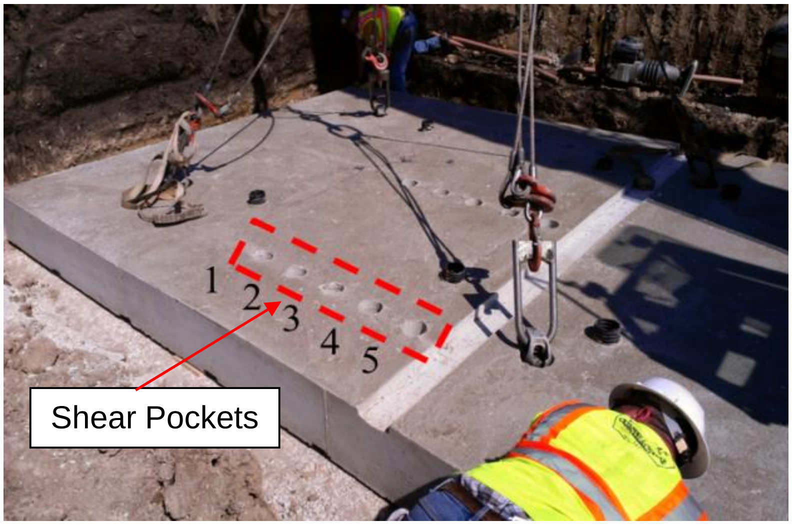

Figure 5-2. Base slab during erection showing predesigned shear pockets for anchor embedment

Counterforts are added along the length of the wall at discrete locations to enhance the serviceability of the face-panel and to increase the stiffness of the system without affording to increase the thickness of the face-panel along the entire length of the wall. In fact, counterfort retaining wall systems also exhibit lower stress states then their cantilever counterparts. Senthil et al (2014) performed a three-dimensional finite element analysis to study the structural performance of both cantilever and counterfort-type retaining walls when subjected to lateral earth pressure. The study shows that retaining walls with counterforts of 1.2 m (3.93 ft) below the top surface of the face-panel exhibit significantly lower stress level than cantilever retaining walls with the same height.

Figure 5-3 shows the front and rear elevations of the proposed system TPCCRW showing the extended counterforts.

(a) Front elevation TPCCRW with wing walls (b) rear view after erection

Figure 5-3. Front and rear elevations of TPCCRW

In this chapter, the overall structural behavior of TPCCRW was experimentally studied and analytically analyzed using Nonlinear Finite Element Analysis (NLFEA). A 20 ft - 2 in. (6.09 m) high, 13 ft – 10 in. (4.21 m) wide full scale TPCCRW prototype was designed meeting the requirements of AASHTO LRFD Specifications.

The system was manufactured in the precast concrete plant of Utility Concrete Product, LLC in Morris, Illinois. Headed anchors were embedded in each counterfort during casting at 1ft (304 mm) spacing with sufficient development length. Starting from the furthermost anchor to the rear face of the face-panel, #7 anchors were used for the first two rows and #6 anchors were used for the remaining three rows. The extended anchors were grouted to a predesigned conical-shape shear pockets in the base-slab as shown in Figure 5-2. The shear pockets in the slab were tapered from 5 in. (127 mm) diameter at the top to 6 in. (152 mm) diameter at the bottom to enhance the bond between components. The dimensions of the proposed TPCCRW are summarized in Figure 5-4 and Figure 5-5

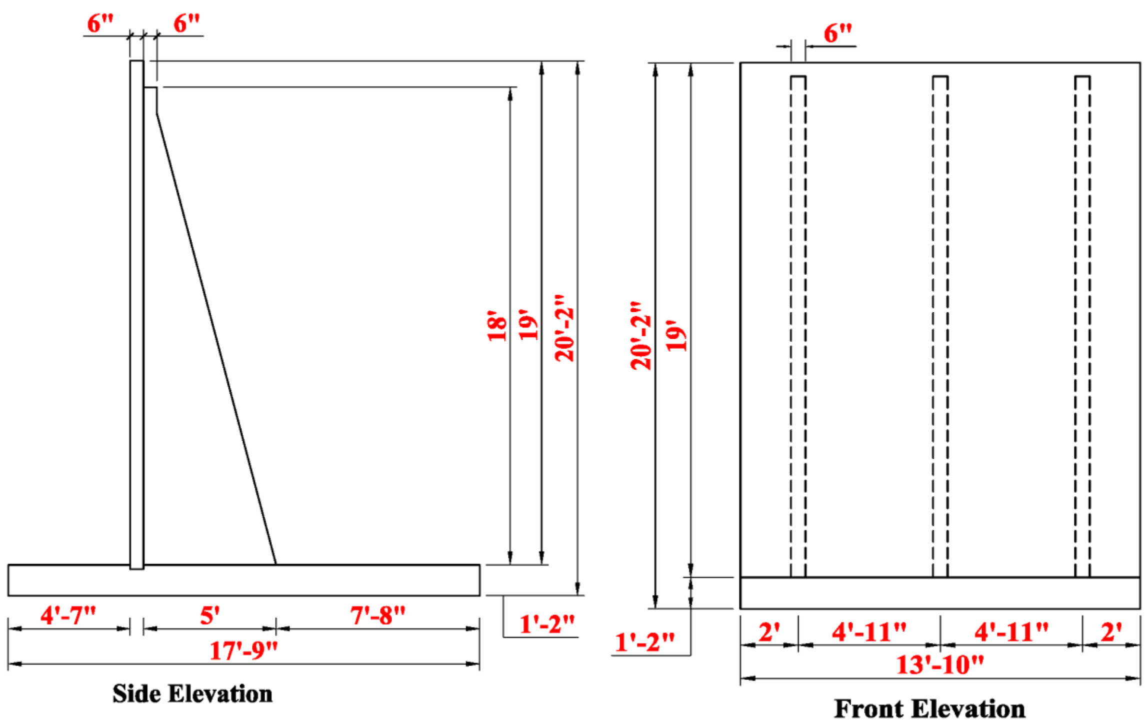

(a) TPCCRW side elevation (b) TPCCRW front elevation and dimensions

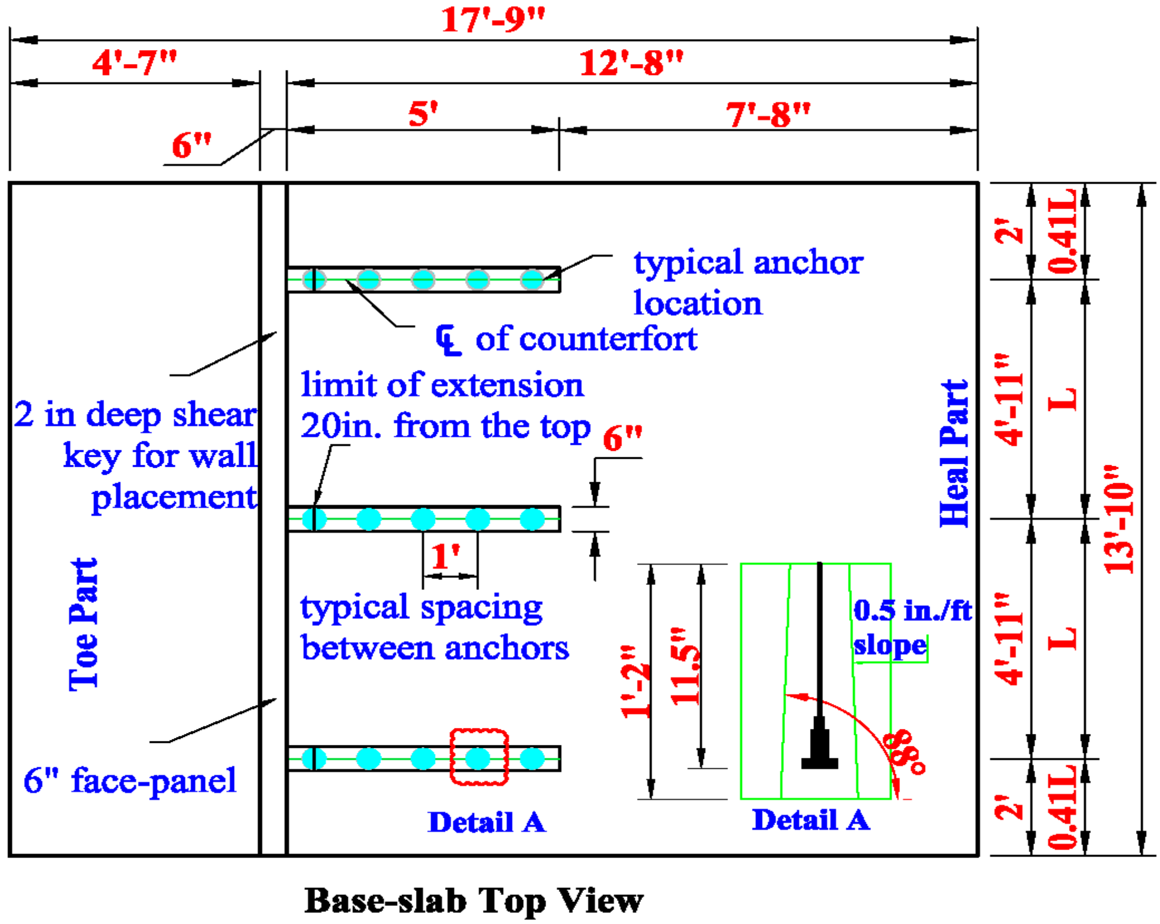

(c) base slab plan view

Figure 5-4. Geometric layouts of TPCCRW

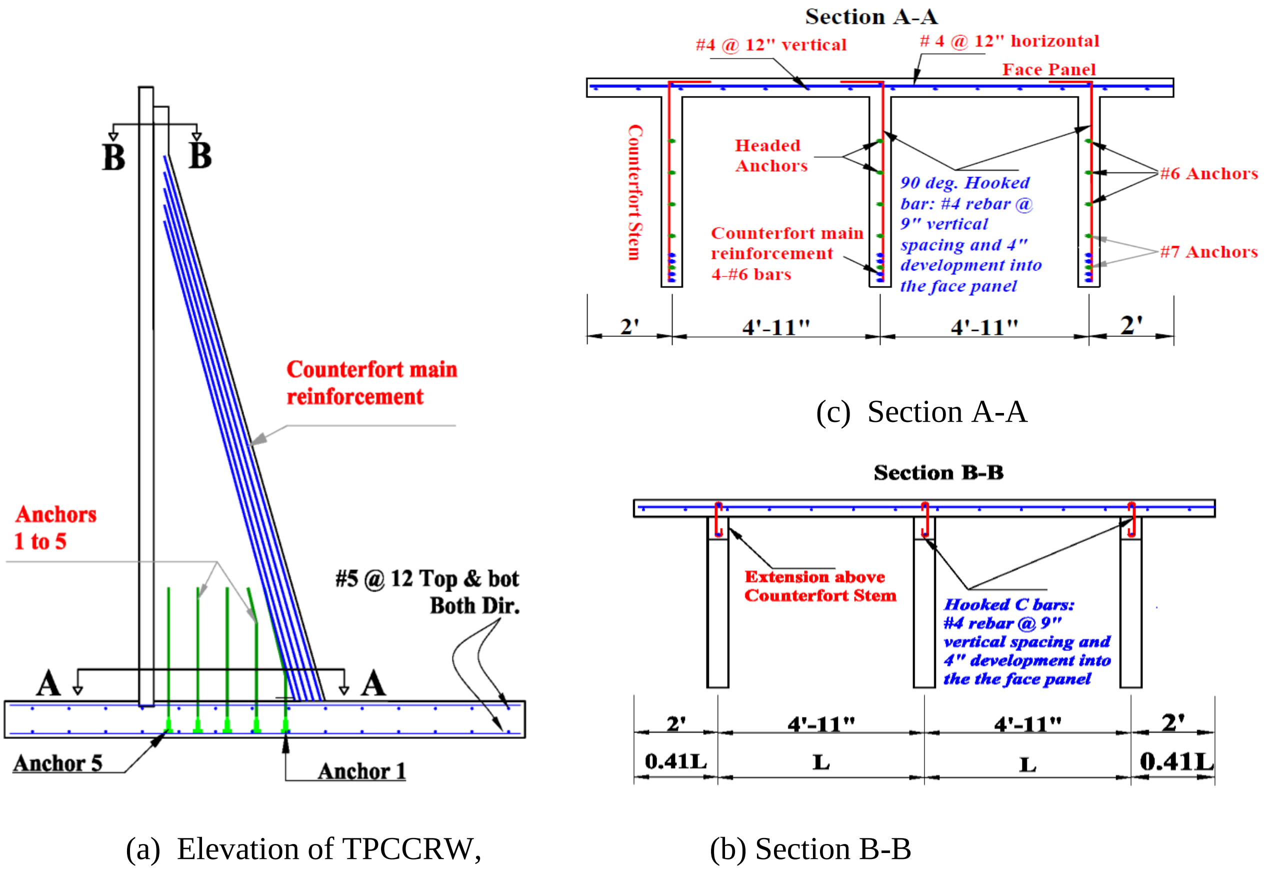

(c) Section A-A

(a) Elevation of TPCCRW,

(b) Section B-B

Figure 5-5. Steel reinforcement details of TPCCRW

5.2. Material properties

The material properties used in the analysis, design, and experimental testing for TCCPRW and the soil backfill in are presented Table 5-1. Soil properties were obtained from the geotechnical report that is presented in Appendix A . For testing purposes, the design assumed active earth pressure to mitigate worst case scenario. However, the results obtained from the experimental testing and the finite element analysis indicated that the deflection at the top of the wall is too small to initiate minimum active pressure as per AASHTO LRFD Table C3.11.1-1. The final design submitted to the precast facility is assumed at-rest soil conditions.

Table 5-1. Material properties used in the design and NLFEA of TCCPRW

Property	Value	Unit	Description
f_y	60	ksi	Steel Yield Strength
E_s	29000	ksi	Steel Modulus of Elasticity
f'_c	7.2	ksi	Concrete Compressive Strength
γ_c	150	pcf	Unit Weight of Concrete
E_c	4888	ksi	Concrete Modulus of Elasticity
n	6		Modular Ratio, Es/Ec = n, per AASHTO LRFD [5.7.1]
γ_d	0.125	kcf	Dry Unit Weight of the Soil
φ_s	28.0	deg	Angle of Internal Friction
k_a	0.361		Coefficient of Active Earth Pressure, AASHTO LRFD
q_{all}*	2.500	ksf	Allowable Soil Bearing Capacity Assumed for Design
q_{all_prov}**	10	ksf	Allowable Soil Bearing Resistance Provided by Geotechnical Report
q_{u_prov}**	15	ksf	Factored Soil Bearing Resistance Provided by Geotechnical Report

* Assumed to obtain worst case scenario for weak soil conditions
** Actual soil conditions in the field
1 ksi = 6.9 MPa, 1 in.= 2.54 cm, 1 pcf = 0.1571 KN/m^3, 1 psf = 0.047 kpa

The concrete mix design and the results of the concrete average compressive strength properties of each component in the TPCCRW are shown in Table 5-2 and Table 5-3, respectively. The ultimate compressive strength of concrete is 7200 psi (49.64 Mpa). It was assigned for design and finite element analysis for both the wall and base slab as shown in Table 5-1.

Table 5-2. Concrete Mix Design used for TPCCRW.

Material proportions for Mix Design	
Material	**Amount, lbs/yd³**
Sand	1325
Coarse aggregate	1527
Cementitious materials	700
w/c ratio	0.38
Air content	6.50%

1 lbs/yd^3 = 0.593 kg/m^3

Table 5-3. Concrete compressive strength of different wall components at 28 days

28 days Concrete compressive strength			
Specimen	**No. of Specimens**	**Specimen Size**	**AVG Ult. Stress, psi**
Base	9	6”x12”	**9400**
Wall	7	6”x12”	**7280**
Grout	4	3”x6”	**7660**

1 psi = 6.9 kPa, 1 in.= 2.54 cm

5.3. Design Limit states and Stability Requirements

Service I and Strength I design limit states are used for load calculations as per AASHTO LRFD specifications Table 3.4.1-1. The load notations and factors are shown in Table 5-4.

Table 5-4. Load Notations and Load Factors

Load Description		Notation	Load Factors		
			Service I	Strength I	
				Min.	Max.
Vertical Loads	Self-weight of face panel Self-weight of base Self-weight of counterfort stem	DC1 DC2 DC3	1.0	0.9	1.25
	Vertical earth pressure on the base heel Vertical earth pressure on the base toe	EV4 EV5	1.0	1.0	1.35
	Vertical surcharge load	LSv	1.0	0.0	1.75
Lateral Load	Horizontal Earth pressure	P_{EH}	1.0	0.9	1.50
	Horizontal surcharge load	LS_h	1.0	0.0	1.75

The check for stability requirements is performed at the Service limit state for the overturning moment, bearing resistance, eccentricity, and sliding. At the strength limit state, stability is checked for bearing resistance, eccentricity and sliding taking into account the minimum and maximum load combinations in accordance to AASHTO LRFD 11.6.3.2, 11.6.3.3, and 11.6.3.6 respectively. The stability checks are summarized in Table 5-5. Analysis of Table 5-5 reveals that the design meets the stability requirements per AASHTO LRFD section 11.6.3. The system was not studied for overall stability. The total service load of 144 kip (640.54 KN) calculated using Service I limit state and the total ultimate load of 216.5 kip (963.03 KN) calculated using Strength I limit state.

Table 5-5. Stability checks based on AASHTO LRFD 11.6.3.

<table>
<tr><th>Limit State</th><th>Stability check</th><th colspan="2">F.O.S./Limit</th><th>Calculated F.O.S.</th><th>Check</th></tr>
<tr><td rowspan="5">Service I</td><td>Failure due to Overturning</td><td colspan="2">2</td><td>3.39</td><td>O.K.</td></tr>
<tr><td>Failure due to Sliding</td><td colspan="2">1.5</td><td>1.55</td><td>O.K.</td></tr>
<tr><td rowspan="2">Eccentricity limits</td><td>1/3 base</td><td>5</td><td rowspan="2">6.22</td><td rowspan="2">O.K.</td></tr>
<tr><td>2/3 base</td><td>10</td></tr>
<tr><td>Bearing Capacity Failure</td><td colspan="2">2.9</td><td>2.47</td><td>O.K.</td></tr>
<tr><td rowspan="4">Strength I</td><td>Failure due to Sliding</td><td colspan="2">1.5</td><td>1.8</td><td>O.K.</td></tr>
<tr><td rowspan="2">Eccentricity limits</td><td>1/6 base</td><td>2.5</td><td rowspan="2">4.12</td><td rowspan="2">O.K.</td></tr>
<tr><td>5/6 base</td><td>12.5</td></tr>
<tr><td>Bearing Capacity Failure</td><td colspan="2">7.25</td><td>6.41</td><td>O.K.</td></tr>
</table>

5.3.1. Nonlinear Finite Element Analysis (NLFEA)

ANSYS® package was used to develop three dimensional finite element model to analyze the structural behavior of TPCCRW as shown in Figure 5-6.

The purpose of finite element modeling is to:

- Verify whether the AASHTO LRFD-based design satisfies structural stability and integrity of the system under both service and ultimate loads,
- Investigate the deflection of wall at top of wall, H/2, and H/3, where H is the height of wall,
- Evaluate the structural behavior of anchors connecting the counterforts and base-slab,
- Investigate required the amount of steel reinforcement in the counterforts.

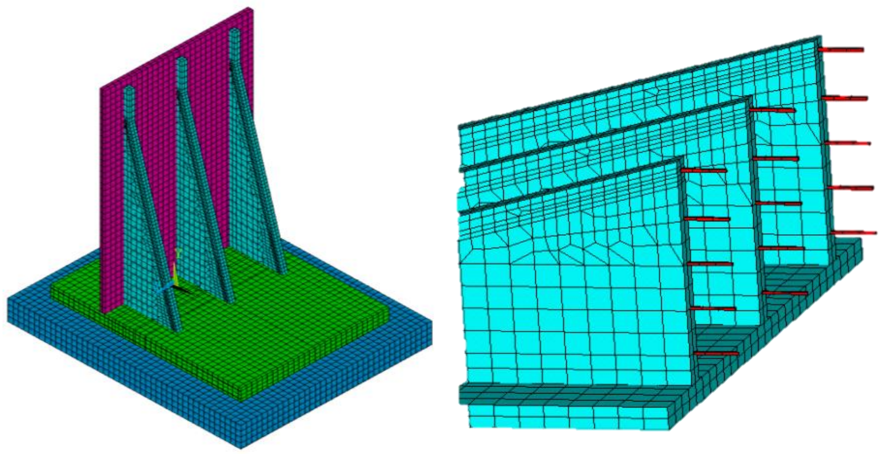

(a) Finite element model geometry of TPCCRW   (b) anchors extending from counterforts

Figure 5-6. Finite Element Model of TPCCRW

5.3.2. <u>Concrete, steel reinforcement and anchors</u>

SOLID65 element was used to simulate the concrete volume. It has the capabilities of simulating both cracking and crushing of concrete. The cracking and crushing of concrete is defined by Willam and Warnke model. Although, the crushing capability of concrete was ignored in several studies to avoid fictitious crushing (Kachlakev et al., 2001, ANSYS User Manual, Zhou et al., 2004, and Si et al., 2008). Instead a uniaxial multilinear stress-strain concrete cylinder test data of actual test specimen was used to define compressive behavior of concrete. A value of 0.2 was used for concrete's poisson's ratio.

The steel reinforcement and anchors are modeled using Link8 element. The steel material assumed to be bilinear elastic-perfectly plastic that is identical in both tension and compression with elastic modulus (E) of 29,000 ksi (200 Gpa) and poisson's ratio of 0.2 (Al-Rousan and Issa, 2011). The interface between the Link8 concrete elements are assumed fully bonded. TARGE 170 and CONTA 174 elements were used to define the frictional interface between the bottom surface of the precast face panel and the top surface of the base-slab. The material models utilized in finite element analysis is presented in Fig 7.

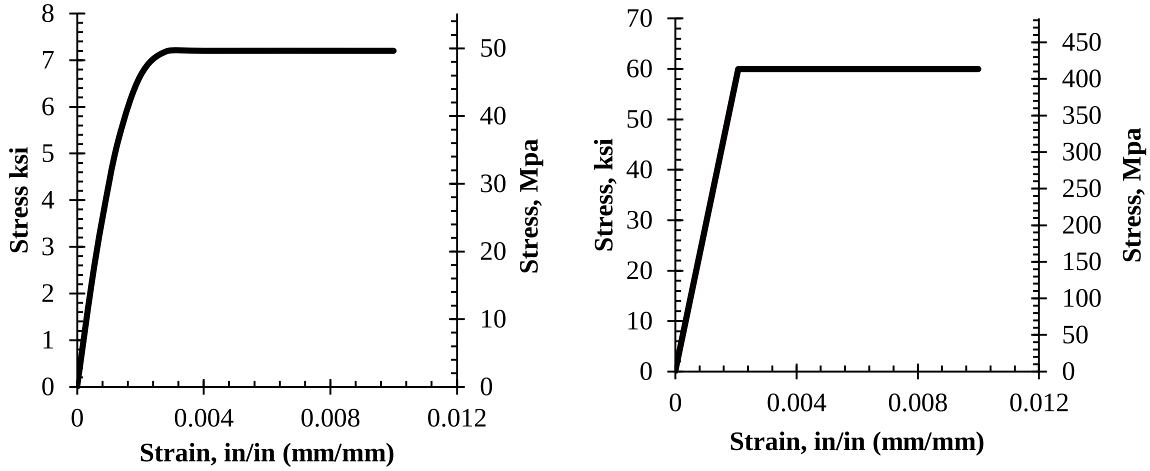

(a) Material model for concrete (b) Material model for steel.

Figure 5-7. Material Properties used in Finite Element Model

5.3.3. Loading and boundary conditions

A perfectly elastic medium is placed below the retaining wall to mitigate soil conditions. The finite element model was focused on studying the structural behavior of TPCCRW. Therefore, soil structure interaction under various soil conditions was ignored. Elastic foundation modulus of 40 ksi (276 Mpa) was assigned to the soil medium which corresponds to medium clay soil (Bowels 2001 and 1996). The analysis was carried out over several load steps. The sequence of load steps includes (1) self-weight of wall, (2) soil backfilling, (3) two feet surcharge load in order to simulate the Service I (AASHTO LRFD) and (4) a nodal load of 200 kip (889.64KN) from the hydraulic cylinders was applied at one third height of wall (H/3) to carry the system to ultimate load capacity (Strength I).

5.3.4. Analysis and discussion of NLFEA results

The deflections of the wall as well as the variation of the strain in the concrete, steel reinforcement, and anchors are discussed below.

Load vs. Deflection curve: deflection results and deflections contours of TPCCRW obtained from finite element analysis at different heights of face panel are shown in Figure 5-8 and Fig 9, respectively. Inspection of Figure 5-8 reveals that, under service loads, the deflection at top of wall was estimated to be around 0.21 in (5.43 mm). In addition, the deflections at mid-height (H/2) and one third height (H/3) of the wall were 0.072 in (1.66 mm) and 0.1 in. (2.53 mm), respectively. When the load is increased to 216.5 kip (963.03 KN) the deflection at top of the wall was 0.44 in (11.13 mm) and the deflections at mid-height (H/2) and one third height (H/3) of wall are 0.2 in (5.16 mm) and 0.13 in (3.29 mm) respectively.

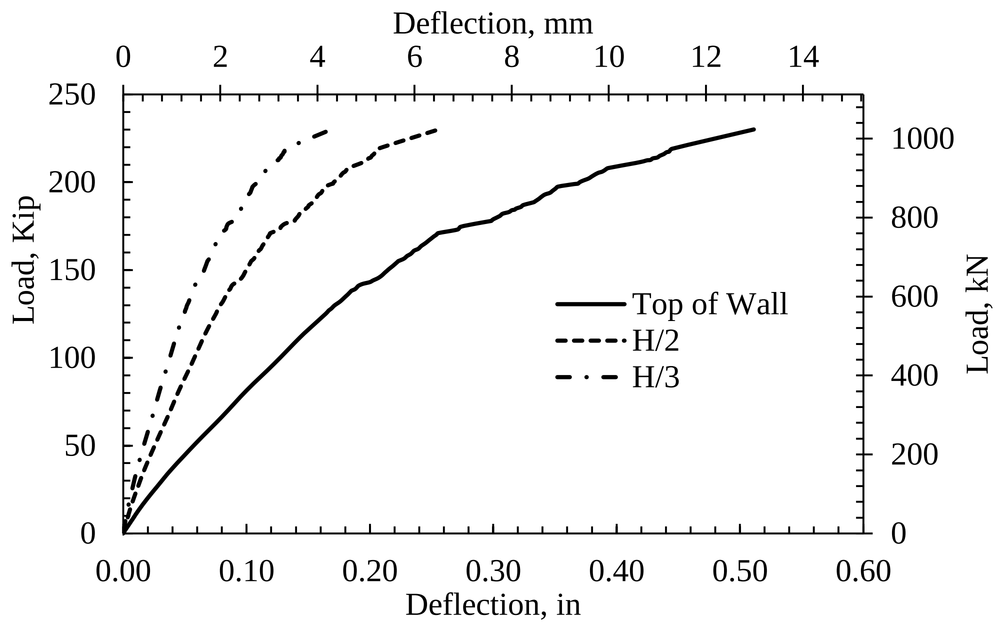

Figure 5-8. Load vs. deflection plots at H/3, H/2, and Top of Wall using ANSYS Package

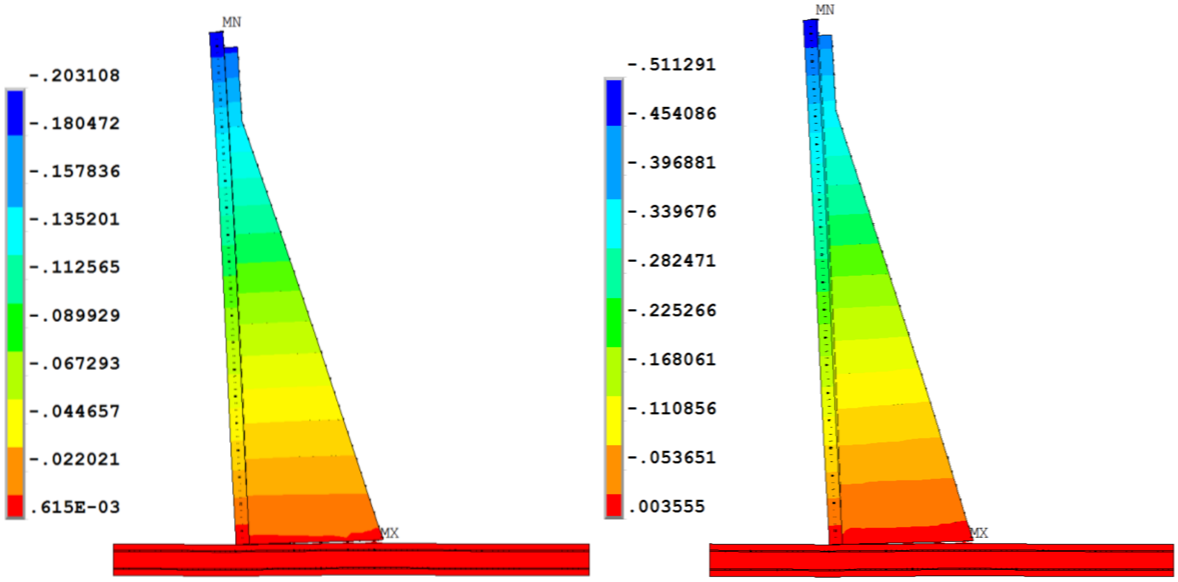

(a) Service load of 144 kip (b) Ultimate load of 216.5 kip

Figure 5-9. Deflection contours results obtained from Finite Element Analysis (ANSYS)

Stress vs. strain results in anchors: The strain variations in the anchors for the middle counterfort are presented in Figure 5-10. Inspection of Figure 5-10 shows that, the strain results values exhibit a decreasing general trend starting from the outermost anchor approaching the face of the face-panel as expected. It reveals that anchor 1, the furthest anchor from the face-panel (#7 anchor), has yielded at a load of 170 kips (756.19 KN). Anchor 2 shows yielding strain of 2083 με at a load of 215 kips (956.4 KN) . In addition, it can be observed that anchor 3, 4, and 5 did not yield. The described behavior of the anchors is expected as the anchors with longer moment arm experience higher flexural moment.

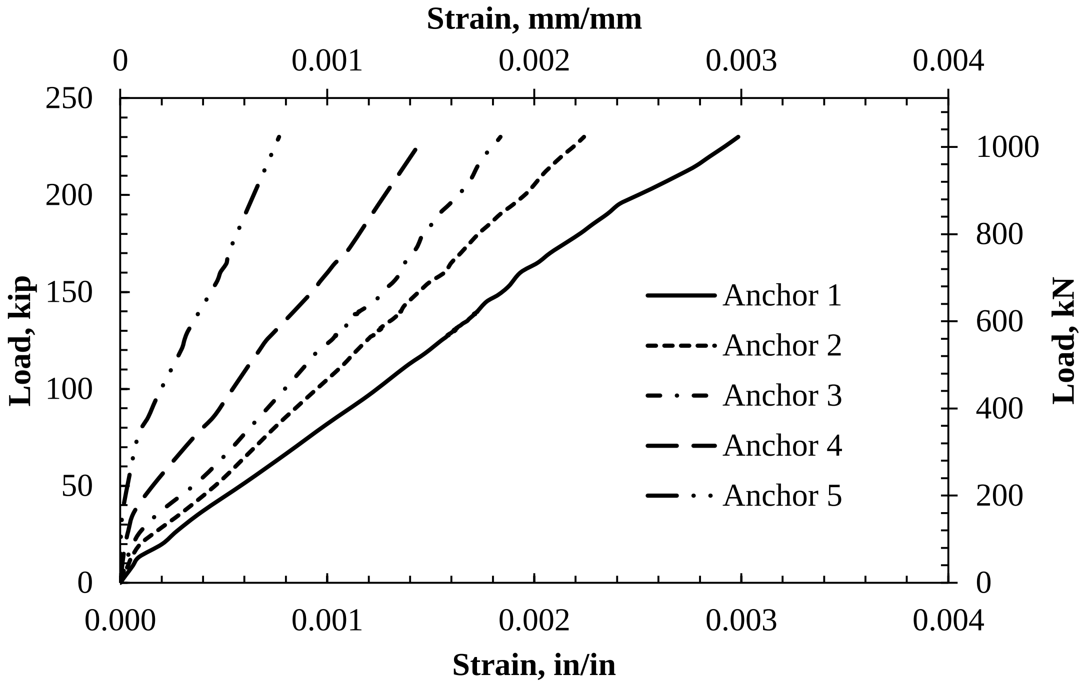

Figure 5-10. Applied load vs. strain at each anchor in the middle counterfort from ANSYS

5.4. Experimental Program

5.4.1. Fabrication

TPCCRW is formed of two totally precast components; the face-panel and counterforts cast as one component and the base-slab as separate component. Based on structural analysis supported by FEA, the face-panel and counterforts are reinforced with one layer of steel reinforcement. Figure 5-11 shows extended L-bars from face-panel to the counterfort. The base-slab is reinforced with two identical layers as shown in Figure 5-11.

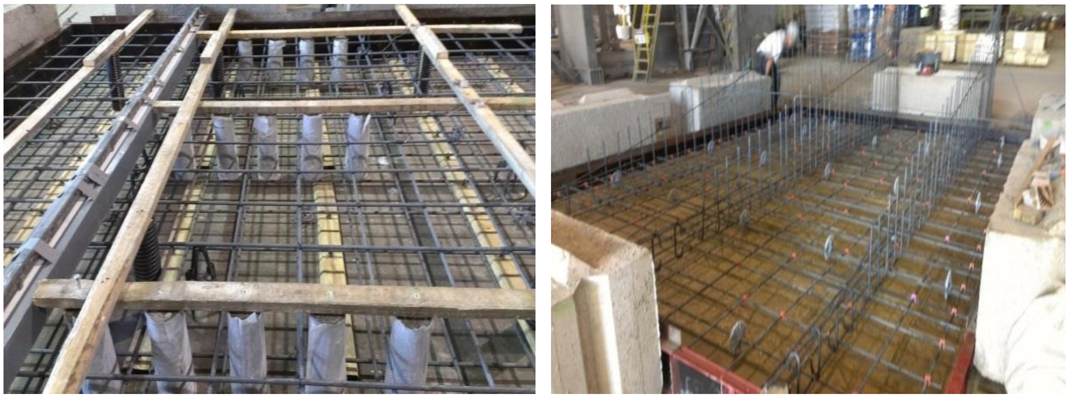

(a) Base slab (b) Face panel and counterforts with extended L-bars

Figure 5-11. Fabrication of the base slab and face panel with counterforts

The steel reinforcement of the TPCCRW at the level of each component is summarized in Table 5-6.

Table 5-6. Reinforcement Details at All Wall Sections

Assembly Part	Number of layers	Vertical	Horizontal	Inclined
Face	1	# 4 @ 12	# 4 @ 12	--
Counterfort	1	# 4 @ 12	# 4 @ 6	4 # 6
Base	2	# 5 @ 12	# 5 @ 12	--
Anchors	--	2#7 and 3#6 on each counterfort		

Each counterfort is connected to the base-slab using 5 headed anchors. Each headed anchor is embedded 11.5 in. (292 mm) in the base-slab. The anchors are at 1 ft (304.8 mm) spacing starting at 6 in. (152.4 mm) from the internal face of the wall. The development length of the L-bars can also be reduced by reducing the spacing between them.

5.4.2. Instrumentation

The purpose of instrumentation is to monitor the structural behavior of the retaining wall during all loading stages. The loading stages start with soil backfilling and end with applying loads to ultimate. Two types of instrumentation sensors were used to monitor the behavior of critical locations on the wall.

The first type is the Linear Variable Differential Transformer (LVDT), which measures the deflection of the wall. Seven LVDTs were placed against the face of the wall at seven different locations. Four of them are at one third of the height of the wall and three at one half of the wall height. The purpose of this configuration is to study the deflection of the wall at the counterforts and at the mid-span between them. The seven LVDTs were fixed to a steel frame against the wall and connected to a portable data logger system (Figure 5-17) that would provide instantaneous reading of the wall deflection, as shown in Figure 5-12.

(a) LVDT installed strain gauge as mounted on site

(a) LVDT connection setup

(b) LVDT locations at H/3 and at H/2

Figure 5-12. Details of instrumentation setup

The second type of instrumentation equipment is the strain gauges. Strain gauges vary in size depending on the location, function, and type of material tested. The size and the gauge factor for the strain gauges used are shown below:

1. 6 mm long with 2.12 gauge factor used for steel
2. 10 mm long with 2.09 gauge factor used for steel
3. 60 mm long with 2.09 gauge factor used for concrete
4. 60 mm long with 2.08 gauge factor used for concrete
5. 90 mm long with 2.09 gauge factor used for concrete

Similar to the application of LVDTs, strain gauges were mounted at the locations of critical interest. The study of strains at these locations provides important information describing the behavior of the retaining wall system.

A total of forty-two strain gauges were installed at different locations. The gauges are divided into concrete mounted strain gauges and steel mounted strain gauges. Twelve strain gauges were mounted on concrete and the rest were mounted on steel.

Among the strain gauges mounted on steel, eleven strain gauges were mounted on the 10 anchors of the left and middle counterfort in a way such that 10 mm strain gauges were mounted on the #7 anchors and 6 mm strain gauges were mounted on the rest # 6 anchors. Another 10 mm strain gauge was mounted on the first # 7 bar of the right counterfort. Three 6 mm strain gauges were mounted on the inclined bars, one for each counterfort at a height of 3ft from the top of the base. In addition, two strain gauges of 6mm length were installed on the extension 30 in. below the top of the wall at the left and middle counterforts.

For the front face panel of the PCCRW, twelve strain gauges 6mm long were mounted on the steel reinforcement of the wall. The distribution was six strain gauges at H/3 level and another six at H/2 level. For each level, the strain gauges were installed at the left mid-span, middle counterfort, right mid-span and right counterfort, in addition to two strain gauges in the vertical direction located at the right mid-span and right counterfort. The purpose of this configuration is to study the strain response of the steel at the locations of positive moment (mid-span) and negative moment (at counterfort).

The last strain gauge distribution at steel is at the level of the base. Two 6mm strain gauges were mounted on the top layer of base reinforcement. The first one is aligned with the middle counterfort and the second one is aligned with right counterfort. Figure 5-13 and Figure 5-14 shows the distribution of strain gauges on steel reinforcement.

(a) (b)

Figure 5-13. (a) & (b) Connection of stain gauge to anchor

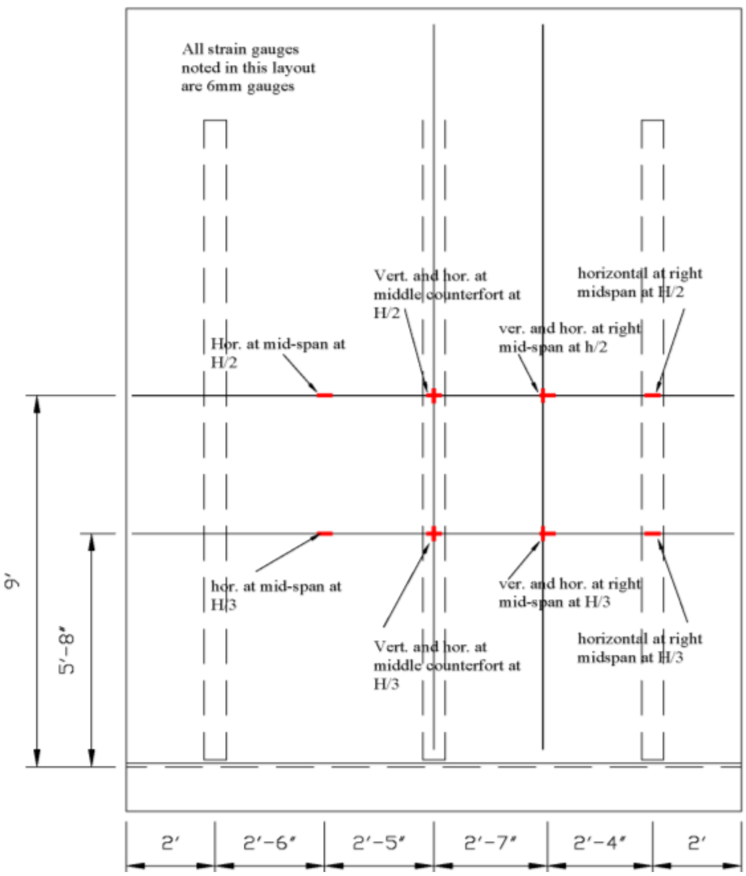

(a) Distribution of strain gauges on the steel reinforcement in the wall face

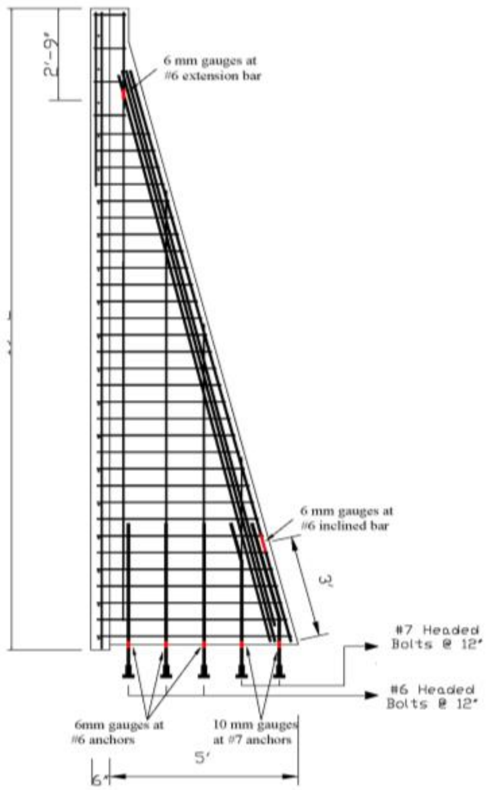

(b) Distribution of strain gauges on the steel reinforcement in the counterforts

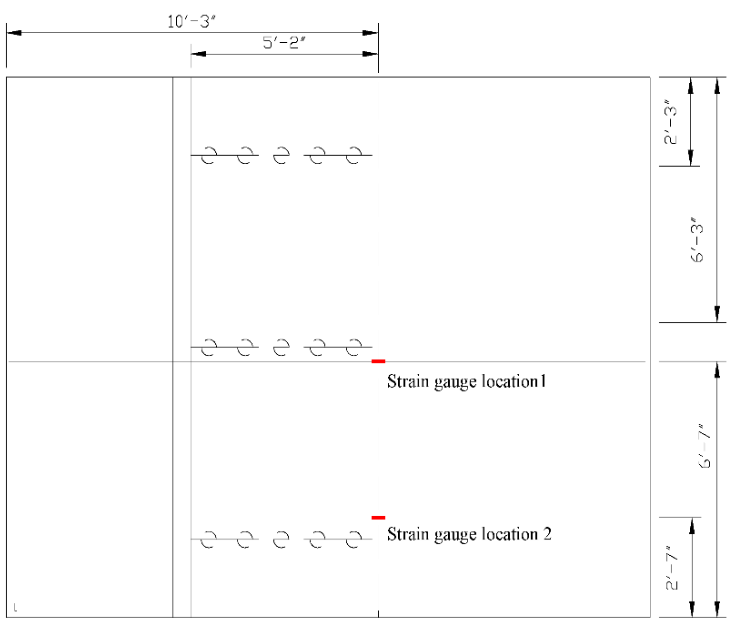

(c) Strain gauge on the steel reinfocement of the base

Figure 5-14. Distribution of strain gauges along the steel reinforcement of (a) wall face (b) counterforts (c) base

For the concrete strain gauges, similar configuration was followed. 90mm strain gauges were mounted on the inclined surface of the middle and right counterfort at 3ft. elevation from the bottom. Two other strain gauges 60mm each were installed on the rear face of the wall at both mid-spans at one third the wall height. For the front face panel, a total of eight 60mm strain gauges were mounted. The distribution is similar to that of the steel in the face. Strain gauges were located at H/3 and at H/2 of the wall. Figure 5-15 illustrates the location of the strain gauges mounted on the surface of concrete.

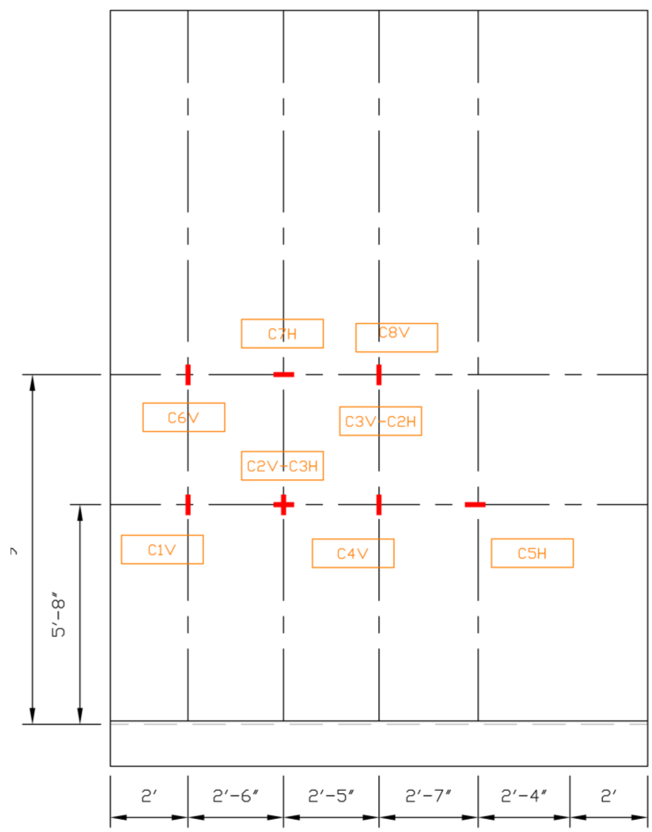

Figure 5-15. Location of concrete strain gauges on wall panel

All Strain Gauges and LVDTs were connected to a portable data acquisition system in order to collect and record data as shown in Figure 5-16 and Figure 5-17. The data acquisition system is mainly composed of a data logger that is connected to a computer unit and strain indicator with switch and balance units. The system was running continuously to ensure constant data collection throughout the whole test duration.

Figure 5-16. Wiring of LVDTs and strain gauges to data acquisition system

Figure 5-17.Portable data logger and data logging equipment for LVDTs and strain gauges

5.4.3. Erection

The erection process starts at the level of the base-slab. The base-slab is cast and delivered to the site. It was placed 2 ft below grade level on spacers, which guaranteed a 1 in. (25.4 mm) offset from the ground in order to allow for grouting below the base. The base was grouted to eliminate any voids so that the base would rest uniformly on the ground. The grout was pumped through four holes until all the voids below the base were filled as shown in Figure 5-18. The wall was erected by aligning each headed anchor with the specified shear pocket of the base slab. Then, the shear pockets were filled with high performance fast setting (15 minutes) grout.

Figure 5-18. Erection and leveling of the base slab

The erection process can be summarized into three stages:

1. Stage 1: placement of the base slab: The base slab is placed, leveled on site. Grout is pumped below the slab to eliminate any voids and to ensure uniform distribution of the soil pressure generating below the base. The erection procedure of the base slab is shown in Figure 5-19 and Figure 5-20.

(a) Preparing the ground under the base slab (b) Leveling the ground under the base slab

Figure 5-19. (a) & (b): Leveling and preparing the ground under the base slab

(a) Erecting the base slab (b) Placing the precast base slab

Figure 5-20. (a) & (b): Placing the precast base slab into its location

2. Stage 2: Erecting the wall component: wall component is erected using steel cables wrapped in designed openings in the counterforts specified for handling purposes. The wall is placed and leveled such that the headed anchors are placed in each specified shear pocket.

(a) and (b) Transportation and lifting of wall face and counterforts

 

(b) and (c) Erection of wall face and counterforts assembly to base slab

 

(d) Final wall assembly (e) 1 in. gap for grouting

Figure 5-21. Retaining wall transportation, erection and assembly

3. Stage 3: Grouting shear pockets: shear pockets are grouted to sustain the required anchorage between the base-slab from one side and the counterforts from the other side through the headed anchors.

Two circular openings were designed in each of the two external counterforts for handling and erection purposes. The effect of wind load on the stability of the system during construction was calculated and was found to be negligible. As a result, the crane was capable of handling the wall without a need for a temporary bracing system.

5.4.4. Setup and Testing Procedure

The erected retaining wall is experimentally tested following the order:

1. Soil Backfilling: soil pressure was applied by backfilling of the retaining wall with soil with 95% compaction level.
2. Surcharge Load: the load was applied using Dozers to simulate the actual condition for live surcharge.
3. Test 1: two hydraulic cylinders applied up to 178 kips (791.78 kN) at one H/3 of the wall acting at 6 points divided over 3 counterforts. It was followed by Hydraulic actuator at the top of the wall delivering 160 kips (711.71 kN).
4. Test 2: two hydraulic cylinders applied up to 136 kips (604.95 kN) at H/3 of the wall acting at 6 points divided over 3 counterforts.
5. Test 3: two hydraulic cylinders applied up to 97 kips (431.47 kN) at H/3 of the wall acting at 2 points on middle counterfort.
6. Test 4: two hydraulic cylinders applied up to 192.4 kips (855.83 kN) at H/3 of the wall acting at 6 points divided over counterfort.

5.4.4.1. Soil Backfilling:

The soil was filled at 6 in. increments. At each increment, soil was compacted using a sheep-foot roller compacting machine. The goal was to maintain 95% compaction level (Figure 5-22). The proctor test revealed that the wet density of the soil was 130 pcf (20.42 kN/m^3). The moisture level by the end of backfilling was estimated to be 12%. The top surface of the soil was finished at almost a leveled surface.

(a) Bulldozer during soil backfilling

(b) Soil backfilling

(c) Soil Compaction using sheep-foot roller

(d) Manual compaction for corners

Figure 5-22. (a) & (b): Backfilling of soil, (c) & (d): Soil compaction

5.4.4.2. <u>Surcharge load:</u>

In order to simulate the surcharge load stated by AAHSTO LRFD that would account for the live load, two vehicular live loads were placed at the top of the backfill. The first and second vehicles weigh 27 kips (120.10 kN) and 37 kips (164.58 kN), respectively. The bulldozer was placed 2 ft away from the wall to maintain a worst case scenario as shown in Figure 5-23. The live load application was also followed by placing a hydraulic cylinder mounted against the bulldozer which was used to apply a lateral load of 16 kips at the top of the wall.

(a) 27K bulldozer (b) 37K bulldozer

Figure 5-23. Application of live load surcharge using a 37 kip (164.6 kN) bulldozer

5.4.4.3. Load application using hydraulic cylinders

Tests 1 to 4 were performed using two hydraulic cylinders as shown in Figure 5-24. Four steel cables of 1.5 in. diameter each, were hooked to the hydraulic cylinders from one side and to a 7 in diameter solid steel section from the other side. The solid steel section served as a connection element to transfer the load from the cylinders to the wall. Representation of the testing setup as performed in the field is shown in Figure 5-26. The cylinders were anchored to a stack of ten concrete blocks for additional support as shown in Figure 5-25.

(a) Hydraulic pump (b) Location of load application

(c) Hydraulic actuators with steel cables extended

(d) Hydraulic pump (e) Setup for hydraulic actuators

(f) South view of setup

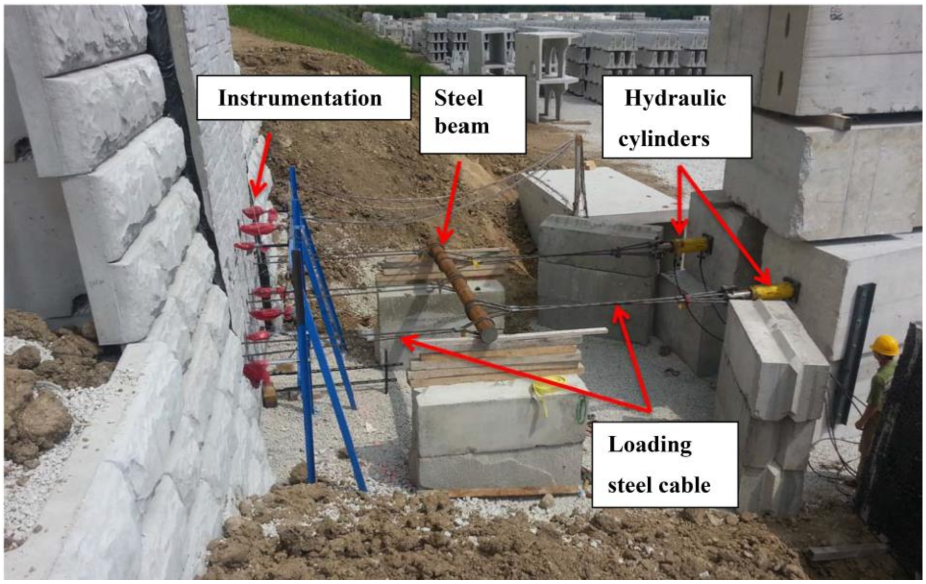

(g) North view of setup

Figure 5-24. Testing Setup for TPCCRW in the field

(a) Rear concrete blocks

(b) Steel rod

(c) Front concrete blocks

(d) Hydraulic actuators

(e) Whole blocks setup

(f) Concrete blocks

Figure 5-25. (a) – (h): Hydraulic actuator test 4 setup

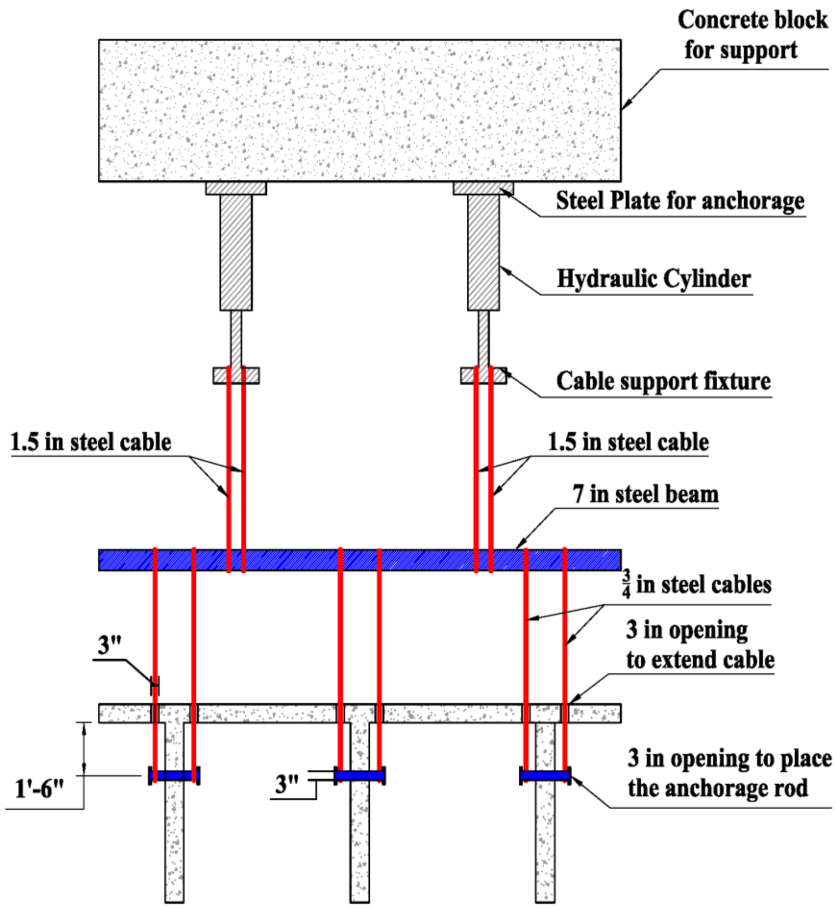

Figure 5-26. Representation of testing setup as performed in the field

5.5. Analysis and discussion of experimental test results

5.5.1. Deflection results

Deflection results are shown in Figure 5-27 and Figure 5-28. The data was collected continuously throughout the scope of the project. The times of the testing are marked on the figures. After each test was executed, the load was removed. The 3 LVDTs located at H/2 showed very similar readings. The deflections at H/2 showed a maximum value of 0.1 in. (2.5 mm) at the end of backfilling. Upon adding the surcharge load, the deflection at H/2 increased to 0.115 in. (2.9 mm). Finally, the registered deflection at Tests 1, 2, 3 and 4 were 0.158 in. (4.01 mm), 0.16 in. (4.1 mm), 0.163 in. (4.16 mm), and 0.212 in. (5.4 mm), respectively.

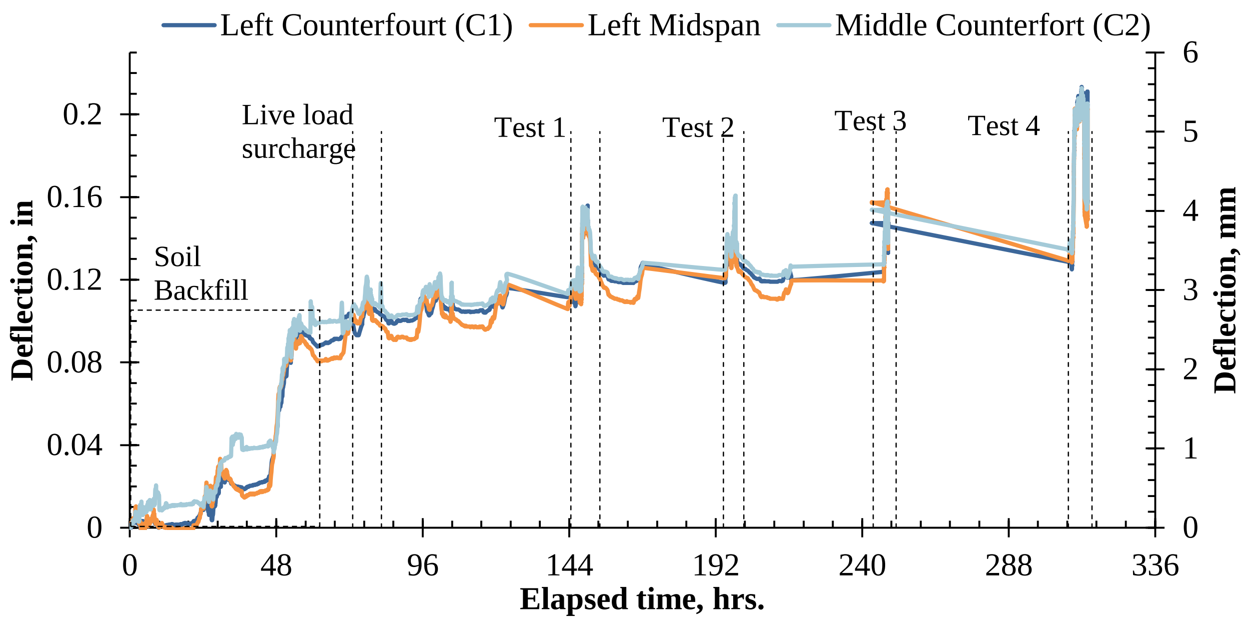

Figure 5-27. Deflection measured by the 3 LVDTs at H/2

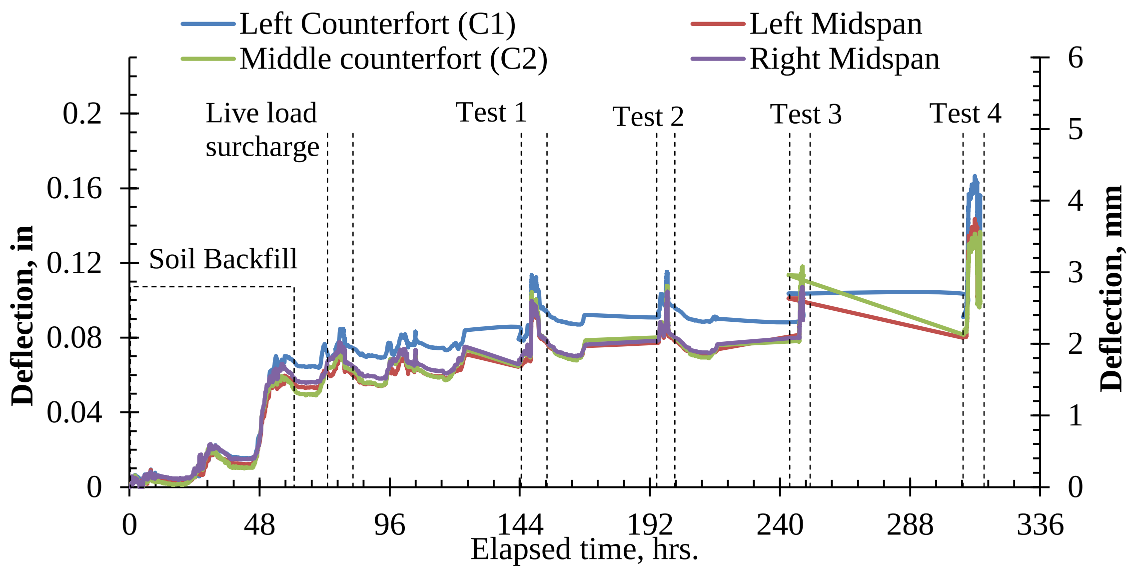

Figure 5-28. Deflection measured by the 4 LVDTs at H/3

Deflection results show that the critical locations at left midspan, middle counterfort and right midspan at H/3 of the wall exhibit a similar behavior. Inspection of Figure 5-28 shows that the maximum deflection at one-third the height (H/3), recorded during Test 4, was found to be 0.167 in. (4.25 mm) at the left counterfort. A slightly smaller value of 0.14 in (3.55 mm) was recorded by the 3 other LVDTs at the same level.

The experimental testing results show consistent deflection values between the counterforts and the midspans of the wall throughout various testing times. This is due to the efficient geometric configuration which minimizes the load resisted by the face-panel. The counterforts are designed to resist the total applied lateral load. On the other hand, the face-panel is designed to resist lateral load due to soil pressure acting in the longitudinal direction spanning between each two counterforts. As a result, using a small Spacing-to-Height ratio (0.245) minimizes the lateral loads due to soil pressure applied to the face-panel.

In order to assume active earth pressure, AASHTO LRFD specifies a deflection-to-height ratio ranging from 0.001 to 0.01 for soil types varying from dense sand to compacted clay, respectively ($0.001 < \Delta/H < 0.01$). The value of deflection necessary to initiate active earth conditions corresponding to wall height of 20 ft - 2 in. (6.09 m) varies from 0.241 in. (6.1 mm) to 2.41 in. (61.2 mm) The maximum deflection results obtained from the experimental testing at service limit state was around 0.212 in. This indicated that the deflection at the top of the wall is too small to initiate minimum active pressure as per AASHTO LRFD Table C3.11.1-1. As a result, the design of the counterfort retaining wall to be applied in future applications should consider at-rest earth conditions.

5.5.2. Strain in the anchors

The maximum strain readings in the headed anchors at the middle and left counterforts are presented in Figure 5-29. Inspection of Figure 5-29 shows that the strain results in the headed anchors varied depending on the location of the anchor with respect to the wall and location of the counterfort. The outermost two anchors from the face-panel experienced the highest strain readings due to their longer moment arm with respect to the wall. These readings gradually decrease in the anchors closer to the wall. The strain readings in anchors 1 and 2 at the middle counterforts were found to be 2659 $\mu\varepsilon$ and 2203 $\mu\varepsilon$ and therefore exceeded 2070 $\mu\varepsilon$ which is the yield limit strain of steel. The strain readings in anchors 1 at the left counterfort was found to be 2421 $\mu\varepsilon$ which also exceeded 2070 $\mu\varepsilon$. However, the reading of anchor 2 showed a strain reading value of 2010 $\mu\varepsilon$ that is very close to the yield limit strain of steel.

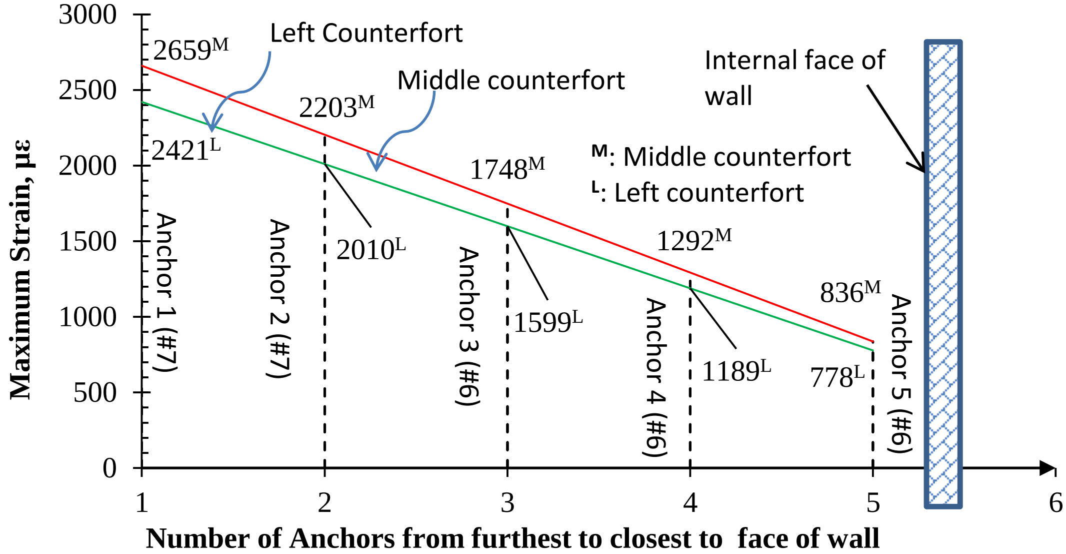

Figure 5-29. Maximum strains in headed anchors at the middle and Left counterforts

The strain variation at the testing times for Anchor 1 (#7 bar) located at the left counterfort throughout various loading conditions is shown in Figure 5-30. During soil backfilling, the strain increased up to 1360 micro-strains (με). It was then followed by gradual increase throughout the scope of testing. This increase was in the form of sharp spikes at the time of testing where the load was applied by hydraulic cylinders. The spikes were followed by drops as soon as the load was removed. This indicates that the anchors did not yield until it was loaded to an ultimate load (Test 4). The yielding limit of the anchor was observed in Test 4 where it reached 2421 με when subjected to ultimate load of 192.4 kip (855.8 kN).

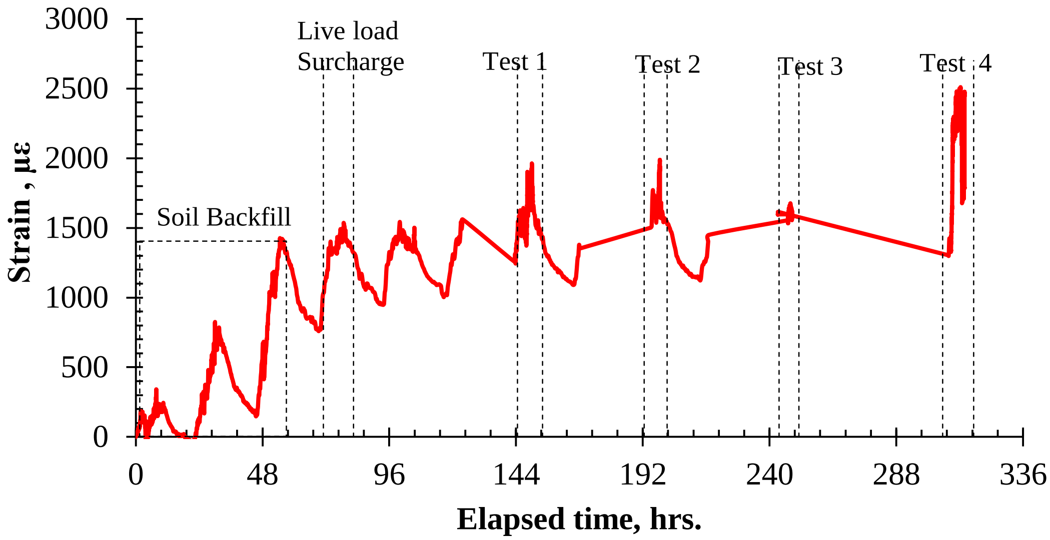

Figure 5-30. Strain variation curve at the times of testing for Anchor 1 in Left Counterfort

The high tensile strain result in the outermost anchors is expected due to the large moment arm measured from the outside face of the face-panel to center of each anchor. As a result, the design is controlled by outermost where #7 bars or higher is recommended. Smaller bar size can be used for anchors close to the face-panel (i.e. Anchors 4 and 5) as they experience smaller tensile strain. The anchors play another important role in maintaining the overall stability of the system.

The plot also shows a repetitive trend of gradual increase followed by a decrease in the strain readings over time between tests. The gradual drop in the strain reading was observed to occur during night-time and vice-versa during the day. This is attributed to the temperature variation between day and night as the test was performed in field conditions.

5.5.3. Face-Panel and main reinforcement in the counterfort

A thorough visual inspection of the face-panel reveals that no visible cracks were observed at the front face of the face-panel during testing. This is attributed to the efficiency of the geometric configuration which helped in lowering the stresses in the face-panel and achieved a successful design using one layer of steel with a wall thickness of 6 in. (152.4 mm). The results showed that no yielding occurred in the main reinforcement of the face-panel. Figure 5-31 represents sample strain readings at the left midspan between counterforts and over the middle counterfort. The maximum strain readings at H/3 at the midspan between the counterforts and over the counterforts were similar and ranged from 500 to 600 με as shown in Figure 5-31.

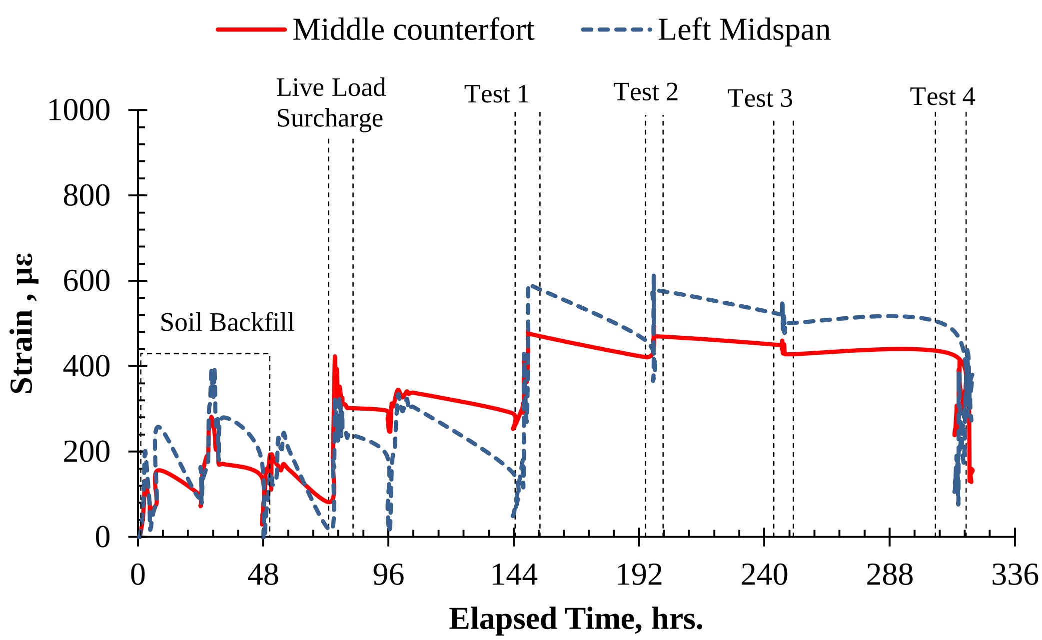

Figure 5-31. Strain vs. time readings for face-panel steel reinforcement located at H/3 at the middle counterfort and left midspan

On the other side, the strain results at the main reinforcement of the left counterfort are represented in Figure 5-32. The strain reading show a maximum value of 1957.5 με recorded in Test 1 and almost similar values recorded in Tests 2, and 4. These values dropped to their initial values after each test. This indicates that the main reinforcement did not undergo yielding. This behavior was not witnessed in Test 3 due to the nature of the loading setup which only focused on studying the behavior of the middle counterfort.

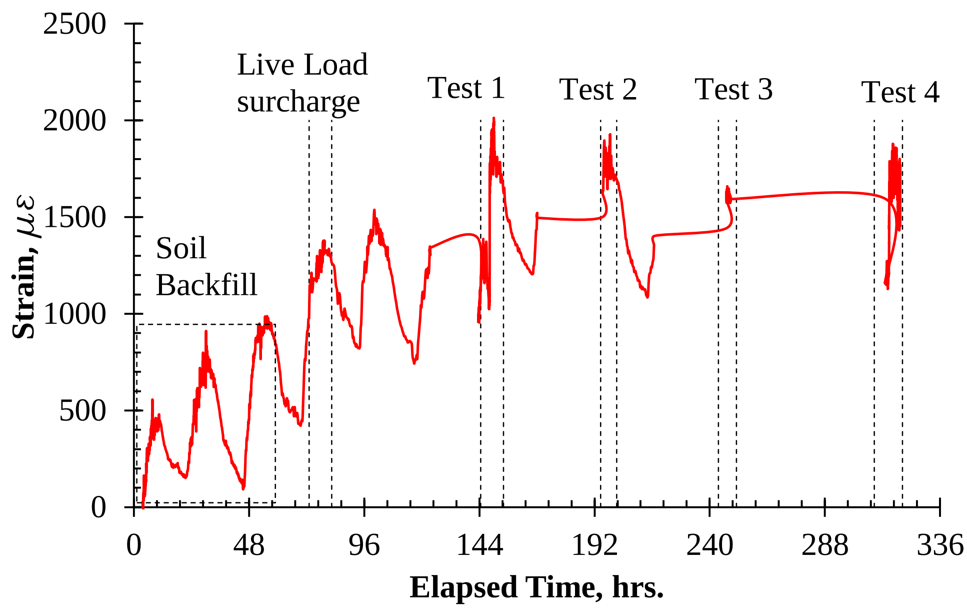

Figure 5-32. Strain readings at the main reinforcement of the right and middle counterforts

It can be also said that cracks developed in the concrete at the level of inclined surface to counterforts, due to high overturning moment resisted by the T-section of the counterforts and the face-panel. This observation was verified using finite element analysis as shown in Figure 5-33.

The finite element analysis revealed a very important aspect of the counterfort behavior. Anchors are subjected to tension when the lateral loads are applied. As a result, cracks are expected to generate at the location of the anchors. These cracks are likely to propagate towards the middle of the counterfort with the increase of the load as mitigated by the finite element analysis shown in Figure 5-33.

In this case, shear failure will be the dominant mode of failure due to the big counterfort depth. Temperature and shrinkage reinforcement (vertical bars) are used to control the mode of failure by arresting the cracks propagating towards the middle of the counterfort web. As a result, the failure mode of the counterforts can be controlled by reducing the spacing of the vertical bars to obtain controlled flexural mode of failure.

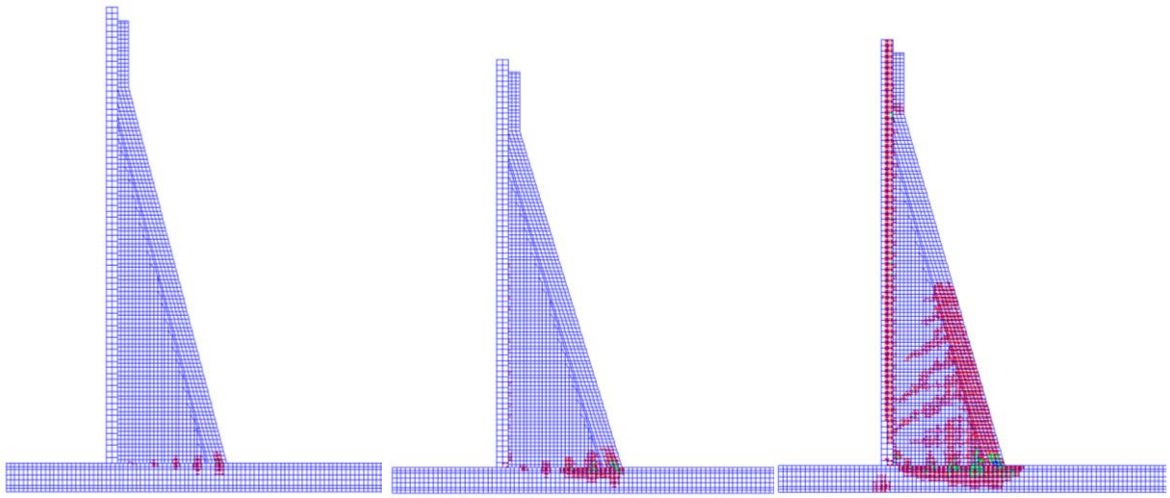

(a) 67 kip (298.03 kN) (b) 144 kip (640.54 kN) (c) 216.5 kip (963.03 kN)

Figure 5-33. Development of cracks in the counterforts and base slab using FEA

5.5.4. Results and analysis for strain in extension steel at top

The strain readings in steel at left and middle counterfort's top extension are shown in Figure 5-34. Analysis of Figure 5-34 shows that the strain readings of the steel reinforcement at the top of the counterforts at the extension steel exhibited no significant changes except in Test 1. In Test 1, a 16 kip (71.17 kN) load was applied at the top of the wall using a hydraulic cylinder mounted against the bulldozer which in turn was used as live load surcharge resulting in high bending stresses at the level of extension steel. These stresses were reflected in a high jump in the strain reading; 1100 $\mu\varepsilon$ in the left counterfort and around 1700 $\mu\varepsilon$ in the middle counterforts as shown in Figure 5-34. These strain readings indicate that the steel at the top of the counterforts did not yield when subjected to lateral load of 16 kips (71.17 kN).

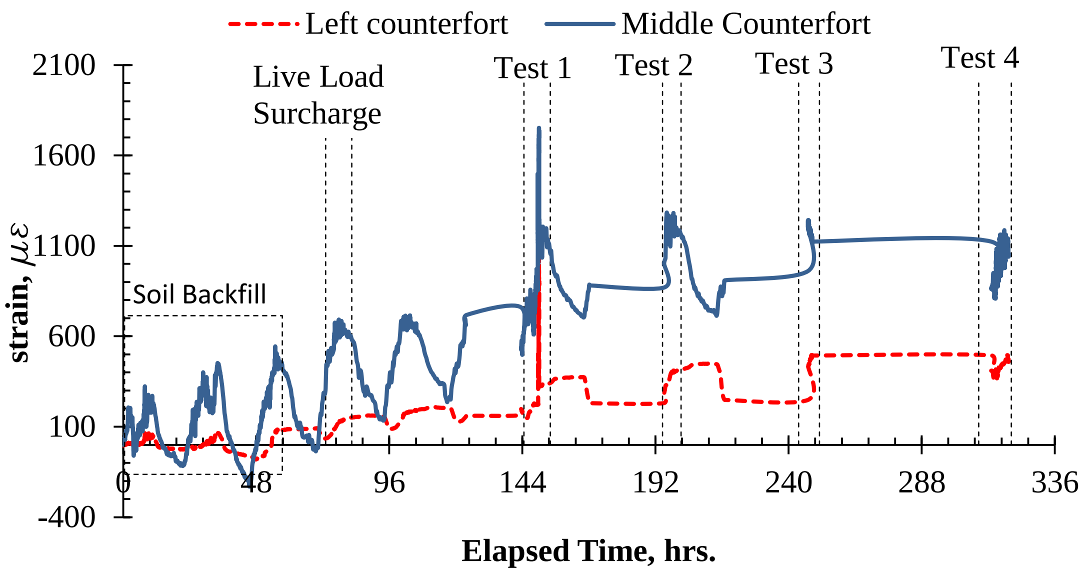

Figure 5-34. Strain readings in steel at left and middle counterfort's top extension

5.6. Validation of NLFEA results with experimental results

At service load, The FEA deflection results at H/2 of wall and H/3 were 0.1 in. (2.5 mm) and 0.065 in. (1.6 mm), respectively. The experimental results showed an average deflection at H/2 and H/3 equals to 0.11 in. (28 mm), and 0.075 in. (1.9 mm), respectively. In addition, the NLFEA deflection at ultimate load at H/2 and H/3 were 0.203 in. (5.1 mm) and 0.13 in. (3.3 mm) respectively. The experimental results at ultimate load showed an average deflection at H/2 and H/3 of 0.22 in. (5.6 mm), and 0.14 in. (3.5 mm), respectively. The NLFEA results are in good agreement with experimental results as shown in Figure 5-35 and Figure 5-36.

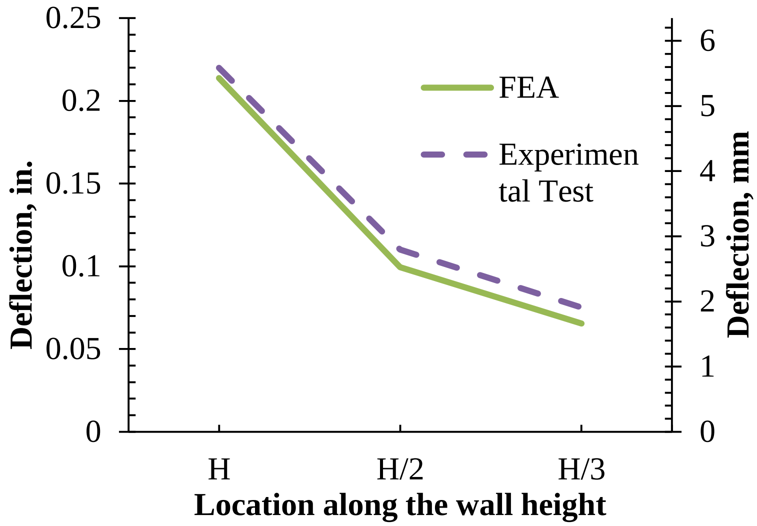

Figure 5-35. Deflection results from the experimental test and NLFEA at service load

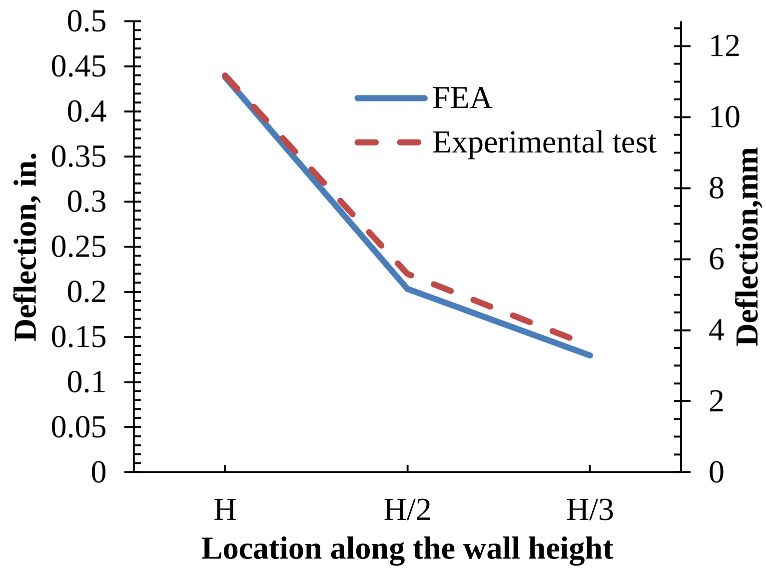

Figure 5-36. Deflection results from the experimental test and NLFEA at Ultimate load

The deflection at the top of the wall was estimated using linear extrapolation for the experimental results. The deflection values at the top were found to be 0.22 in. (5.6 mm) at service load and 0.44 in. (11.17 mm) at ultimate load. The results obtained from linear extrapolation were confirmed using NLFEA as shown in Figure 5-35 and Figure 5-36. The experimental test results compared to NLFEA results are summarized in Table 5-7.

Table 5-7. Summary of Deflection results compared to NLFEA

Load level	Location	Experimental data (in)	NLFEA data (in)	% difference
Ultimate Load (216 kip)	H	0.440	0.438	0.40
	H/2	0.220	0.203	7.59
	H/3	0.140	0.129	7.57
service Load (144 Kip)	H	0.220	0.214	2.82
	H/2	0.110	0.099	9.62
	H/3	0.075	0.065	12.74

1 in.= 25.4 mm, 1 kip = 4.448 kN

On the other hand, The FEA results of the headed anchors showed a good correlation with the experimental test results. The finite element analysis showed that, at ultimate load, the strain was estimated to be around 2780 με in the outermost anchor at 215.5 kip (963.03 kN) load (Test 4). In addition, the trend obtained from the finite element analysis at ultimate load showed that yielding occurs at the first two anchors (Anchors 1 and 2). The strain readings in the anchors decreased when moving closer to the face-panel (moving from anchor 1 to 5).

Comparison of strain readings in the anchors between the experimental test results and the FEA results are presented in Figure 5-37. Inspection of Figure 5-37 shows that the results obtained from the finite element analysis are validated with those obtained from the experimental testing. The anchors exhibited a consistent trend with that of the experimental results. The finite element model verified the behavior of TPCCRW exhibited during experimental testing.

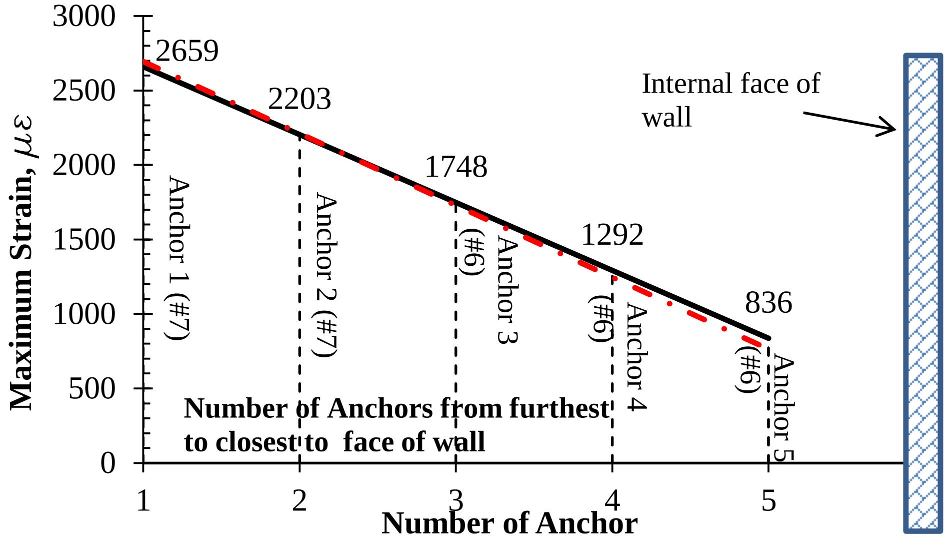

Figure 5-37. Comparison of strain readings in the anchors between experimental results and NLFEA

6. PULLOUT BEHAVIOR OF HEADED ANCHORS USED IN TOTALLY PRECAST CONCRETE COUNTERFORT RETAINING WALL SYSTEM

6.1. Introduction

The study performed by Farhat et al. (2016) outlined the design process of the proposed system. The lateral loads applied to the proposed retaining wall system include lateral soil pressure, and live surcharge load. These loads result in overturning moment at the bottom of the counterforts. The headed anchors are designed to resist the entire applied overturning moment in the form of axial tension as shown in Figure 6-1. In particular, the anchors are designed to yield before breakout in concrete. However, under axial tensile loads, the load carrying capacity of the headed anchors is controlled by the mode of failure anticipated at the anchor-shear pocket level. The mode of failure can be either fracture in steel, grout frictional pullout, or concrete conical breakout (ACI-318). Therefore, short knowledge in the actual mode of failure may result in deference between the design assumptions and the actual structural performance.

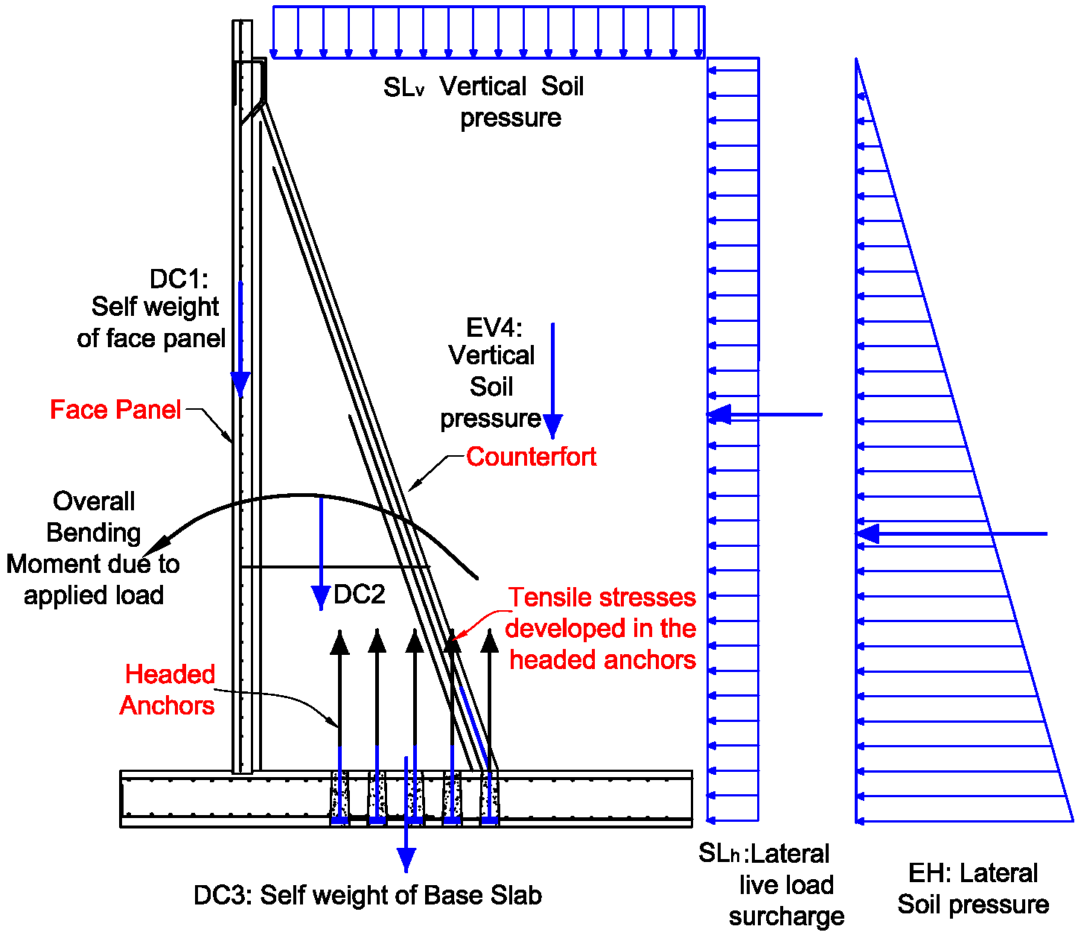

Figure 6-1. Load resistance behavior of headed anchors under applied load

The full scale experimental testing was conducted to assess the overall structural behavior of the system. However, additional investigation of the behavior of the headed anchors at the level of the grouted shear pockets is required.

In this study, an experimental testing program was conducted to examine the pullout behavior of the headed anchors. The study took into account different bar sizes ranging from #6 to #9 bars which can be used in the design process. The study also took into consideration two different commercially available grout types and headed anchors. The anchors were studied with different embedded length to examine the change in the mode of failure associated with changing the embedment depth of the headed anchors. In addition, a detailed 3D finite element analysis was performed using ANSYS package to further investigate the damage development in the anchors and shear pocket under axial loading conditions. The model was calibrated using the results obtained from the experimental testing. Finally, the results obtained from the experimental testing and finite element analysis were compared to the results obtained from the design codes.

6.2. Test Specimens

The experimental testing program was carried out on 18 precast concrete blocks. The following parameters were considered during this study:

- Type of headed anchor: Two commercially available headed anchors were used. The first type is labeled as “D” and the second type is labeled as “P”. The specifications and details for type “D” anchors are shown in Table 6-1. Type “P” has the same specifications as Type “D” but with a head thickness of *38* mm (1.5 in.). It should be mentioned that all bars were epoxy coated to consider worst-case scenario.
- Size of headed anchor: #29 (#9), #25 (#8), #22 (#7), and #19 (#6) headed anchors were considered.
- Type of concrete grout: Two commercially available considered types were considered. These types of grout are certified by the Illinois Department of Transportation (IDOT). The first type of grout is labeled as “Adv” and the second type was labeled as “SG”.
- Embedment depth of headed anchors: The four different embedment depths were 317 mm (12.5 in.), 254 mm (10 in.), 203 mm (8 in.), and 152.4 mm (6 in).

Table 6-1. Specifications and details for headed anchors Type “D”.

Label SI (US)	Bar Diameter mm (in.)	Head Diameter mm (in.)	Head Thickness mm (in.)	P_u kN (lbs)
(#19) #6	19.05 (0.75)	60.12 (2.367)	14.3 (0.563)	176.15 (39.6)
(#22) #7	22.23 (0.875)	70.21 (2.764)	15.88 (0.625)	240.2 (54)
(#25) #8	25.4 (1.0)	80.57 (3.172)	15.88 (0.625)	316.27 (71.1)
(#29) #9	28.65 (1.128)	90.65 (3.569)	17.48 (0.688)	400.34 (90)

The concrete testing specimens were divided into two groups as follows:

1. The first group (labeled A) is composed of 9 concrete blocks having dimensions of 508 mm x 533 mm (20 in. x 21 in.) and 355 mm (14 in.) thickness. All specimens were reinforced with 5 #16 (#5) bars in long direction and 4 #13 (#4) bars in short direction at the top and bottom. Each specimen has a truncated cylindrical shear pocket at the middle with 127 mm (5 in.) top diameter and 152 mm (6 in.) bottom diameter. The geometric details of Group A are presented Figure 6-2.

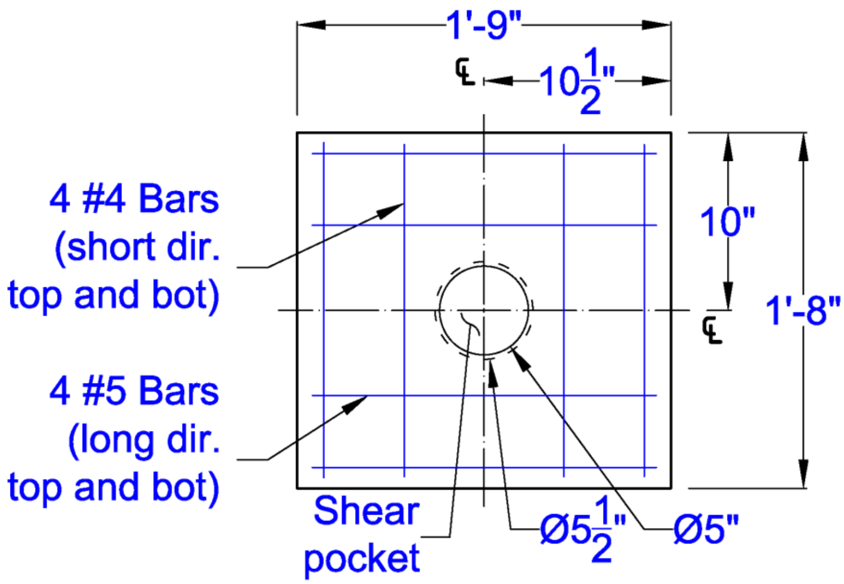

(a) Plan view of precast block type A (1 in. = 25.4 mm)

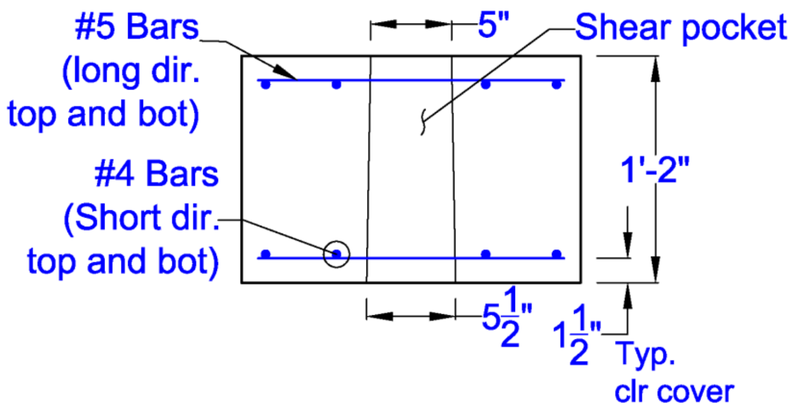

(b) Cross section of precast block type A (1 in. = 25.4 mm)

Figure 6-2 Dimensions and details for the cross section of Block A.

2. The second group (labeled B) is composed of 9 concrete blocks having dimensions of 20 in. x 21 in. and 6 in. thickness. All specimens were reinforced with 5 #16 (#5) bars in long direction and 4 #13 (#4) bars at the top only. Each specimen has a truncated cylindrical shear pocket at the middle with 114 mm (4.5 in.) top diameter and 127 mm (5 in.) bottom diameter. The geometric details of Blocks Type B are presented in Figure 6-3.

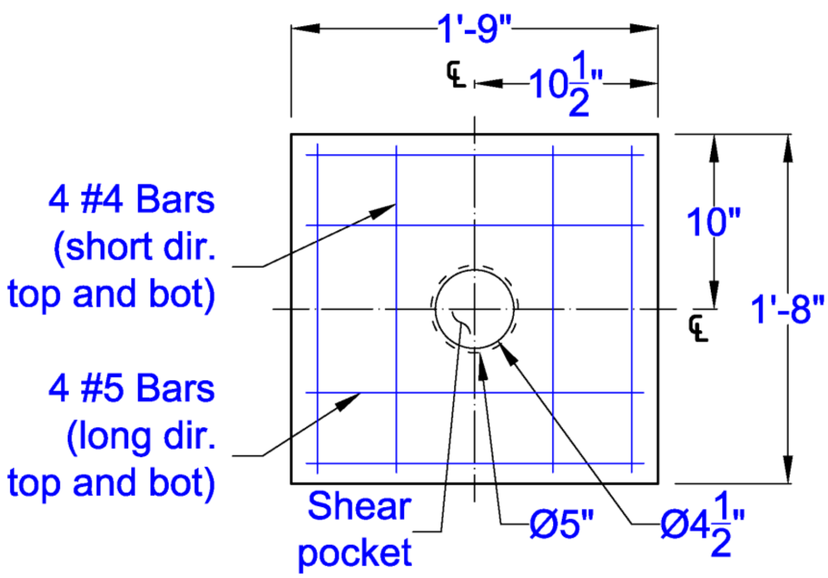

(a) Plan view of precast block type B (1 in. = 25.4 mm)

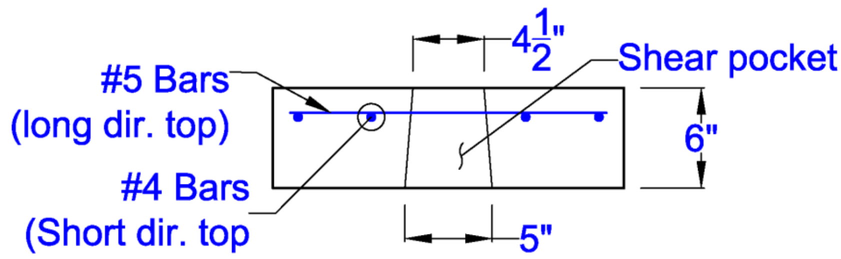

(b) Cross section of precast block type B (1 in. = 25.4 mm)

Figure 6-3. Dimensions and details for the cross section of Block B.

6.3. <u>Material properties</u>

The precast concrete blocks were prepared at the Utility Concrete Products precast plant located in Morris, IL and shipped to UIC for testing. The specimens were cast and cured in optimum conditions in the precast plant. The average concrete compressive strength for the blocks was about 62 Mpa (9000 psi) for all blocks. The grout material was bought by UIC from local suppliers. The grout was mixed and cast at UIC using the proportions provided by supplier. The grout was mixed with 11.33 kg (25 lbs) of pea gravel having a maximum aggregate size of 9.5 mm (3/8 in). The average compressive strength for the grout was about 41.36 Mpa (6000 psi) for all samples. The mix design for the concrete used for the blocks and the two types of the grout is presented in Table 6-2. The headed steel anchors were epoxy-coated grade 60 steel.

Table 6-2 Concrete Mix Design for precast concrete blocks and grout

Material proportions for Mix Design			
Material	**Concrete for Blocks, kg/m^3 (lbs/yd^3)**	**Adv Grout, kg/m^3 (lbs/yd^3)**	**SG Grout, kg/m^3 (lbs/yd^3)**
Sand	785.7 (1325.0)	0.0 (0.0)	0.0 (0.0)
Coarse aggregate	905.5 (1527.0)	678.5 (1144.1)	702.2 (1184.2)
Cementitious materials	415.1 (700.0)	1356.8 (2288.1)	1404.5 (2368.4)
water	157.7 (266.0)	226.6 (382.1)	191.6 (323.1)
w/c ratio	0.38	0.167	0.136
Air content	6.50%	NA	NA

1 lbs/yd^3 = 0.593 kg/m^3

6.4. Experimental Program

6.4.1. Testing schedule

The testing schedule for all concrete blocks is presented in Table 6-3.

Table 6-3. Details for the testing schedule

Qty.	Anchor size and type	Grout Type	Notation	Remarks
2	#29 (#9)-D	Adv	A-#29D-ADV-1 l_d= 318 mm (12.5 in.)	• Block Type: A • Thickness = 355mm (14 in.) • Reinforcing Mat: 5 #16 (#5) Top and Bottom in long direction and 4 #13 (#4) Top and Bottom in short direction • Purpose: Test typical thickness of slab with similar reinforcement. 7.
		SG	A-#29D-SG-2 l_d = 318 mm (12.5 in.)	
1	#25 (#8)-D	Adv	A-#25D-ADV-1	
1	#25 (#8)-P	Adv	A-#25P-ADV-1	
2	#22 (#7)-D	Adv	A-#22D-ADV-1	
		SG	A-#22D-ADV-1	
3	#29 (#9)-D	Adv	A-#29D-ADV-1 l_d = 254 mm (10 in.)	
		Adv	A-#29D-ADV-2 l_d = 203 mm (8 in.)	
		Adv	A-#29D-ADV-3 l_d = 152 mm (6 in.)	
2	#22 (#7)-D	SG	B-#22D-SG-1	

		SG	B-#22D-SG-2	• Block Type: B • Thickness = 177mm (7 in.) • Reinforcing Mat: 5 #16 (#5) Top only in long direction and 4 #13 (#4) Top only in short direction • Purpose: Test small thickness to get breakout on top face only.
1	#22 (#7)-P	SG	B-#22P-SG-1	
1	#25 (#8)-P	SG	B-#25P-SG-2	
2	#25 (#8)-D	SG	B-#25D-SG-1	
		SG	B-#25D-SG-2	
1	#29 (#9)-D	SG	B-#29D-SG-1	
2	#19 (#6)-D	SG	B-#19D-SG-1	
		SG	B-#19D-SG-2	

6.4.2. Specimens preparation

As mentioned earlier, the shear pocket within the concrete blocks were formed at the precast yard using conical cylinders were wrapped with debonding agent. The debonding agent left traces of grease on the interior face of the shear pockets. Therefore, every shear pocket was sand blasted using black diamond abrasive sand at a pressure of 1.03 Mpa (150 psi). After sandblasting, the specimens were cleaned using pressurized air to remove all dust particles remaining from the sand blasting process. Each shear pocket was sealed from the bottom using Styrofoam and filled with clean water allowing it to cure for 24 hours before grouting as shown in Figure 6-4.

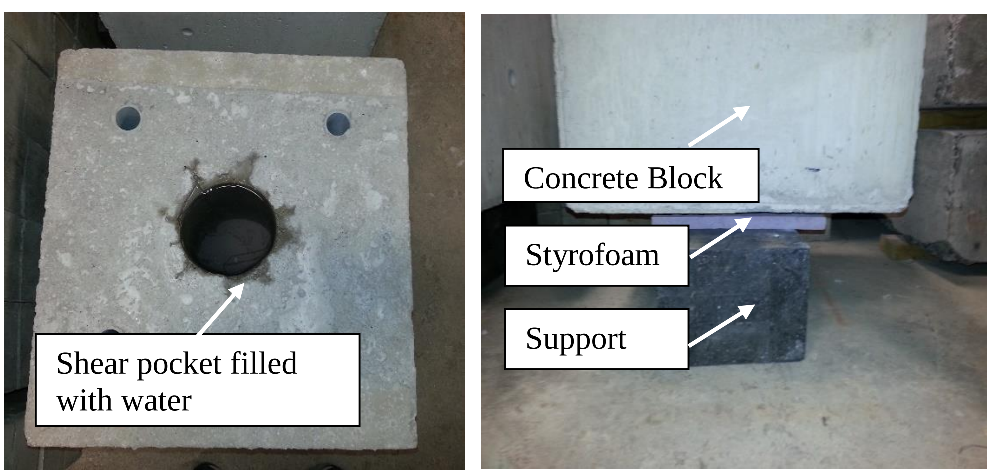

(a) Shear pocket cured with water (b) Curing setup of shear pocket

Figure 6-4 Curing setup for test specimens

The grout was mixed according to the proportions provided by the manufacturer using a mechanical mixer with rotating blades. Each grout bag (22.67 kg (50 lbs)) was dry-mixed for 10 minutes in order to thoroughly mix all the bag constituents. Around 3/4 of the mixture water were added to the grout. The remaining water amount was added later to achieve flowability. The components were mixed for around five minutes.

A special frame was designed to align the headed anchors before casting. Each anchor was placed and leveled in the center of the shear pocket at the desired embedment depth. The curing water was drained out of the shear pocket right before grouting. The specimens preparation setup is shown in Figure 6-5.

Figure 6-5. Specimen preparation setup

6.4.3. Experimental testing

The experimental testing was conducted using a Tinius Olsen automatic hydraulic machine. The tests were performed using a controlled strain rate for steel of 1000 $\mu\varepsilon$/min. The testing machine is composed of two hydraulic systems. A fixed system used to support the top of the concrete block during testing, and a movable system with a loading jaw to apply the load. Each specimen was loaded on the machine and the steel bar was caught with the loading jaw. The experimental setup is presented in Figure 6-6.

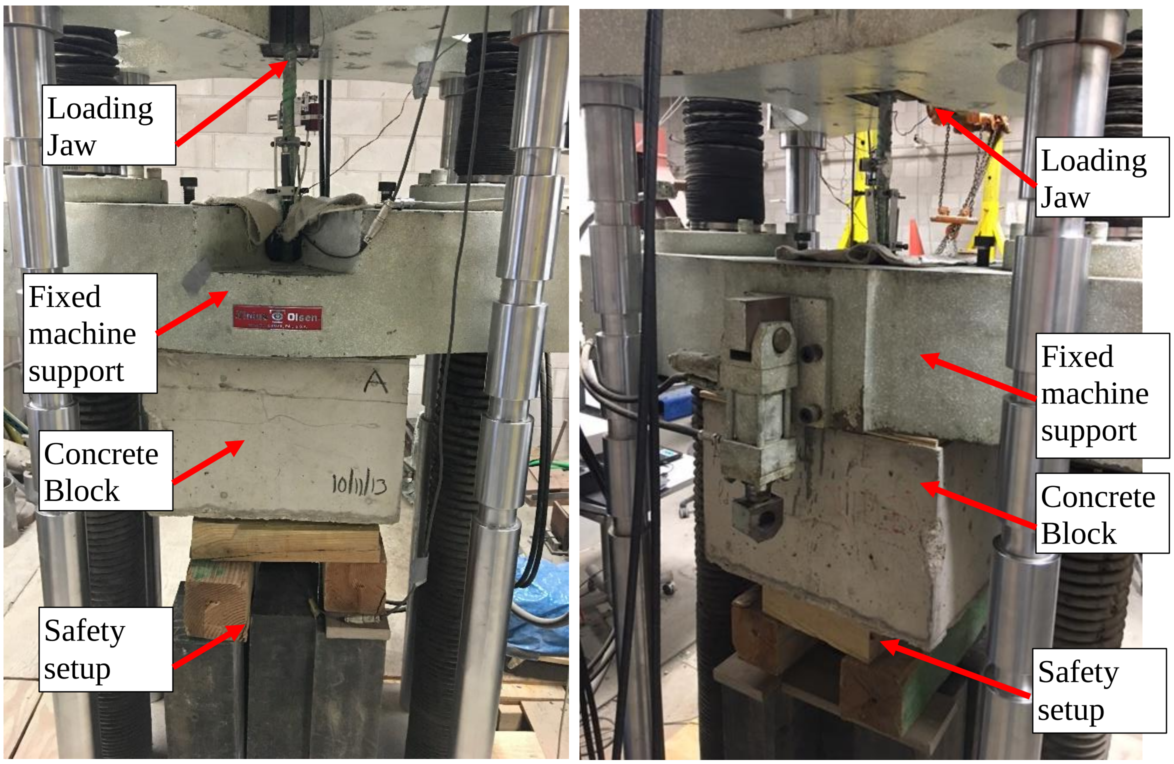

(a) Front view of experimental testing setup (b) Rear view of experimental testing setup

Figure 6-6. Experimental testing setup for the pullout blocks

6.4.4. Instrumentation

Tinius Olsen extensometer with a gauge length of 50.8 mm (2 in.) was used to control the strain rate during testing through feedback signal. The extensometer was mounted on the steel headed bar. In addition, a strain gauge and a Linear Variable Differential Transducer (LVDT) (placed in a special fixture), were used to measure the strain in the steel headed bar as backup readings. The total gauge length of the LVDT fixture was 100 mm (3.93 in.). in order to measure the relative slip, a hole was drilled at the bottom of the blocks at the center line of the steel headed bars and a 25 mm (0.98 in.) LVDT was mounted at the bottom using a designed aluminum fixture. Figure 6-7 represents the typical instrumentation setup.

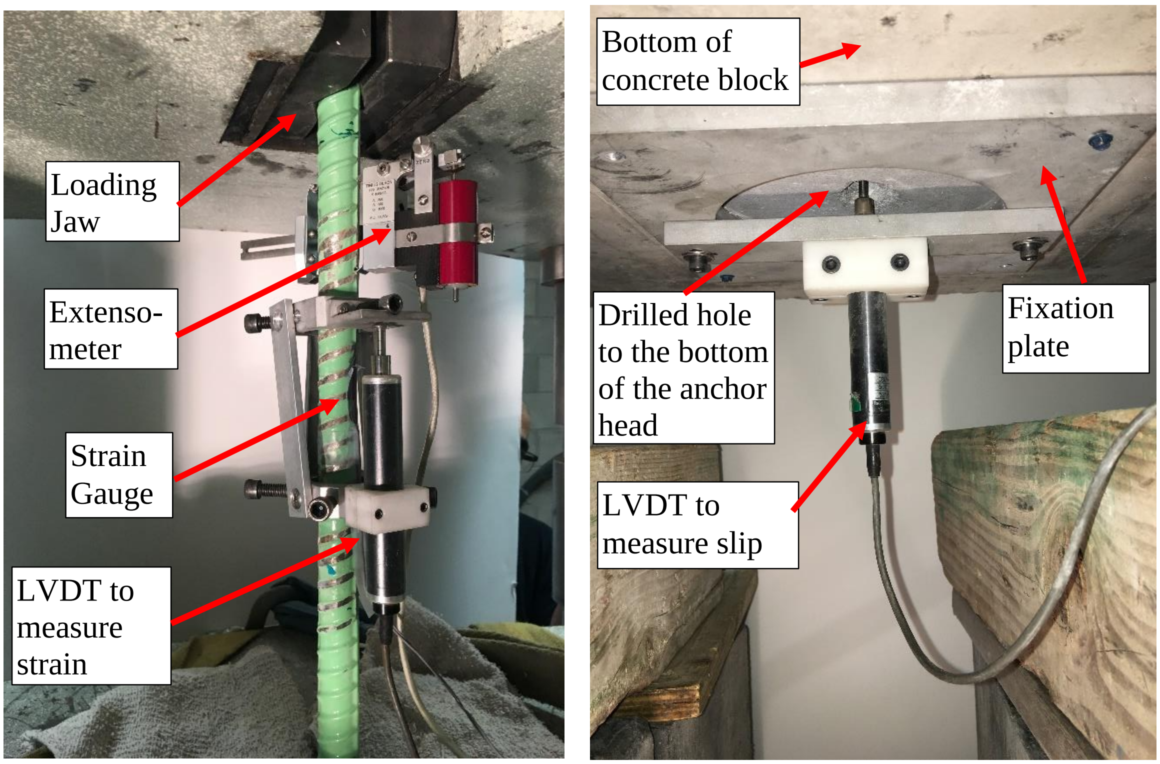

(a) Instrumentation on headed anchor   (b) LVDT at the bottom to measure anchor slip

Figure 6-7. Typical instrumentation setup for the testing blocks

6.4.5. <u>Discussion of experimental test results</u>

6.4.5.1. <u>Effect of bar size</u>

The stress versus strain results of #29 (#9), #25 (#8), and #22 (#7) anchors obtained from the experimental testing are presented in Figure 6-8. Inspection of Figure 6-8 shows that all headed anchors, regardless of bar size, failed by yielding of steel before breakout of concrete. They yielded at a stress around 143.68 Mpa (60 ksi). The post yielding behavior of all anchors is characterized by strain hardening with an increase in stress. The testing was stopped when the strain in the steel anchor exceeded 40,000 με.

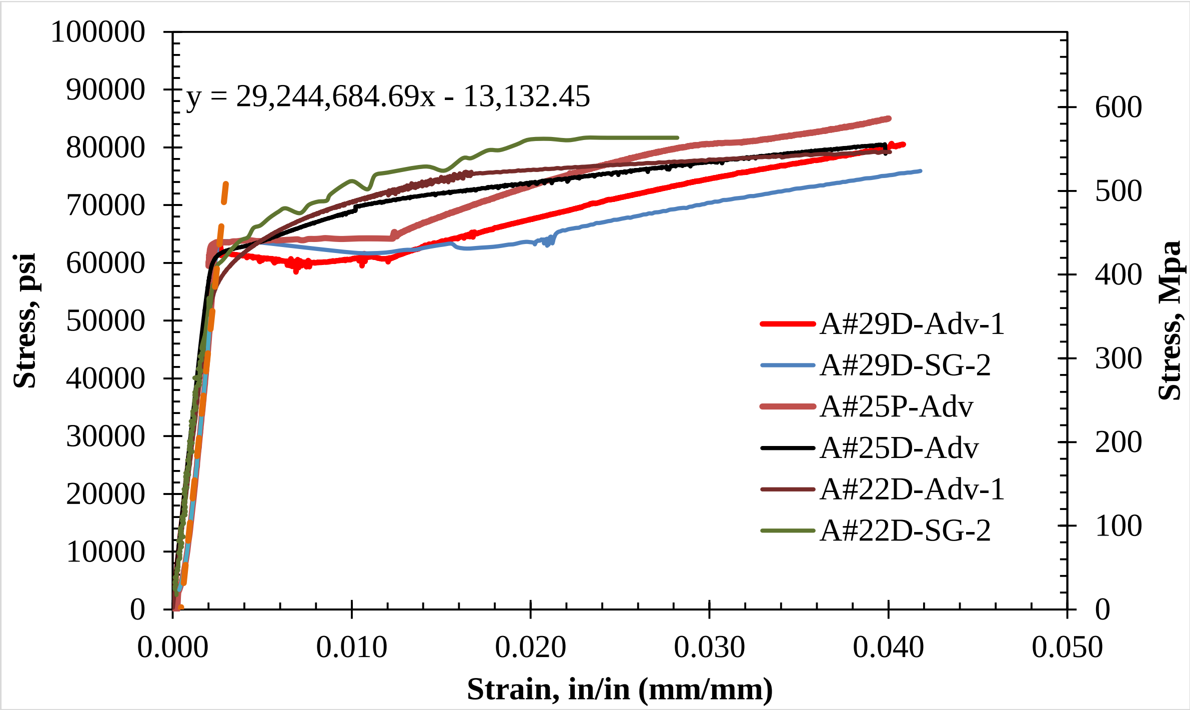

Figure 6-8. Stress versus strain results for Block A specimens with different anchor size

Table 6-4 summarizes the experimental test results for each testing block based on the type of headed anchor. Analysis of Table 6-4 reveals that all headed anchors registered a modulus of elasticity of around 200 Gpa (29,000 ksi). The anchor bars experienced yielding before concrete breakout. This mode of failure was consistent for all three bar sizes. Concrete blocks cast with #25P (#8P) and #25D (#8D) headed anchors (A-#25D-ADV-1, A-#25P-ADV-1) did not show significant difference in the overall behavior. Moreover, block cast with grout type “SG” (A-#29D-SG-2 and A-#22D-SG-1) did show any significant difference in performance compared to the specimens cast with grout type “Adv” (A-#29D-ADV-1 and A-#22D-ADV-1). The ultimate load listed in Table 6-4 represents the load registered by each specimen at the time when the test was ended. The tests were stopped when the strain in the anchor bar exceeded 40,000 με (expect for A-#22D-SG-1).

Table 6-4. Experimental test results for Type A blocks with different bar sizes.

Notation (embed. = 318 mm (12.5 in.))	**Ultimate load**	**Strain at Ultimate load**	**Modulus of elasticity**	**Behavior**
	kN (kips)	**(με)**	**Gpa (ksi)**	
A#29D-Adv-1	358.8 (80.6)	40192	202.71 (29400)	Yielding in anchor
A#29D-SG-2	386.5 (86.8)	48547	201.96 (29292)	Yielding in anchor
A#25D-Adv	283.0 (63.6)	39804	204.62 (29677)	Yielding in anchor
A#25P-Adv	351.2 (78.9)	55110	201.64 (29244)	Yielding in anchor
A#22D-Adv-1	214.4 (48.2)	49009	194.74 (28244)	Yielding in anchor
A#22D-SG-2	218.1 (49.0)	23100	198.30 (28761)	Yielding in anchor

6.4.5.2. Effect of bar embedment depth

The stress versus strain results of #29 (#9) anchors with different embedment depths obtained from the experimental testing are presented in Figure 6-9. Inspection of Figure 6-9 shows that all headed anchors, failed by yielding of steel before breakout of concrete for all cases. The stress versus strain behavior is very consistent for all embedment cases.

According to 318-14 section 25.4.4.2, the development length of epoxy coated headed anchors in tension shall be 14.8 d_b, and not less than 8 d_b or 6 in. with compressive strength not exceeding 41 Mpa (6000 psi). The blocks were tested under axial tensile loading conditions. The conclusions based on this section depend on the quality of grout, good sandblasting, and the fact that the shear pockets solely contain grout material with no confinement reinforcement.

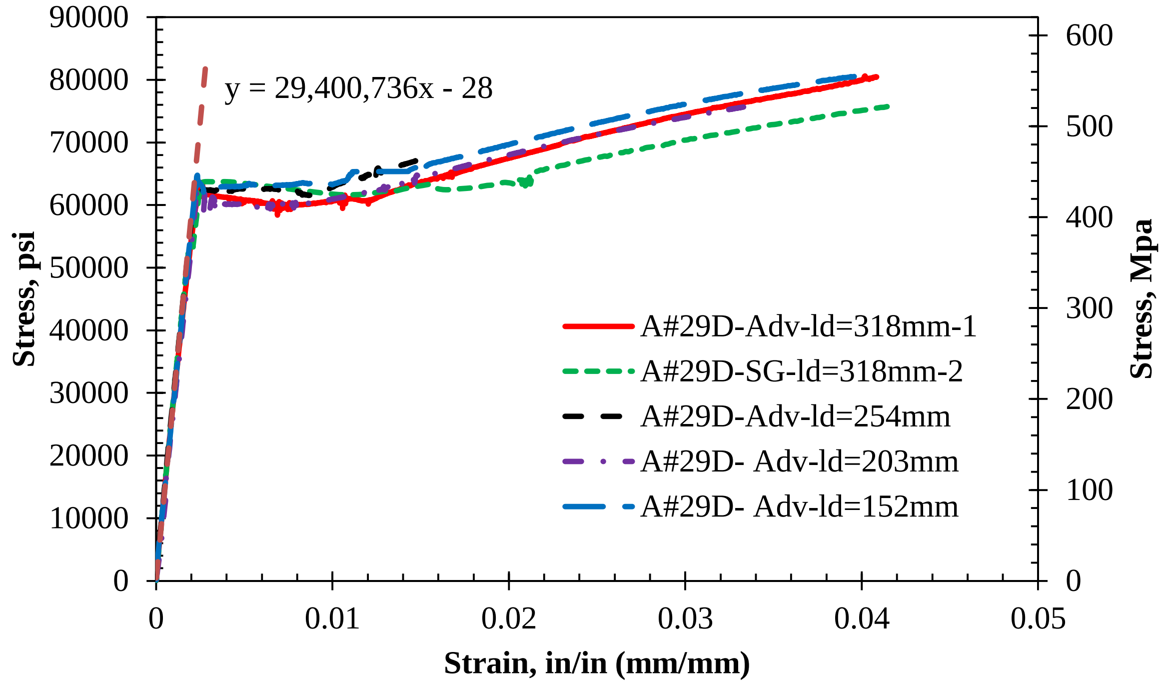

Figure 6-9. Stress versus strain results for Block A specimens with different embedment depth

The tests were stopped when the strain in the anchor bar reached almost 40,000 με of when fracture in the headed steel bar occurred. This result indicates that yielding in the headed steel bar is expected for all cases including shallow embedment depth.

Table 6-5 summarizes the experimental test results for each testing block based on the embedment depth (l_d) of headed anchor. Analysis of The tests were stopped when the strain in the anchor bar reached almost 40,000 με of when fracture in the headed steel bar occurred. This result indicates that yielding in the headed steel bar is expected for all cases including shallow embedment depth.

Table 6-5 reveals that all headed anchors registered a modulus of elasticity of around 200 Gpa (29,000 ksi). Similar to the case of different bar sizes, the anchor bars experienced yielding before concrete breakout. This mode of failure was consistent for all embedment depths. The ultimate load listed in The tests were stopped when the strain in the anchor bar reached almost 40,000 με of when fracture in the headed steel bar occurred. This result indicates that yielding in the headed steel bar is expected for all cases including shallow embedment depth.

Table 6-5 represents the load registered by each specimen at the time of ending the test. The tests were stopped when the strain in the anchor bar reached almost 40,000 με of when fracture in the headed steel bar occurred. This result indicates that yielding in the headed steel bar is expected for all cases including shallow embedment depth.

Table 6-5. Experimental test results for headed blocks with different embedment depths.

Notation	Embed. depth, l_d	Embed. depth to bar ratio,	Ultimate load	Strain at Ultimate load	Mod. of elasticity	Behavior
	mm (in.)		kN (kips)	(με)	Gpa (ksi)	
A#29D-Adv-l_d = 318 mm (12.5 in.)-1	317.5 (12.5)	11.1 d_b	358.7 (80.6)	40192	202.71 (29,401)	Yielding in anchor
A#29D-SG-l_d =318 mm (12.5 in.).- 2	317.5 (12.5)	11.1 d_b	348.1 (78.2)	48547	201.96 (29,292)	Yielding in anchor
A#29D- Adv -l_d = 254 mm (10 in.)	254 (10.0)	8.8 d_b	365.3 (82.1)	39,992	200.36 (29,060)	Yielding in anchor
A#29D- Adv-l_d = 203 mm (8 in.)	203.2 (8.0)	7.1 d_b	339.2 (76.2)	34388	197.28 (29,613)	Yielding in anchor
A#29D- Adv-l_d = 152 mm (6 in.)	152.4 (6.0)	5.3 d_b	358.6 (80.6)	39732	196.96 (28,568)	Yielding in anchor

6.4.5.3. Mode of failure

The mode of failure for the 355.6 (14 in.) specimens (Blocks A) was characterized by yielding of the headed steel anchor at a stress around 413.68 Mpa (60 ksi) followed by strain hardening behavior and necking until fracture of the bar. This result was consistent for all headed anchors with all embedment depths except for the l_d = 152 mm (6 in.) The specimen with 152 mm (6 in.) embedment depth (l_d = 6 in.) the mode of failure was characterized by yielding of steel anchor at a stress of 413.68 Mpa (60 ksi) and breakout of concrete when ultimate load was applied. The cracks extended from the periphery of the grouted shear pocket to the corners of the concrete block. Figure 6-10 shows the mode of failure of all Type A blocks.

(a) Mode of failure of A#9-Adv-ld=12.5in. (typical) (b) Mode of failure of A#9-Adv-6 in.

Figure 6-10. Mode of failure for all Type A specimens and for A#9D-adv with 6 in. embedment depth.

Type B blocks exhibited concrete breakout mode of failure before any yielding in the steel anchors. The typical mode of failure for all Type B specimens is shown in Figure 6-11.

Cracks extended from the periphery of the grouted shear pocket to the corners of the concrete block. This mode of failure was attributed to the small block thickness of Type B specimens. This result indicates that a slab thickness of 152 mm (6 in.) is insufficient to obtain full development length of the headed anchors. After propagation of cracks in the concrete, the shear pockets exhibited separation from the concrete block at the bond interface.

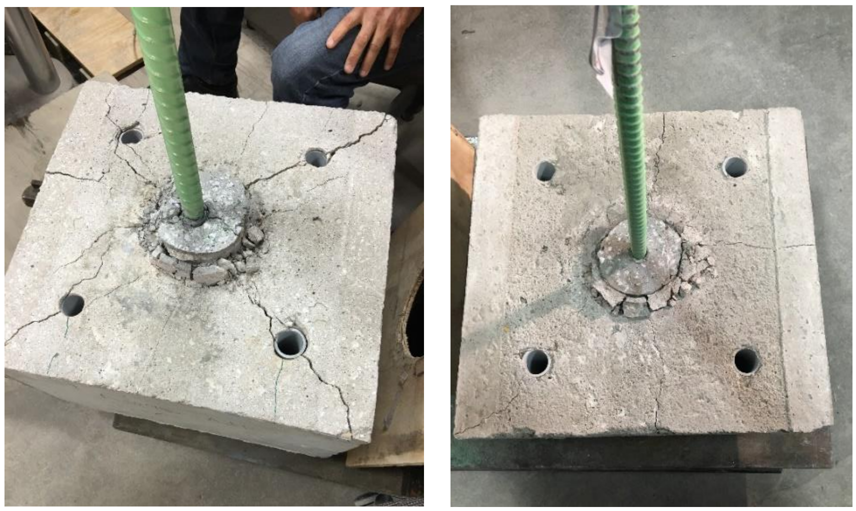

Figure 6-11. Mode of failure of Type B blocks with #7 and #8 bars (typical failure)

6.5. <u>Finite Element Analysis</u>

A detailed nonlinear finite element model was developed using ANSYS® package to analyze the pullout behavior of the headed anchors. The purpose of finite element modeling was to:

- Investigate the pullout behavior of the headed anchors used in TPCCRW.
- Investigate the mode of failure of anchor-shear pocket system,

6.5.1. <u>Finite element model: concrete, grout, anchors, and steel reinforcement</u>

Concrete volume was modeled using SOLID 65 element that is specialized for modeling concrete materials. It allows simulating the cracking and crushing behaviors of concrete. The simulation of cracking and crushing is based on Willam and Warnke model. A uniaxial multilinear stress-strain curve was obtained from concrete cylinder testing and input to the model to define compressive behavior of concrete. A value of 0.2 was used for Poisson's ratio of concrete. The compressive strength, modulus of rupture, and modulus of elasticity of precast concrete were set to 62.1 Mpa (9000 psi), 4.9 Mpa (711 psi), and 37.23 Gpa (5400 ksi), respectively. The modulus of rupture and modulus of elasticity of concrete were calculated according to ACI 318-14 Eq. 19.2.3.1 and Eq.19.2.2.1, respectively. The grout material was modeled separately. The same analytical model was used for the grout, however, the material properties were changed. The compressive strength and flexural strengths of the grout material were set to 41.4 Mpa (6000 psi), 4.0 Mpa (581 psi), and 30.33 Gpa (4400 ksi), respectively.

The headed anchors were modeled using solid 185. This general-purpose element can be used to model steel material. It is defined by eight nodes with three translational degrees of freedom (x, y, and z) at each node. This element can provide plasticity capability. The anchors were modeled with a modulus of elasticity of 200 Gpa (29,000 ksi) and a Poisson's ratio of 0.3.

Steel reinforcement is modeled using Link8 element. The steel material was assumed to be bilinear elastic-perfectly plastic that is identical in both tension and compression with elastic modulus (E) of 200 Gpa (29,000 ksi) and Poisson's ratio of 0.3. The interface between the Link8 concrete elements are assumed fully bonded. The material properties for all components used in finite element analysis are summarized in Table 6-6.

Table 6-6. Material properties for all components used finite element analysis

Component	Property	Value	Unit	Description
Concrete Block	f'_c	62.1 (9000)	Mpa (psi)	Compressive Strength of concrete block
	f_r	4.9 (711)	Mpa (psi)	Modulus of rupture of concrete block
	γ_c	2402.8 (150)	kg/m^3 (pcf)	Unit Weight of Concrete

	E_c	37.23 (5400)	Gpa (ksi)	Modulus of Elasticity of concrete block
	η_c	0.2		Poisson's Ratio
Grout	f'_c	41.4 (6000)	Mpa (psi)	Compressive Strength of grout material
	f_r	4.0 (581)	Mpa (psi)	Modulus of rupture of grout material
	γ_g	2402.8 (150)	kg/m^3 (pcf)	Unit Weight of Concrete
	E_c	30.33 (4400)	Gpa (ksi)	Modulus of Elasticity of grout material
	η_c	0.2		Poisson's Ratio
Headed anchors and steel reinforcement	f_y	413.7 (60)	Mpa (ksi)	Yield Strength of steel
	E_s	200 (29000)	Gpa (ksi)	Modulus of Elasticity of steel
	η_s	0.3		Poisson's Ratio
	γ_s	7849.0 (490)	kg/m^3 (pcf)	Unit Weight of steel

The nonlinear material property for headed steel anchors was taken from results obtained from experimental testing. The stress versus strain obtained was divided into an ascending linear portion until the yielding point at strain of 2,070 με and stress of 413.7 Mpa (60 ksi), a plateau characterized by large strain increase (until 10,000 με) with a slight increase in stress, and a strain hardening portion with increasing strain and stress. The material model using in the FEA for headed anchors is shown in Figure 6-12.

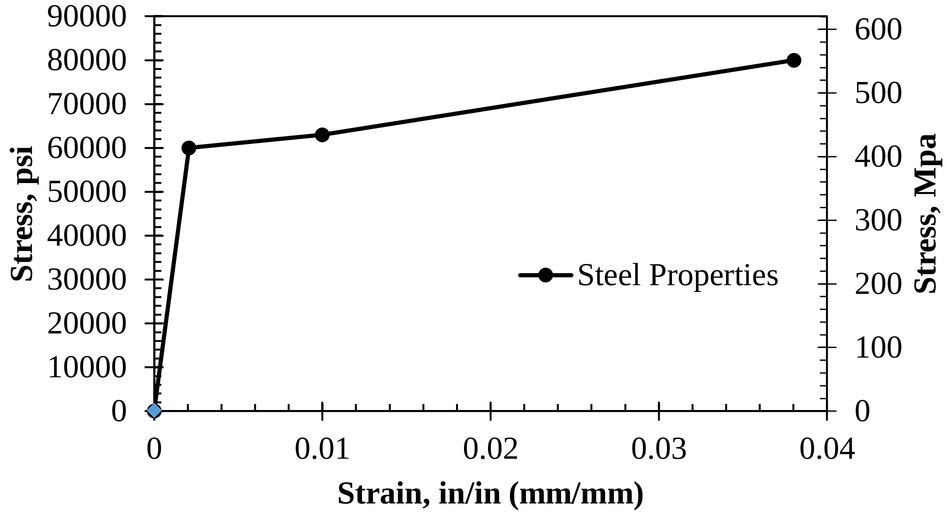

Figure 6-12. Material properties for steel headed anchors used in FEA

6.5.2. Loading and boundary conditions

The boundary conditions were set to mimic the actual testing conditions. The top face of the concrete block excluding the grout zone was restrained from translation in the vertical direction. The loading was applied in the form of displacement in the steel anchor. A total displacement of 50.8 mm (2 in.) was assigned to the top nodes of the steel anchor. A representation of the boundary and loading conditions are shown in Figure 6-13. In order to reduce the computation time, one quarter of the mode was modeled and quarter symmetry boundary conditions were applied. The finite element model and the boundary conditions are shown in Figure 6-13.

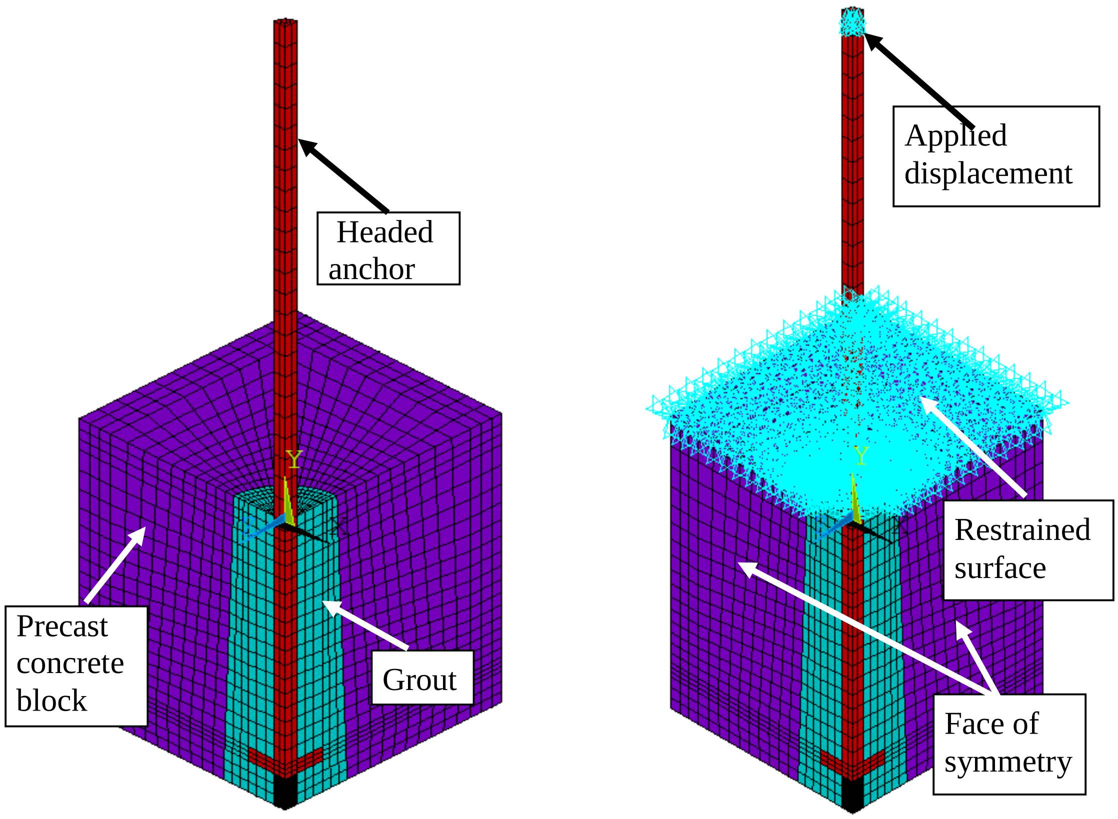

Figure 6-13. Finite element model and boundary conditions

6.5.3. Analysis and discussion of NLFEA results

The structural behavior and the mode of failure of the headed anchors-shear pocket system is discussed based on the finite element analysis results.

6.5.3.1. Behavior of headed anchors:

The results obtained from the finite element analysis show that all headed anchors yielded when the tensile stresses reached 413.7 Mpa (60 ksi). The load versus strain results obtained from the finite element analysis for #29 (#9), #25 (#8), and #22(#7) headed anchors are shown in Figure 6-14. Inspection of Figure 6-14 reveals that #29 (#9) headed anchor yielded at a load of 266.9 kN (60,000 lbs). In addition, #25 (#8) headed anchors yielded at a load of 210.84 kN (47,400 lbs) and #22 (#7) headed anchors yielded at a load of 162.8 kN (36,000 lbs). The general behavior of the headed anchor depicted that of the assigned material property because the mode of failure of the headed bars was characterized by yielding before major damage in the concrete. Therefore, all headed anchors were characterized by an increasing elastic behavior until reaching the yielding point of 413.7 Mpa (60ksi), followed by a plateau with slight increase in the stress until reaching a strain of 10,000 με, and followed by a strain hardening behavior.

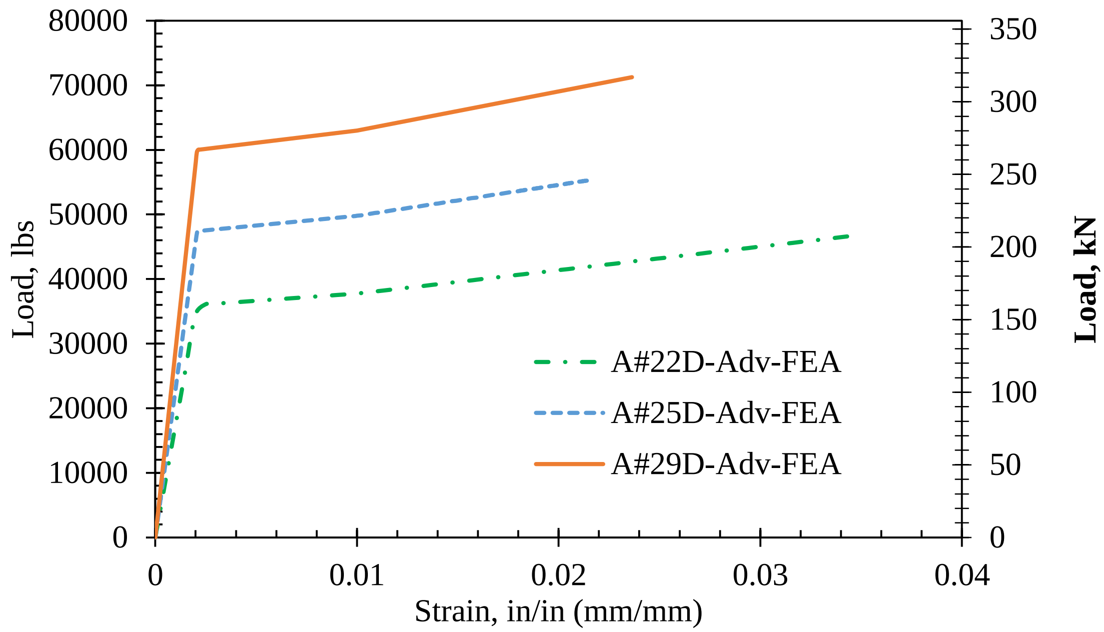

Figure 6-14. Load versus strain results obtained from the finite element analysis using for #9, #8, and #7 headed anchors

6.5.3.2. Behavior of shear pocket:

The results obtained from the finite element analysis show that development of minor cracks in the shear pocket after yielding of headed anchors. It was noticed that the cracks propagated in a conical shape at an angle varying between 26° and 42° as shown in Figure

6-15. This observation is consistent with ACI 318-14 code and AISC CCD method for calculating the breakout capacity of concrete.

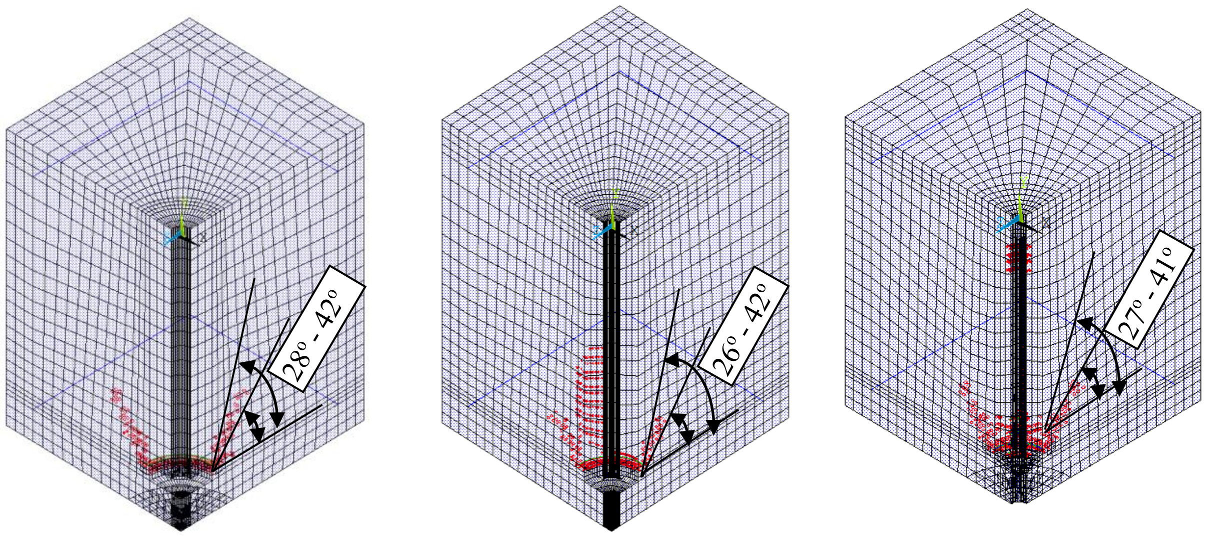

(a) Number 9 anchor (b) Number 8 anchor (c) Number 7 anchor

Figure 6-15. Development of cracks in the shear pocket from finite element analysis

6.6. Validation of NLFEA results with experimental results

The results obtained from the finite element analysis were compared to those obtained from the experimental investigation. Figure 6-16 represents the load versus strain for all specimens having an embedment depth of 317 mm (12.5 in). obtained from the experimental test results and the FEA. Investigation of Figure 6-16 reveals a very good correlation between the experimental testing results and the finite element analysis results. The finite element model was capable of predicting the structural behavior and the mode of failure of the pullout specimens.

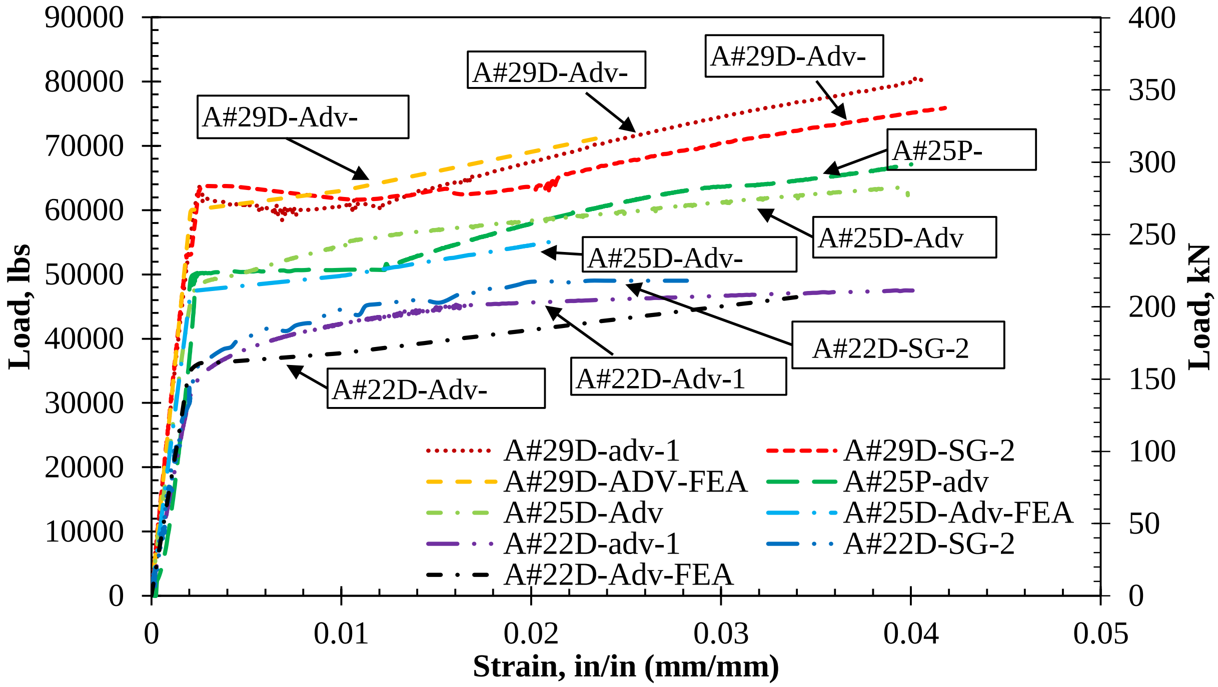

Figure 6-16. Load versus strain for all specimens having an embedment depth of 318 mm (12.5 in.) obtained from the experimental test results and the FEA

6.7. Comparison with design codes

reveals that there is a close correlation between the experimental test results and AISC "Base Plate and Anchor Design Guide" for concentric compressive axial load. The average percentage difference between the experimental result and AISC was around 13.3% for #29 (#9) anchors, 1.8% for #25 (#8) anchors, and 11.7% for #22 (#7) anchors. The ASCE CCD method was found correlate well with #9 and #8 headed anchors with 317 mm (12.5 in). embedment length. The percentage differences between the experimental test results and ASCE CCD method for #29 (#9) and #25 (#8) were 5.24% and 6.32%, respectively. However, the ASCE CCD method was found to overestimate the strength of #22 (#7) anchors (percentage difference is 36.1%). Moreover, when the embedment length was reduced the estimated strength using CCD method showed very conservative results compared to experimental testing results. to underestimate the strength of the headed anchors. The studies performed by Thompson et al., DeVries, and Francesco Marchetto at the university of Texas did not correlate well with the experimental test results. The ACI 318-14 Concrete Breakout Strength in Tension (ACI 318-14 17.4.2) was found to underestimate the concrete breakout capacity. In fact, this method does not take into account the effect of the size of the headed anchors.

Table 6-7 shows a comparison between the results obtained from the experimental testing, design codes, and studies found in the literature. Analysis of reveals that there is a close correlation between the experimental test results and AISC “Base Plate and Anchor Design Guide” for concentric compressive axial load. The average percentage difference between the experimental result and AISC was around 13.3% for #29 (#9) anchors, 1.8% for #25 (#8) anchors, and 11.7% for #22 (#7) anchors. The ASCE CCD method was found correlate well with #9 and #8 headed anchors with 317 mm (12.5 in). embedment length. The percentage differences between the experimental test results and ASCE CCD method for #29 (#9) and #25 (#8) were 5.24% and 6.32%, respectively. However, the ASCE CCD method was found to overestimate the strength of #22 (#7) anchors (percentage difference is 36.1%). Moreover, when the embedment length was reduced the estimated strength using CCD method showed very conservative results compared to experimental testing results. to underestimate the strength of the headed anchors. The studies performed by Thompson et al., DeVries, and Francesco Marchetto at the university of Texas did not correlate well with the experimental test results. The ACI 318-14 Concrete Breakout Strength in Tension (ACI 318-

14 17.4.2) was found to underestimate the concrete breakout capacity. In fact, this method does not take into account the effect of the size of the headed anchors.

Table 6-7 reveals that there is a close correlation between the experimental test results and AISC "Base Plate and Anchor Design Guide" for concentric compressive axial load. The average percentage difference between the experimental result and AISC was around 13.3% for #29 (#9) anchors, 1.8% for #25 (#8) anchors, and 11.7% for #22 (#7) anchors. The ASCE CCD method was found correlate well with #9 and #8 headed anchors with 317 mm (12.5 in). embedment length. The percentage differences between the experimental test results and ASCE CCD method for #29 (#9) and #25 (#8) were 5.24% and 6.32%, respectively. However, the ASCE CCD method was found to overestimate the strength of #22 (#7) anchors (percentage difference is 36.1%). Moreover, when the embedment length was reduced the estimated strength using CCD method showed very conservative results compared to experimental testing results. to underestimate the strength of the headed anchors. The studies performed by Thompson et al., DeVries, and Francesco Marchetto at the university of Texas did not correlate well with the experimental test results. The ACI 318-14 Concrete Breakout Strength in Tension (ACI 318-14 17.4.2) was found to underestimate the concrete breakout capacity. In fact, this method does not take into account the effect of the size of the headed anchors.

Table 6-7. Comparison between experimental test results, design codes, and studies in literature

Method	Failure load, kN (kip)					
	#29 l_d = 317 mm (12.5 in.)	#29 l_d = 254 mm (10 in.)	#29 l_d = 203 mm (8 in.)	#29 l_d = 152 mm (6 in.)	#25 l_d = 317 mm (12.5 in.)	#22 l_d = 317 mm (12.5 in.)

Experimental Test results		353.32 (79.43)	365.20 (82.10)	339.04 (76.22)	358.48 (80.59)	316.98 (71.26)	216.18 (48.60)
AISC – Concentric Compressive Axial Load		408.57 (91.85)	408.57 (91.85)	408.57 (91.85)	408.57 (91.85)	322.90 (72.59)	244.96 (55.07)
AISC – Tensile Axial Load	Concrete Pullout Strength	1153.60 (259.34)	1153.60 (259.34)	1153.60 (259.34)	1153.60 (259.34)	911.75 (204.97)	691.65 (155.49)
	CCD	235.00 (52.83)	164.50 (36.98)	114.45 (25.73)	70.86 (15.93)	235.00 (52.83)	235.00 (52.83)
ACI 318 - 14	Concrete Breakout Strength in Tension	102.09 (22.95)	102.09 (22.95)	102.09 (22.95)	102.09 (22.95)	102.09 (22.95)	102.09 (22.95)
UT – DeVries et al		359.19 (80.75)	359.19 (80.75)	359.19 (80.75)	359.19 (80.75)	290.16 (65.23)	252.93 (56.86)
UT – Thompson	Bearing Strength	298.12 (67.02)	298.12 (67.02)	298.12 (67.02)	298.12 (67.02)	265.03 (59.58)	230.82 (51.89)
Francesco Marchetto	Design Values	290.47 (65.30)	290.47 (65.30)	290.47 (65.30)	290.47 (65.30)	496.73 (111.67)	490.91 (110.36)

(1) Averaged between A-#29D-ADV-1 and A-#29D-SG-2

(2) Averaged between A-#25D-ADV-1 and A-#25P-ADV-2

(3) Averaged between A-#22D-ADV-1 and A-#22P-SG-2

7. SUMMARY AND CONCLUSIONS

7.1. Summary

This research was conducted to evaluate the structural performance of Totally Precast Concrete Counterfort Retaining Wall (TPCCRW) system for highway applications. The study was divide into four sections.

In the first section, the study develops the design principles for TPCCRW. The system was compared to an existing counterfort cast in place retaining wall system. The comparison was focused on design, structural efficiency, and economic aspects. A parametric study was performed to assess the performance of the proposed system in increasing heights.

In the second section, description and illustrations of the construction procedures and practices involved in the Totally Precast Concrete Counterfort Retaining Wall system were presented. The main advantages of the proposed system are: 1) the enhanced durability compared to its cast-in-place counterpart, 2) reduced traffic interruption due to this construction, and 3) fast track construction. It provides the contractor with the capability to fabricate all the components off-site and to transport them to the construction site in order to immediately proceed with the construction process. The guidelines for fabrication off-site and the construction processes of the proposed retaining wall system were detailed.

In the third section, a full scale experimental testing and nonlinear finite element analysis were performed to examine the overall structural behavior of the proposed system. The tested model was 20 ft - 2 in. (6.09 m) high and 13 ft – 10 in. (4.21 m) wide. The wall was optimized using conventional beam theory and finite element analysis.

The wall was subjected to soil backfilling, live load surcharge, and additional load using hydraulic cylinders reaching up to 192.4 kips (855.83 kN) to carry the system to ultimate load. The deflection in the face panel at H/3 and H/2 was monitored. In addition, strain readings in the headed anchors, counterforts main reinforcement, face panel, and base slab were monitored and presented. The results of the finite element analysis were compared and validated with the experimental testing results.

In the fourth section, an experimental study and nonlinear finite element analysis were performed to examine the overall breakout behavior of headed anchors subjected to tensile loading. Eighteen precast concrete blocks of 508 mm x 533 mm (21 in. x 20 in.) having a shear pocket identical to those used in TPCCRW were prepared, grouted with headed anchors, instrumented and experimentally tested. The specimens were prepared using minimum area of steel reinforcement and the shear pockets were sandblasted before grouting. The study took into consideration two different block thicknesses of 355 mm and 152 mm (14 in. and 6 in.), two IDOT certified types of headed anchors and types of concrete grout, different bar sizes of #29 (#9), #25 (#8), #22 (#7), and #19 (#6), and different embedment depths of 317 mm (12.5 in.), 254 mm (10 in.), 203 mm (8 in.), and 152.4 mm (6 in). The blocks were tested under axial tensile loading conditions. The conclusions based on this section depend on the quality of grout, good sandblasting, and the fact that the shear pockets solely contain grout material with no confinement reinforcement.

7.2. Conclusion

7.2.1. Design principles of TPCCRW

The following conclusions can be drawn from the first section of this study:

- Totally precast concrete counterfort retaining wall system is an efficient solution for fast track construction. It also provides the advantage of minimal energy use, accelerated construction, the use of high strength construction materials in a consistent and accurate fabrication process, congestion reduction, and safety promotion.
- A reduction in the counterfort spacing-to-base length ratio from 0.84 for a typical design to 0.35 causes a significant reduction in concrete volume reaching 57%. This results in cost savings in both materials and time of construction.
- Counterfort extension to heel length ratio of 0.6 has shown to be optimum for the design of the proposed system. It results in significant reduction in the weight of the components reaching 54% compared to the existing structure. Simultaneously, it satisfies the code requirements for moment and shear strengths.
- The tapered design of the shear pocket enhances the resistance of the anchors against pullout loads. The results show that the grout used is capable of resisting the shear and bearing forces and maintain the integrity between the wall component and the base slab.
- The headed anchors, which extend from the counterforts to the base slab, are verified to maintain the integrity of the system by resisting the shear forces at the interface between the wall and the base components.
- The proposed system is a cost-efficient and structurally adequate alternative that can be used in bridge and highway applications.

7.2.2. Fabrication and construction procedures

The following conclusions can be drawn from the second section of this study:

This system provides the contractor with the capability to prefabricate all the components off-site and to transport them to the construction site in order to immediately proceed with the construction process. The guidelines for fabrication off-site and the construction processes of the proposed retaining wall system were presented. A crane is needed in the second and third stages of the erection process. However, it is optional in the fourth stage depending on the safety measures adopted by the contractor and wind exposure. Each phase of the erection process must be followed by leveling and alignment work before placing the grout. The estimated construction period of the system is approximately 8 hours if fast setting grout is used. The guidelines presented help accelerate the learning experience of the contractors which results in time saving during construction.

7.2.3. Full scale experimental testing and finite element analysis of TPCCRW

Based on the experimental testing and the FEA results presented in the third section, the following can be concluded:

- Headed anchors showed excellent performance in maintaining the composite action between the precast wall and the base slab at service and ultimate loads. This was verified by the NLFEA and the experimental testing. The deflection measured at the mid-height of the wall was found to be around 0.2 in. Counterforts added stiffness to the structure by increasing the section at which the bending moment due to the applied load is resisted. The L-bars that connected the face-panel to the stems were found to be very effective in maintaining the composite action between both components.
- The strain readings in the anchors indicate that the outermost anchors experience the highest strain. The design is controlled by outermost anchors and smaller bar size can be

used for anchors close to the face-panel as they experience smaller tensile strain. In addition, the strain readings in the main steel of the counterforts showed that the counterforts are resisting the entire applied later load. Therefore, two assumptions can be made by the designer:

- The anchors should be properly designed properly to resist the entire applied bending moment and shear forces
- When the anchors are designed, and the main steel in the counterforts should be designed to resist the entire lateral load assuming that the bottom of the counterforts is fully bonded to the base slab.
- The anchors play another important role in maintaining the overall stability of the system.
- The steel in the face-panel showed insignificant and almost equivalent readings in the positive and negative regions. This supports the assumption that the cross section can be significantly reduced and one layer of steel can be used to resist both positive and negative bending moments. This reduces the overall concrete volume, which provides great advantages in transportation and cost reduction.
- Cracks can initiate in the regions of the internal anchors, which are subjected to tensile stresses. These cracks propagate towards the web of the counterforts with the increase of load. The spacing between vertical reinforcements in the web should be reduced to 6 in. in order to provide arrest mechanism of the cracks and prevent shear failure in the counterforts as verified by FEA.

- Totally Precast Concrete Counterfort retaining wall system exhibits a good performance to be utilized for highway applications. It satisfies the need for fast track construction. Although the impact factor specified by AASHTO LRFD specifications was implemented in the design, further research might be required to study the behavior of TCCPRW under traffic collision force.

7.2.4. Pullout behavior of headed anchors used in TPCCRW

Based on the experimental testing and the FEA results presented in the fourth section, the following can be concluded:

- The experimental test results showed good correlation with the AISC design guide for anchor rods. ACI 318-14 seemed to underestimate the concrete breakout capacity.
- The difference in the type did not show any effect on the overall performance of the headed anchors.
- The headed anchor size and the difference in the embedment depth did not affect the failure mode. Specimen with 152 mm (6 in.) embedment depth failed by yielding of steel anchor and breakout of concrete at ultimate load. However, this only occurred at ultimate load after yielding of the headed anchors. It can be safely assumed in the structural design that the headed anchors will yield before breakout of concrete regardless of the headed anchor size, grout type, and embedment depth of at least 152 mm (6 in.).
- Finite element analysis confirms angle of crack propagation in the shear pocket with the AISC design guide for headed anchors. The angle varied between 26^{o} and 42^{o}.
- The headed anchor size and the difference in the embedment depth did not affect the failure mode. Specimens with 152 mm (6 in.) embedment depth failed by yielding of steel

anchor and breakout of concrete at ultimate load. However, this only occurred at ultimate load after yielding of the headed anchors. It can be safely assumed in the structural design that the headed anchors will yield before breakout of concrete regardless of the headed anchor size, grout type, and embedment depth more than 152 mm (6 in.) (preferably 254 mm (10 in.) to be on the safe side).

- Based on the results obtained from the experimental testing program and the nonlinear finite element analysis, headed anchors of any size (up to #29 (#9)) and any embedment depth (not less than 152 mm (6 in.)) can be safely used in the design of TPCCRW without the risk of concrete breakout before yielding of steel.

7.3. Recommendation for Future Work

1. This work entails a full study for the structural performance of TPCCRW. This work can be extended to involve totally precast concrete counterfort abutment systems for bridge application. The implementation of such system will result in reduction in construction time, expenses, and environmental costs. The finite element model was calibrated based on the experimental testing results. Therefore, the application of this model can be extended to account for loads applied on abutments.

2. The study presented in this thesis took into account service and strength limit states as per ASSHTO LRFD. However, the structural performance of TPCCRW under Extreme Event limit state can be evaluated. This includes studying the structural performance under impact load due to collision when a barrier is located at the top of the wall. The study should Test Level 5 (TL-5) collision load as per AASHTO/MASH criteria.

3. Investigate the adequacy of the proposed system to be used in railway application. This can be done using finite element analysis by taking into account surcharge loads corresponding to rail applications.

CITED REFERENCES

AASHTO (American Association of State Highway and Transportation Officials). 2012. LRFD bridge design specifications. Washington, D.C. customary U.S. unit.

ACI Committee, American Concrete Institute, and International Organization for Standardization. "Building code requirements for structural concrete (ACI 318-14) and commentary." American Concrete Institute, 2014.

Al-Rousan R., and M. Issa. 2011. Fatigue performance of reinforced concrete beams strengthened with CFRP sheets, *Construction and Building Materials*, 25(8). (August): pp. 3520-3529.

American Concrete Institute (2011). Building Code Requirements for Structural Concrete (ACI 318–11) and Commentary.

ANSYS User's Manual (Release 11.0 Documentation), ANSYS, Inc., Canonsburg, Pennsylvania, USA

ANSYS User's Manual (Release 11.0 Documentation), ANSYS, Inc., Canonsburg, Pennsylvania, USA

Badie S. S., M. C. Baishya, and M. K. Tadros. 1998. NUDECK- An efficient and economical precast prestressed bridge deck system. *PCI Journal*. 43(5). (Sept.-Oct.): pp. 56-74.

Billington S. L., R. W. Barnes, and J. E. Breen. 2001. Alternate Substructure Systems for Standard Highway Bridges. Journal of Bridge Engineering, 6 (2), (Mar.-Apr.): pp. 87-94.

Billington, S. L., R. W. Barnes, and J. E. Breen. 1999. “A precast segmental substructure system for standard bridges.” *PCI journal*. 44(4): pp. 56-73.

Biswas M. 1986. Precast Bridge Deck Design Systems. *PCI Journal*. 31(2). (Mar.-Apr.): pp. 40-94.

Bowles E. J. 1996. Foundation analysis and design. McGraw-Hill. ISBN-0-07-912247-7. pp. 313-317.

Bowles, E. Joseph. 2001. Foundation analysis and design. McGraw-Hill. ISBN-10: 0071188444

Cannon RW, Burdette EG, Funk RR (1975) Anchorage to concrete—Report No. CEB 75-32. Tennessee Valley Authority, Knoxville.

Culmo M. P. 1991. Bridge deck rehabilitation using precast concrete slabs. *Eight Annual International Bridge Conference*, Paper No. IBC-91-55: pp. 389-396.

Culmo M. P. 2002. Rapid bridge deck replacement with full-depth precast concrete slabs. *Transportation Research Record 1712. Transportation Research Board. Washington D.C.:* pp. 139-146.

Culmo M.P. 2009. Connection Details for Prefabricated Bridge Elements and Systems. *FHWA-IF-09-010*. (March): pp. 568.

Darwish I., M. Kasi, and Alfred Benesch & Company. 2013. Innovative Precast Concrete Cantilever Retaining Wall System. ASPIRE (Spring): pp 2.

Delhomme, F., Roure, T., Arrieta, B., & Limam, A. (2016). Pullout behavior of cast-in-place headed and bonded anchors with different embedment depths. Materials and Structures, 49(5), 1843-1859.

Donkada S., and D. Menon, 2012. Optimal design of reinforced concrete retaining avails. *The Indian Concrete Journal.* (April): pp. 9-18.

Eligehausen R, Balogh T (1995) Behavior of fasteners loaded in cracked reinforced concrete. ACI Struct J 92(3):365–379

Farhat, M., and Issa, M.A., "Design Principles of Totally Precast Concrete Counterfort Retaining Wall System Compared to Existing Cast-In-Place Structures," Paper Submitted to the PCI Journal, 2016, In Review.

Farhat, M., and Issa, M.A., "Fabrication and Construction of Totally Precast Concrete Counterfort Retaining Wall System for Highways," Paper Submitted to the Practice Periodical of Structural Engineering, 2016, In Review.

Farhat, M., Ibrahim, M., Issa, M.A., and Rahman, M., "Full Scale Experimental Testing and Finite Element Analysis of Totally Prefabricated Counterfort Retaining Wall System," Paper Submitted to *PCI Journal*, 2016, In Review.

Farhat, M., M. A. Issa, M. Rahman. 2015. Design Optimization and Modeling of Totally Precast Concrete Counterfort Retaining Wall System. *Proc. of 16th European Bridge Conference*, Edinburgh, Scotland. June 25th, 2015.

Farhat, M., M. Rahman, M. Ibrahim, M. A. Issa. 2014. Design, Fabrication, Modeling and Experimental Study of a Totally Precast Concrete Counterfort Retaining Wall System for

Highways. *Proc. Of 2014 Pci Convention and National Bridge Conference*, Washington D.C., Paper no. 112.

Fuchs, W.; Eligehausen, R.; and Breen, J., 1995, "Concrete Capacity Design (CCD) Approach for Fastening to Concrete," ACI Structural Journal, V. 92, No. 1, Jan.-Feb. 1995, pp. 73-93.

Goldberg, D. (1987). "Precast Prestressed Concrete Bridge Deck Panels." *PCI Journal*, 32(2), 26-45.

Goldberg, D. 1987. "Precast Prestressed Concrete Bridge Deck Panels," PCI Journal, 32 (2). (Mar.-Apr): pp 26-45.

Guide, S. D. (2006). Base plate and anchor rod design. AISC, Chicago.

Hewes J. T. 2013. Analysis of the State of the Art of Precast Concrete Bridge Substructure Systems. AZTrans: The Arizona Laboratory for Applied Transportation Research. Final Report FHWA-AZ-13-687: PP. 124

Hieber, D., J. M. Wacker, M. O. Eberhard, and J. F. Stanton. 2005. State-of-the-art report on precast concrete systems for rapid construction of bridges. Rep. No. WA-RD 594.1, Washington State Department of Transportation.

Issa, M., Idriss, A. T., Kaspar, I. I., & Khayyat, S. Y. (1995c). Full depth precast and precast, prestressed concrete bridge deck panels. PCI journal, 40(1), 59-80.

Issa, M., Yousif, A. A., & Issa, M. A. (1995a). Construction procedures for rapid replacement of bridge decks. *Concrete International*, *17*(2), 49-52.

Issa, M., Yousif, A. A., & Issa, M. A. (2000). Experimental behavior of full-depth precast concrete panels for bridge rehabilitation. *ACI Structural Journal*, *97*(3), 397-407.

Issa, M., Yousif, A. A., Issa, M. A., Kaspar, I. I., & Khayyat, S. Y. (1995b). Field performance of full depth precast concrete panels in bridge deck reconstruction. *PCI Journal*, *40*(3), 82-108.

Issa, M., Yousif, A. A., Issa, M. A., Kaspar, I. I., & Khayyat, S. Y. (1998). Analysis of full depth precast concrete bridge deck panels. *PCI journal*,*43*(1), 74-85.

Kachlakev, D., T. Miller, S. Yim, K. Chansawat, and T. Potisuk. 2001. Finite element modeling of concrete structures strengthened with FRP laminates.*Final report, SPR, 316*.

Kachlakev, D., T. Miller, S. Yim, K. Chansawat, and T. Potisuk. 2001. Finite element modeling of concrete structures strengthened with FRP laminates.Final report, SPR, 316.

Kim, T. H. 2013. Comparison of Totally Prefabricated Bridge Substructure Designed According to Korea Highway Bridge Design (KHBD) and AASHTO-LRFD. *International Journal of Concrete Structures and Materials*. 7(4): pp 319–332.

Lee NH, Kim KS, Bang GCJ, Park KR (2007) Tensile headed anchor with large diameter and deep embedment in concrete. ACI Structural Journal 104(4):479–486

LoBuono, and Armstrong and Associates. 1996. Development of Precast Bridge Structures. *Report Prepared for Florida Department of Transportation*.: pp. 1-25.

McMakin PJ, Slutter RG, Fisher JW (1973) Headed steel anchor under combined loading. Eng J, AISC, Second Quart 10:43–52.

Medlock R., M. Hyzak, and L. Wolf. 2002. Innovative Prefabrication in Texas Bridges. Proceedings of the Texas Section. ASCE. (Spring Meeting): pp. 1-6.

Medlock R., M. Hyzak, and L. Wolf. 2002. Innovative Prefabrication in Texas Bridges. *Proceedings of the Texas Section. ASCE*. (Spring Meeting): pp. 1-6.

Nelson Stud Welding (1966) Concrete Anchor Test No. 7— Project number 802. Nelson Division, Lorain.

Oliva, M. G., D. Unlu, and P. Okumus. 2011. Rapid Bridge Construction Technology: Precast Elements for Substructure. *Rep. No. WHRP 07-08*.

PCI-NER Technical committee. (2001) "Precast Deck Panel Guidelines," *Precast/Prestressed concrete Institute New England Region*, Rep. No. PCINER-01-PDPG, 13.

PCI-NER Technical committee. (2002) "Full depth precast concrete deck slabs,", Precast/Prestressed Concrete Institute New England Region, Rep. No. PCINER-02- FDPCDS, 18.

Qian, S., & Li, V. C. (2011). Headed anchor/engineered cementitious composites (ECC) pullout behavior. Journal of Advanced Concrete Technology, 9(3), 339-351.

Richard Alan DeVries. Anchorage of Headed Reinforcement in Concrete. PhD thesis, The University of Texas at Austin, December 1996.

Rodriguez M, Lotze D, Gross JH, Zhang YG, Klingner RE, Graves HL (2001) Dynamic behavior of tensile anchors to concrete. ACI Struct J 98(4):511–524.

Rodriguez M, Zhang YG, Lotze D, Herman L, Graves HL, Richard E, Lingner RE (1997) Dynamic behaviour of anchors in cracked and uncracked concrete: a progress report. Nucl Eng Des 168:23–24.

Sattler K (1962) Betrachtungen u¨ber neuere Verdu¨belungen im Verdbundbau, Bauingenieur, Heft 1.

Senthil K., M. A. Iqbal, and A. Kumar. 2014. Behavior of cantilever and counterfort retaining walls subjected to lateral earth pressure. *International Journal of Geotechnical Engineering.* 8(2): pp. 167-181

Si B. J., Z. G. Sun, Q. H. Ai, D. S. Wang, and Q. X. Wang. 2008. Experiments and simulation of flexural-shear dominated RC bridge piers under reversed cyclic loading. *The 14th World Conference on Earthquake Engineering*. (October): pp. 12-17.

Si B. J., Z. G. Sun, Q. H. Ai, D. S. Wang, and Q. X. Wang. 2008. Experiments and simulation of flexural-shear dominated RC bridge piers under reversed cyclic loading. The 14th World Conference on Earthquake Engineering. (October): pp. 12-17.

Stamnas, P. E., and M. D. Whittemore. 2005. All-Precast Substructure Accelerates Construction of Prestressed Concrete Bridge in New Hampshire. PCI Journal. 50(3): pp 26-39.

Tadros, M.K. and Baishya, M.C. (1998) “Rapid replacement of bridge decks,” *National Cooperative Highway Research Program*, NCHRP Report 407, Washington D.C., 51

Tarek Refaat Bashandy. Application of Headed Bars in Concrete Members. PhD thesis, The University of Texas at Austin, 1996.

Zhou S., D. C. Rizos, and M. F. Petrou. 2004. Effects of Superstructure Flexibility on Strength of Reinforced Concrete Bridge Decks. *Computers & Structures*. 82(1): pp.13-23.

.

Appendix A. **SUBGRADE TESTING REPORT**

Mc Cleary Engineering

"Specializing in Geotechnical Solutions"

July 11, 2013

Tom Heraty
Utility Concrete Products, LLC
2495 W. Bungalow Road
Morris, IL 60450

Re: Summary Report of Footing Subgrade Inspection and Fill Testing.

Mr. Heraty:

On July 8, 9 & 10, 2013, Randy Safranski performed density testing with a nuclear density machine. The test was performed at approximate depths of 19.5 ft below top of wall and 12 ft. below top of wall. Some construction of the embankment was witnessed by Randy and it appeared that the lift thickness was in the realm of 8 inch loose lifts.

The material being placed as backfill of the test wall was visually classified to be a brown gravelly Clay till material to simply a gravelly till material. It is cohesive with a large portion of gravel sized aggregate. The proctors used for the gravelly clay till and the gravelly till materials were 122.5 pcf SDD at an optimum moisture content of 11.8% and 127.1 pcf SDD at an optimum moisture content of 10.8%, respectively. The results of the nuclear density tests are included as attachments to this report. As can be seen in these reports approximately 91% compaction was achieved in the second day of testing. The material was placed wet of optimum reducing the chance of obtaining the targeted 95% compaction.

Two Shelby tubes were pushed into the fill material 7.5 ft. below the top of wall. These two samples were weighed and measured to determine their insitu unit wt. The results were 130.0 pcf and 129.8 pcf. Using the average of these two unit weights, a $K_a \approx 0.75$ a lateral earth pressure is estimated to be in the realm of 1850 psf for a 19 ft. fill height (approximately 1 ft. below the top of the wall). The resulting load on the wall is estimated to be 17500 lb/ft. of wall.

We believe this to be appropriate due to the soft to medium stiff consistency of the cohesive fill placed behind the test wall. The K_a was estimated from Figure 14-6 of the US ARMY publication TM5-818-1. The use of cohesion can result in a net negative undrained loading on the wall stem which we do not believe to be realistic for this test wall application.

On June 10th Jeff Safranski tested the foundation subgrade soils with a Dynamic Cone Penetrometer, DCP, to see if the subgrade soils met your design assumption of 2500 psf. The results are shown in the table below.

T-1 NE	blows/1 foot	IBV	Q_u tons/ft^2
First foot	40	31.54	10.09
Second foot	70	64.51	20.64
Third foot	100	100.05	32.02

T-2 NW	blows/1 foot	IBV	Q_u tons/ft^2
First foot	39	30.26	9.68
Second foot	80	75.53	24.17
Third foot	105	111.65	35.73

T-3 SE	blows/1 foot	IBV	Q_u tons/ft^2
First foot	38	29.07	9.30
Second foot	90	87.64	28.04
Third foot	115	119.32	38.18

T-4 SW	blows/1 foot	IBV	Q_u tons/ft^2
First foot	42	33.54	10.73
Second foot	65	58.15	18.61
Third foot	66	59.27	18.97

Table 1.0, DCP test results

As can be seen the strength of the subgrade soils are quite strong. This was confirmed by comparing these results to the borings taken for the yard expansion project. Boring 4 of the 2007 report appears to be the closest existing boring to the prototype wall test site. The September 2007 report is attached for your reference. As you can see in this boring there exists a hard till material with unconfined compressive strengths, Qu's, in the realm of 4 tsf. The Qu's determined by the DCP are exaggerated as the blow counts increase to the number of blows/ft encountered at this site. For your purposes we believe the Qu to be well above the desired 2500 psf design assumption used for this wall.

If you have any questions please don't hesitate to contact me at (815) 830-6405 or via email at terry@mcclearyengineering.com.

Respectfully submitted,

Terrence L. McCleary

Terrence L. McCleary

STATE OF ILLINOIS
062-050019
TERRENCE L.
MC CLEARY
LICENSED ENGINEER

Date: June 11, 2013 **Sheet:** 1 of 1

Midwest Testing Services, Inc
3705 Progress Blvd.
Peru, IL 61354
Phone 815-223-6696 Fax 815-223-6659

REPORT OF IN-PLACE DENSITY TESTS

Report Number: 001
Date of Test: June 11, 2013
Contractor: Stott Construction
Project: Utility Concrete Products
Retaining Wall Construction
Morris, IL

Architect or Engineer: McCleary Engineering
Equipment Compacting: Vibratory Plate
Source of Material: Central Limestone
Soil Type: CA-06 Crushed Stone
Water Required: No
Aeration Required: No

Test #	Location	Depth Below Sub-Grade Elevation	Field		Laboratory		% of Maximum Dry Density	Specification Requirements
			Dry Density (PCF)	Moisture Content %	Maximum Dry Density (PCF)	Optimum Moisture Content %		
01	NW Area	Grade	131.8	7.1%	135.4	8.7%	97.3%	95%
02	NE Area	Grade	132.1	7.5%	135.4	8.7%	97.6%	95%
03	SE Area	Grade	130.8	7.0%	135.4	8.7%	96.6%	95%
04	SW Area	Grade	129.8	8.0%	135.4	8.7%	95.9%	95%
05	Center Area	Grade	130.2	7.7%	135.4	8.7%	96.2%	95%

Remarks:

Method Used : Nuclear Density Gauge

Original To:
Copies To:

Midwest Testing Services, Inc.

By: Joseph E. Safranski P.E.

Date: July 8, 2013 **Sheet:** 1 of 1

Midwest Testing Services, Inc

3705 Progress Blvd.
Peru, IL 61354
Phone 815-223-6696 Fax 815-223-6659

REPORT OF IN-PLACE DENSITY TESTS

Report Number: 002
Contractor: Stott Construction
Date of Test: July 8, 2013
Project: Utility Concrete Products
Retaining Wall Construction
Morris, IL

Architect or Engineer: McCleary Engineering
Equipment Compacting: Vibratory Plate
Source of Material: On-Site
Soil Type: Brown Gray Clay Till
Water Required: No
Aeration Required: No

Test #	Location	Depth Below Top of Wall Elevation	Field Dry Density (PCF)	Field Moisture Content %	Laboratory Maximum Dry Density (PCF)	Laboratory Optimum Moisture Content %	% of Maximum Dry Density	Specification Requirements
01	West Side of Wall	19.5'	109.2	16.1%	122.5	11.8%	89.1%	95%

Remarks:

Method Used : Nuclear Density Gauge

Original To:
Copies To:

Midwest Testing Services, Inc.

By: Joseph E. Safranski P.E.

Date: July 9, 2013 **Sheet:** 1 of 1

Midwest Testing Services, Inc

3705 Progress Blvd.

Peru, IL 61354

Phone 815-223-6696 Fax 815-223-6659

REPORT OF IN-PLACE DENSITY TESTS

Report Number: 003

Contractor: Stott Construction

Date of Test: July 9, 2013

Project: Utility Concrete Products
Retaining Wall Construction
Morris, IL

Architect or Engineer: McCleary Engineering

Equipment Compacting: Vibratory Plate

Source of Material: On-Site

Soil Type: Brown Gravely Till

Water Required: No

Aeration Required: No

Test #	Location	Depth Below Top of Wall Elevation	Field		Laboratory		% of Maximum Dry Density	Specification Requirements
			Dry Density (PCF)	Moisture Content %	Maximum Dry Density (PCF)	Optimum Moisture Content %		
01	North Side of Wall	14'	120.2	14.0%	127.1	10.8%	94.6%	95%
02	Center of Wall	14'	117.3	15.2%	127.1	10.8%	92.3%	95%
03	South Side of Wall	14'	118.6	14.5%	127.1	10.8%	93.3%	95%
04	South Inner Partion of Wall	14'	117.7	14.8%	127.1	10.8%	92.6%	95%

Remarks:

Method Used : Nuclear Density Gauge

Original To:

Copies To:

Midwest Testing Services, Inc.

By: Joseph E. Safranski P.E.

Date: July 10, 2013 **Sheet:** 1 of 1

Midwest Testing Services, Inc
3705 Progress Blvd.
Peru, IL 61354
Phone 815-223-6696 Fax 815-223-6659

REPORT OF IN-PLACE DENSITY TESTS

Report Number: 004
Contractor: Stott Construction
Date of Test: July 10, 2013
Project: Utility Concrete Products
Retaining Wall Construction
Morris, IL
Architect or Engineer: McCleary Engineering
Equipment Compacting: Vibratory Plate
Source of Material: On-Site
Soil Type: Brown Gravely Till
Water Required: No
Aeration Required: No

Test #	Location	Depth Below Top of Wall Elevation	Field		Laboratory		% of Maximum Dry Density	Specification Requirements
			Dry Density (PCF)	Moisture Content %	Maximum Dry Density (PCF)	Optimum Moisture Content %		
01	6-Feet West of Wall	7.5'	115.9	12.6%	127.1	10.8%	91.2%	95%
02	12-Feet West of Wall	7.5'	115.5	11.5%	127.1	10.8%	90.9%	95%

Remarks:

Method Used : Nuclear Density Gauge

Original To:
Copies To:

Midwest Testing Services, Inc.

By: Joseph E. Safranski P.E.

J. E. Safranski, P.E.

Business Phone: 815-223-6696
Fax Phone: 815-223-6659
E-Mail: mts37@comcast.net

Midwest Testing Services, Inc.
3705 Progress Boulevard
Peru, Illinois 61354

07/10/2013

McCleary Engneering
3705 Progress Blvd. Suite 2
Peru, IL. 61354

Attn: Terry McCleary

RE: Soil Wet Unit Weight
Utility Concrete
Morris, IL. 60450

Dear Sir,

On July 10, 2013, as requested Shelby Tube testing was completed, to determine the unit weight of the soil for the above referenced project.

Below are the results of the completed testing:

Shelby Tube #1

130.0 Lbs. Per Cubic Foot (Wet Weight)

Shelby Tube #2

129.8 Lbs. Per Cubic Foot (Wet Weight)

If you have any questions or concerns regarding this report, please contact our office at your convenience.

VITA

MAEN FARHAT

1013 Harlem Ave. Apt 1D, Forest Park, IL 60130|(312) 927-5583|
maen.farhat@gmail.com

EDUCATION

a) **Doctor of Philosophy,** Civil and Material Engineering, University of Illinois at Chicago (UIC), USA, December 2016.
Thesis: Structural Behavior of Full Scale Totally Precast Concrete Counterfort Retaining Wall System.
b) **Bachelor of Science,** Civil Engineering, Lebanese University, Beirut, Lebanon, July 2012.

RESEARCH INTRESTS

- Accelerated Bridge Construction
- Finite Element Method
- Pavements and bridges
- Seismic and Wind Analysis
- HDPE crossties for high speed rail
- Ultra-High Performance Concrete
- Durability of concrete materials
- Prestressed Concrete

ACADEMIC CAREER EXPERIENCE

Research Assistant, University of Illinois**,** Chicago, IL. (August 2012- present)
Advisor: Prof. Mohsen Issa

- ***Totally precast concrete counterfort retaining wall system (Ph.D. thesis work)*** *($47,048 by Utility Concrete Products, Morris, IL, May 2013 - Sep. 2013):*

  Performed a full-scale experimental testing program and detailed nonlinear finite element analysis to assess the structural behavior of innovative totally precast concrete counterfort retaining wall system. The testing program was divided into design, fabrication, erection, instrumentation, testing setup, soil backfilling, and load application. Real time data was collected during testing.

  In addition, an experimental testing program was conducted to examine the pullout behavior and the mode of failure of headed anchors that are used in the Totally Precast Concrete Counterfort Retaining Wall system. I am currently working to publish this section of the thesis.

- ***Recycled composite rail crossties for high speed rail applications*** *($402,308 by NURail- USDOT/RITA, Oct 2013-present):*

a) This project is part of a collaborative effort with NURail center, Urbana-Champaign, IL to improve the track-bridge interaction using composite materials. I assisted in conducting an experimental testing program to assess the performance of recycled, high-density polyethylene, crossties for high-speed rail applications and developed calibrated material models for use in full-scale analytical analyses. The testing program evaluated the mechanical properties, temperature effect, fastening system interactions and long-term performance of the composite plastic crossties.

b) Performed a nonlinear finite element analysis to investigate the structural behavior HDPE railway crossties for high-speed rail applications.

- ***Effect of early-age concrete elastic properties on fatigue damage in PCC pavements containing fibers*** *($300,000 ICT/IDOT-ongoing):*

  I was fully involved in conducting a comprehensive experimental testing program to study the effect of elastic properties on the fatigue damage of concrete at an early age of opening to traffic. The program contains concrete mixing and fresh properties, flexure toughness with various fiber content and types, strength measurements, fracture mechanics, fatigue testing, maturity meters, relative dynamic modulus, static modulus of elasticity, hardened air content, effect of fatigue on the freeze/thaw performance, effect of fatigue on doweled slab system at an early age, etc…

- ***Performance of limestone and inorganic processing additions (IPA) in concrete for pavements and bridge decks*** *($400,000 ICT/IDOT-May 2011-Dec 2013):*

  Involved in performing a detailed experimental testing program such as concrete mixing, compression test, chloride penetration, freeze/thaw cycles, etc…

- ***Performance of optimized railway concrete crossties prestressed with Basalt FRP (****C1 Pultrusions LLC, $171,786 Aug. 2016-Jul. 2021****):***

  Developed an innovative prestressing technique to allow prestressing BFRP bars without subjecting them to crushing. Crossties were tested for positive seat bending and negative bending.

- ***Rehabilitation of existing building structures using advanced FRP materials***
- ***Assessment of current condition of existing concrete structures using concrete cores.***
- ***Performed finite element simulation and participated in the experimental testing program of composite plastic lumbers used for structural application***

  The testing program included flexural bending, compression, screw pullout, full support-deck system testing

- ***Implementation of advanced instrumentation techniques*** *(strain gauges, LVDT…)* for structural testing applications.
- ***Attended 3-days Non-Destructive Testing (NDT) of concrete workshop in August 2012 in Chicago, IL.*** *The workshop was organized Germann Instruments Inc. and was taught by Dr. Nick Carino.*

Teaching Assistant, University of Illinois at Chicago**,** Chicago, IL.

Aided in teaching the following courses by grading assignments, giving review lectures, and replacing the professor when he was away for conferences and emergency:

- *Reinforced Concrete Design - CME 310 (Spring semesters of 2013, 2015, and 2016):*
- *Bridge Design I - CME 406 (Fall 2014):*
- *Advanced Design of Reinforced Concrete - CME 400 (Fall 2015):*
- *Composition and Properties of Concrete- CME 300 (lecture and Labs) (Fall 2016):*
- *Concrete Plates and Shells design- CME 500* (Spring 2016)

TEACHING INTERESTS

- Strength of Materials
- Bridge Design
- Design of steel structures
- Statics
- Reinforced concrete design (I and II)
- Composition and properties of concrete
- Prestressed Concrete (I and II)
- Structural Analysis

PHD SKILLS

Experimental Testing	Conducted numerous experimental testing programs. These programs required knowledge in running high caliber machines (Instron and Tinius Olsen), experimental setup preparation, ASTM standards, instrumentation techniques (LVDT, strain gauges, load cells, etc…), and analyzing the test results. Examples of experimental testing skills include Fracture Mechanics, Flexure Toughness, Ultra High Performance Concrete (UHPC) testing, etc…
Finite Element Analysis	Performed a variety of simulations using Nonlinear Finite Element Analysis. I used FEM to analyze concrete structures and understand the real behavior of structures before testing. I am experienced in using ANSYS package and Sap2000.

Proposal writing	Participated with my advisor in writing several proposals to funded projects for different agencies such as ICT/IDOT, Illinois Tollway Authority, and others
Communicat-ion	Presented 10 technical presentations and poster sessions to industry experts and research pioneers in professional conferences around the US. Authored and co-authored 12 journal and proceeding publications.

THEORETICAL BACKGROUND

During my stay at UIC, I worked to reinforce my theoretical background with the necessary advanced courses that allowed me to further understand the real behavior of structures. The advanced courses I took at UIC gave me the knowledge necessary to start a successful academic career. These courses include:

- CME 430: Theory of Elasticity
- CME 537: Theory of Plasticity
- CME 400: Advanced Concrete Design
- CME 406: Bridge Design
- CME 536: Nondestructive Testing of Concrete
- CME 594: Sustainability Engineering
- CME 433 and 533: Fracture Mechanics I & II
- CME 520: Earthquake Engineering
- CME 500: Design of Concrete Plates and Shells
- CME 544: Structural Dynamics
- CME 534: Finite Element Analysis II
- CME 454: Design of Tall Building Structures

STRUCURAL ENGINEERING DESIGN SKILLS

I took several Special Problems courses in which I developed several design spreadsheets, Mathcad files, and Finite Element Analysis for several design projects, including:

- Investigated the adequacy of existing segmental box girder bridge to meet the AASHTO LRFD design specifications,
- Developed caisson design spreadsheets according to AREMA and performed L-pile simulations for them.
- Designed abutments and retaining walls according to AASHTO LRFD criteria,
- Designed Twin cell reinforced concrete box culverts (AASHTO LRFD),
- Revising existing counterfort abutment and retaining systems from AASHTO LFD to conform with the latest AASHTO LRFD design specifications

- Finite Element Modeling of pedestrian bridge

ACADEMIC DISTINCTIONS AND AWARDS

- Won the AAAEA scholarship for the Illinois section, *October 2015*
- Precast/Prestressed Concrete Institute (PCI) award to present a poster and presentation at the 60th anniversary PCI Convection and National Bridge Conference (2014), Washington, D.C. *September 2014*

SOFTWARE AND COMPUTER SKILLS

- ANSYS
- Matlab, Mathcad
- ETABS, SAP2000, AutoCAD

EXTRA CURRICULAR ACTIVITIES

May 2014 and 2015	Mentored high school students during "Physics Day" at Reavis High School, Burbank, IL.
May 2015- 2016	Board member (secretary) in the AAAEA student chapter at UIC
May 2015	Assisted ASCE chapter students at UIC to design and build the concrete canoe for the 2015 Midwest Regional Competition held at Notre Dame, IN.
April 2015	Assisted in organizing the AAAEA educational seminar held at HBM Engineering Group, LLC.
Oct 2014	Assisted in organizing the AAAEA educational seminar held at UIC.
July 2014	Participated in orientations and tours held for multiple high school and middle school students to introduce them to civil engineering.

PROFESSIONAL AFFILIATIONS

ASCE, American Society of Civil Engineers, Associate Member.
PCI, Precast/Prestressed Concrete Institute, Student Member.
ASME, American Society of Mechanical Engineers, Student Member.
ACI, American Concrete Institute, Student Member.
NURail, National University Rail (NURail) Center, Student Member.

PUBLICATIONS

1. Farhat, M., Issa, M.A., and Jose Prado, B. F. “Pullout Behavior of Headed Anchors Used in Totally Precast Concrete Counterfort Retaining Wall System,” Paper Submitted to PCI Journal, In Review.
2. Farhat, M., Ibrahim, M., Bassim, R., and Issa, M. A., "Effect of Early Opening to Traffic on the Fracture Mechanics Parameters of IDOT Concrete Pavement Mix Designs," Papers Submitted to the ACI Concrete International. Under Review.
3. Ibrahim, M., Farhat, M., Bassim, R., and Issa, M. A., "Evaluation of the Maturity and Dynamic Modulus Tests for the Strength Prediction of IDOT Concrete Pavement and Patches Mix Designs at Early Opening to Traffic," Papers Submitted to the ACI Concrete International. Under Review.
4. Farhat, M., and Issa, M.A., “Design Principles of Totally Prefabricated Counterfort Retaining Wall System Compared to Existing Cast-In-Place Structures,” Accepted for publication in PCI Journal. Date of acceptance: October 31, 2016.
5. Farhat, M., and Issa, M.A., “Fabrication and Construction of Totally Prefabricated Counterfort Retaining Wall System for Highways,” Paper Submitted to the Practice Periodical of Structural Engineering, Accepted for publication on October 10, 2016.
6. Farhat, M., Ibrahim, M., Issa, M.A., and Rahman, M., “Full Scale Experimental Testing and Finite Element Analysis of Totally Prefabricated Counterfort Retaining Wall System,” Paper Submitted to *PCI Journal*, Accepted for publication in PCI Journal. Date of acceptance: October 31, 2016.
7. Ibrahim, M.A., Farhat, M., Issa, M.A., and Amanda, J.A., “Effect of Material Constituents on the Mechanical and Fracture Mechanics Properties of UHPC,” Paper Submitted to ACI Materials Journal, Under Review.
8. Farhat, M., Rahman, M., Ibrahim, M., and Issa, M. A., “Design Optimization and Modeling of a Totally Precast Concrete Counterfort Retaining Wall System” In the proceedings of the 2015 European Bridge Conference, Edinburgh., UK, 22-25 June 2015.
9. Farhat, M., Rahman, M., Ibrahim, M., and Issa, M. A., “Design, Fabrication, Modeling and Experimental Study of a Totally Precast Concrete Counterfort Retaining Wall System for Highways” In the proceedings of the 2014 PCI/NBC conference, Washington D.C., CA, 06-09 September 2014.
10. Lotfy, I., Farhat, M., and Issa, M., "Effect of Pre-drilling, Loading Rate and Temperature Variation on the Behavior of Railroad Spikes used for High

Density Polyethylene Crossties", Journal of Rail and Rapid Transit; In press, DOI: 0954409715620755, first published on December 10, 2015.

11. Lotfy, I., Farhat, M., and Issa, M. A., "Structural Behavior of Rail Fastening System used for Recycled Plastic Composite Crossties" In the proceedings of the 2015 Joint Rail and Rapid Transit, San Jose, CA, 23-25 March 2015.
12. Lotfy, I., Farhat, M., and Issa, M. A., "Temperature Effect on the performance of Glass Fiber Reinforced High Density Polyethylene Composite Railroad Crossties" Journal of Rail and Rapid Transit; In press, accepted for publication on 17 March 2015. DOI: 10.1177/0954409715583384
13. Lotfy, I., Farhat, M., Issa, M. A., and Al-Obaidi, M., "Flexural behavior of high-density polyethylene railroad crossties", Journal of Rail and Rapid Transit, Vol. 230, No. 3, March 2016, pp. 813-824.

PRESENTATIONS AND CONFERENCE INVOLVEMENT

1. Farhat M., Rahman M., and Issa M. A., "Performance of Concrete Railway Ties Prestressed with Basalt FRP." Poster session at the 2016 NURail/Rees annual meeting in Urbana-Champaign, IL, July, 2016.
2. Farhat M., Rahman M., Ibrahim M., and Issa M. A., "Totally Prefabricated Counterfort Substructure System for Highway and Railway Applications." Poster session at the 2015 NURail annual meeting in Chicago, IL, June, 2015.
3. Lotfy I., Farhat M., and Issa M., "Experimental Evaluation and Modeling of Fastening System for Plastic Composite Crossties." Two posters at the 2015 NURail annual meeting in Chicago, IL, June, 2015.
4. Farhat M., Rahman M., Ibrahim M., and Issa M. A., "Totally Prefabricated Counterfort Substructure System for Highway Applications" Poster session in the 2014 PCI/NBC Conference Washington, DC, September, 2014.
5. Farhat M., Rahman M., Ibrahim M., and Issa M. A., "Design, Fabrication, Modeling and Experimental Study of A Totally Precast Concrete Counterfort Retaining Wall System For Highways" Presentation at the 2014 PCI/NBC Conference Washington, DC, September, 2014.
6. Farhat M., Rahman M., Ibrahim M., and Issa M. A., "Totally Prefabricated Counterfort Substructure System for Highway and Railway Applications." Presentation and Poster session in the 2014 NURail annual meeting in Altoona, PA, August, 2014.
7. Lotfy I., Farhat M., and Issa M., "Experimental Evaluation and Modeling of Fastening System for Plastic Composite Crossties." presentation and two posters in the 2014 NURail annual meeting in Altoona, PA, August, 2014.

8. “National University Rail Center (NURail) booth.” Represented the NURail center at The 2014 AREMA Annual Conference and Exposition, Chicago, IL, October, 2014.
9. Chaired the “Vehicle-Track Interaction” session in the “Railroad Infrastructure Engineering” technical track at the 2014 Joint Rail Conference in Colorado Springs, CO, April 2014
10. Farhat M., Lotfy I., and Issa M., “Finite element analysis for pullout, lateral restraint and flexural behavior of HDPE crossties”, presentation in the 2014 Joint Rail Conference in Colorado Springs, CO, Special Session: 10-3 National University Rail (NURail) Center - Research & Education 2, April, 2014.
11. Al-Obaidi M., Lotfy I., Farhat M., and Issa M., “Effect of temperature on the mechanical properties of HDPE railroad crossties”, presentation in the 2014 Joint Rail Conference in Colorado Springs, CO, Special Session: 10-3 National University Rail (NURail) Center - Research & Education 2, April, 2014.
12. Lotfy I., Farhat M., and Issa M., “Assessment of HDPE railroad crossties performance using static and cyclic testing”, presentation in the 2014 Joint Rail Conference in Colorado Springs, CO, Special Session: 10-3 National University Rail (NURail) Center - Research & Education 2, April, 2014.
13. “National University Rail Center (NURail) booth.” Represented the NURail center at The 2013 AREMA Annual Conference and Exposition, Rail Interchange Expo Center, Indianapolis, IN, October, 2013.
14. “National University Rail Center (NURail) booth.” Represented the NURail center at The 2013 AREMA Annual Conference and Exposition, Rail Interchange Expo Center, Indianapolis, IN, October, 2013.
15. Lotfy I., Farhat M., and Issa M., “Testing and Simulation of Fastening System for HDPE Crossties.” Poster presented in the 2013 NURail annual meeting in Urbana-Champaign, IL, Poster Session, September, 2013.
16. Lotfy I., Farhat M., and Issa M., “Flexural behavior of High Density Polyethylene Railroad Crossties.” Poster presented in the 2013 NURail annual meeting in Urbana-Champaign, IL, Poster Session, September, 2013.
17. Lotfy I., Farhat M., Al-Obaidi M., and Issa M., “Testing and performance simulation of plastic rail ties” presentation and poster in the 2013 Joint Rail Conference in Knoxville, TN, Special Session: 10-4 NURail: Research Projects (Technical), April, 2013.

REFRENCES

Mohsen A. Issa, Ph.D., P.E., S.E., F.ACI, F.ASCE (Ph.D. Advisor)
Professor of Structural and Material Engineering,
Director, Structural and Concrete Research Laboratory
University of Illinois at Chicago, Department of Civil & Materials Engineering
2095 Engineering Research Facility, (M/C 246)
842 West Taylor Street, Chicago, IL 60607
Phone:(312) 996-3432, cell: (312) 375-8186, e-mail: **missa@uic.edu**

Krishna R. Reddy, PhD, PE, DGE, FASCE, ENV SP (Ph.D. committee member)
Professor of Civil & Environmental Engineering
Director, Sustainable Engineering Research Laboratory
Director, Geotechnical & Geoenvironmental Engineering Laboratory
Department of Civil & Materials Engineering, University of Illinois at Chicago
Engineering Research Facility, 842 West Taylor Street Chicago, IL 60607-7023
Phone: 312-996-4755, Cell:630-849-0207, e-mail: **kreddy@uic.edu**

Craig Foster, Ph.D., (Ph.D. committee member)
Associate Professor
Department of Civil and Materials Engineering (MC 246), University of Illinois at Chicago
3085 Engineering Research Facility, 842 West Taylor Street Chicago, IL 60607-7023
Tel: (312)-996-8086 , *e-mail*: **fosterc@uic.edu**

Ahmed Shabana, Ph.D. (Ph.D. committee member)
UIC Distinguished Professor, Richard and Loan Hill Professor of Engineering
Director of The Multibody System Dynamics Laboratory
Room 2031, Engineering Research Facility, 842 West Taylor Street Chicago, IL 60607-7023
Phone: (312) 996-3600 e-mail: **shabana@uic.edu**

Moussa Issa, Ph.D., P.E, S.E.
Chief Structural Engineer at HBM Engineering Group, LLC., Hillside, IL.
4415 Harrison St #231, Hillside, IL 60162
Tel: (312) 355-0364, *e-mail*: **Moussa.issa@hbmengineering.com**